













TECH BRIEFS

NATIONAL AERONAUTICS AND SPACE ADMINISTRATION

-  **Technology Focus**
-  **Electronics/Computers**
-  **Software**
-  **Materials**
-  **Mechanics/Machinery**
-  **Manufacturing**
-  **Bio-Medical**
-  **Physical Sciences**
-  **Information Sciences**
-  **Books and Reports**

INTRODUCTION

Tech Briefs are short announcements of innovations originating from research and development activities of the National Aeronautics and Space Administration. They emphasize information considered likely to be transferable across industrial, regional, or disciplinary lines and are issued to encourage commercial application.

Availability of NASA Tech Briefs and TSPs

Requests for individual Tech Briefs or for Technical Support Packages (TSPs) announced herein should be addressed to

National Technology Transfer Center

Telephone No. (800) 678-6882 or via World Wide Web at www.nttc.edu

Please reference the control numbers appearing at the end of each Tech Brief. Information on NASA's Innovative Partnerships Program (IPP), its documents, and services is also available at the same facility or on the World Wide Web at <http://ipp.nasa.gov>.

Innovative Partnerships Offices are located at NASA field centers to provide technology-transfer access to industrial users. Inquiries can be made by contacting NASA field centers listed below.

NASA Field Centers and Program Offices

Ames Research Center

Lisa L. Lockyer
(650) 604-1754
lisa.l.lockyer@nasa.gov

Dryden Flight Research Center

Gregory Poteat
(661) 276-3872
greg.poteat@dfrc.nasa.gov

Glenn Research Center

Kathy Needham
(216) 433-2802
kathleen.k.needham@nasa.gov

Goddard Space Flight Center

Nona Cheeks
(301) 286-5810
nona.k.cheeks@nasa.gov

Jet Propulsion Laboratory

Ken Wolfenbarger
(818) 354-3821
james.k.wolfenbarger@jpl.nasa.gov

Johnson Space Center

Michele Brekke
(281) 483-4614
michele.a.brekke@nasa.gov

Kennedy Space Center

David R. Makufka
(321) 867-6227
david.r.makufka@nasa.gov

Langley Research Center

Martin Waszak
(757) 864-4015
martin.r.waszak@nasa.gov

Marshall Space Flight Center

Jim Dowdy
(256) 544-7604
jim.dowdy@msfc.nasa.gov

Stennis Space Center

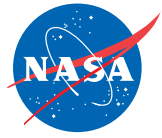
John Bailey
(228) 688-1660
john.w.bailey@nasa.gov

Carl Ray, Program Executive

Small Business Innovation
Research (SBIR) & Small
Business Technology
Transfer (STTR) Programs
(202) 358-4652
carl.g.ray@nasa.gov

Doug Comstock, Director

Innovative Partnerships
Program Office
(202) 358-2560
doug.comstock@nasa.gov



TECH BRIEFS

NATIONAL AERONAUTICS AND SPACE ADMINISTRATION



5 Technology Focus: Composites & Coating

- 5 Rapid Fabrication of Carbide Matrix/Carbon Fiber Composites
- 5 Coating Thermoelectric Devices To Suppress Sublimation
- 6 Ultrahigh-Temperature Ceramics
- 7 Improved C/SiC Ceramic Composites Made Using PIP
- 7 Coating Carbon Fibers With Platinum



9 Electronics/Computers

- 9 Two-Band, Low-Loss Microwave Window
- 9 MCM Polarimetric Radiometers for Planar Arrays
- 10 Aperture-Coupled Thin-Membrane L-Band Antenna
- 11 WGM-Based Photonic Local Oscillators and Modulators
- 13 Focal-Plane Arrays of Quantum-Dot Infrared Photodetectors
- 14 Laser Range and Bearing Finder With No Moving Parts
- 14 Microrectenna: A Terahertz Antenna and Rectifier on a Chip
- 15 Miniature L-Band Radar Transceiver
- 17 Robotic Vision-Based Localization in an Urban Environment
- 18 Programs for Testing an SSME-Monitoring System
- 19 Cathodoluminescent Source of Intense White Light
- 20 Displaying and Analyzing Antenna Radiation Patterns
- 20 Payload Operations Support Team Tools
- 21 Space-Shuttle Emulator Software
- 21 Soft Real-Time PID Control on a VME Computer
- 22 Analyzing Radio-Frequency Coverage for the ISS



23 Materials

- 23 Nanorod-Based Fast-Response Pressure-Sensitive Paints



25 Mechanics/Machinery

- 25 Capacitors Would Help Protect Against Hypervelocity Impacts

- 25 Diaphragm Pump With Resonant Piezoelectric Drive
- 26 Improved Quick-Release Pin Mechanism
- 26 Designing Rolling-Element Bearings
- 27 Reverse-Tangent Injection in a Centrifugal Compressor
- 28 Inertial Measurements for Aero-assisted Navigation (IMAN)
- 28 Analysis of Complex Valve and Feed Systems
- 29 Improved Path Planning Onboard the Mars Exploration Rovers
- 29 Robust, Flexible Motion Control for the Mars Explorer Rovers
- 29 Solar Sail Spaceflight Simulation



31 Manufacturing & Prototyping

- 31 Fluorine-Based DRIE of Fused Silica
- 31 Mechanical Alloying for Making Thermoelectric Compounds
- 32 Process for High-Rate Fabrication of Alumina Nanotemplates
- 33 Electroform/Plasma-Spray Laminates for X-Ray Optics



35 Physical Sciences

- 35 An Automated Flying-Insect Detection System
- 36 Calligraphic Poling of Ferroelectric Material
- 38 Blackbody Cavity for Calibrations at 200 to 273 K
- 39 KML Super Overlay to WMS Translator
- 39 High-Performance Tiled WMS and KML Web Server
- 39 Modeling of Radiative Transfer in Protostellar Disks
- 40 Composite Pulse Tube
- 40 Photometric Calibration of Consumer Video Cameras
- 41 Criterion for Identifying Vortices in High-Pressure Flows
- 42 Amplified Thermionic Cooling Using Arrays of Nanowires
- 43 Delamination-Indicating Thermal Barrier Coatings
- 44 Preventing Raman Lasing in High-Q WGM Resonators
- 44 Procedures for Tuning a Multiresonator Photonic Filter

- 45 Robust Mapping of Incoherent Fiber-Optic Bundles
- 47 Extended-Range Ultrarefractive 1D Photonic Crystal Prisms
- 48 Rapid Analysis of Mass Distribution of Radiation Shielding
- 48 Modeling Magnetic Properties in EZTB
- 48 Deep Space Network Antenna Logic Controller
- 49 Modeling Carbon and Hydrocarbon Molecular Structures in EZTB
- 49 BigView Image Viewing on Tiled Displays
- 49 Imaging Sensor Flight and Test Equipment Software
- 50 Processing AIRS Scientific Data Through Level 2
- 50 Triaxial Probe Magnetic Data Analysis
- 51 Analyzing Responses of Chemical Sensor Arrays
- 51 PREDICTS
- 51 Software Compensates Electronic-Nose Readings for Humidity
- 52 Space Propulsion Design and Analysis
- 52 Parallelization of the Coupled Earthquake Model

53 Information Sciences

- 53 Automated Recognition of 3D Features in GPR Images
- 53 Algorithm Plans Collision-Free Path for Robotic Manipulator
- 54 Hybrid Automated Diagnosis of Discrete/Continuous Systems
- 55 State-Estimation Algorithm Based on Computer Vision
- 56 Representing Functions in n Dimensions to Arbitrary Accuracy
- 57 Accumulate-Repeat-Accumulate-Accumulate Codes
- 58 Interface for Physics Simulation Engines
- 59 ISPATOM: A Generic Real-Time Data Processing Tool Without Programming
- 59 Automated Diagnosis and Control of Complex Systems
- 60 Program Management Tool
- 60 Flyby Geometry Optimization Tool
- 61 Displaying Properties of PDFs
- 61 Modular Filter and Source-Management Upgrade of RADAC
- 61 Automatic Command Sequence Generation
- 62 Generating Scenarios When Data Are Missing
- 62 CASPER Version 2.0
- 63 Mission Simulation Toolkit
- 63 Solving Equations of Multibody Dynamics
- 63 Mapped Landmark Algorithm for Precision Landing

- 64 WMAP C&DH Software
- 64 Web-Based Environment for Maintaining Legacy Software
- 64 Information Metacatalog for a Grid
- 65 Grid Task Execution
- 65 Parallel-Processing Software for Correlating Stereo Images
- 65 Knowledge Base Editor (SharpKBE)
- 66 Parallel Computing With Satellite Orbit Analysis Program
- 67 Automated Sequence Generation Process and Software
- 67 Periodic, On-Demand, and User-Specified Information Reconciliation
- 67 Simulating Operations at a Spaceport
- 68 Web-Based Real-Time Emergency Monitoring
- 68 Real-Time Data Display
- 69 Master Metadata Repository and Metadata-Management System
- 69 Collaborative Resource Allocation
- 70 Model Checker for Java Programs

73 Books & Reports

- 73 Telescope Formation at L2 for Observing Earth's Atmosphere
- 73 Ultraviolet-Resistant Bacterial Spores
- 73 Launching Payloads Into Orbit at Relatively Low Cost
- 73 Effects of Bone Morphogenic Proteins on Engineered Cartilage

This document was prepared under the sponsorship of the National Aeronautics and Space Administration. Neither the United States Government nor any person acting on behalf of the United States Government assumes any liability resulting from the use of the information contained in this document, or warrants that such use will be free from privately owned rights.



❏ Rapid Fabrication of Carbide Matrix/Carbon Fiber Composites Melt infiltration offers advantages over chemical vapor infiltration.

Marshall Space Flight Center, Alabama

Composites of zirconium carbide matrix material reinforced with carbon fibers can be fabricated relatively rapidly in a process that includes a melt infiltration step. Heretofore, these and other ceramic matrix composites have been made in a chemical vapor infiltration (CVI) process that takes months. The finished products of the CVI process are highly porous and cannot withstand temperatures above 3,000 °F ($\approx 1,600$ °C). In contrast, the melt-infiltration-based process takes only a few days, and the composite products are more nearly fully dense and have withstood temperatures as high as 4,350 °F ($\approx 2,400$ °C) in a highly oxidizing thrust chamber environment. Moreover, because the melt-infiltration-based process takes much less time, the finished products are expected to cost much less.

Fabrication begins with the preparation of a carbon fiber preform that, typically, is of the size and shape of a part to be fabricated. By use of low-temperature ultraviolet-enhanced chemical vapor deposition, the carbon fibers in the preform are coated with one or more interfacial material(s), which could include oxides. The interfacial material helps to protect the fibers against chemical attack during the remainder of the fabrication process and against oxidation during subsequent use; it also enables slippage between the fibers and the matrix material, thereby helping to deflect cracks and distribute loads. Once the fibers have been coated with the interfacial material, the fiber preform is further infiltrated with a controlled amount of additional carbon, which serves as a reactant for the formation of the carbide matrix material.

The next step is melt infiltration. The preform is exposed to molten zirconium, which wicks into the preform, drawn by capillary action. The molten metal fills most of the interstices of the preform and reacts with the added carbon to form the zirconium carbide matrix material. The zirconium does not react with the underlying fibers because they are protected by the interfacial material(s). The success of the melt-infiltration step depends on interface material selection and uniform coating of the fibers, infiltration with the correct amount of carbon, and careful control of temperature and rate of heating.

*This work was done by Brian E. Williams and Robert E. Benander of Ultramet for Marshall Space Flight Center. Further information is contained in a TSP (see page 1).
MFS-31847*

❏ Coating Thermoelectric Devices To Suppress Sublimation

Thermoelectric materials are covered with adherent, chemically stable metal outer layers.

NASA's Jet Propulsion Laboratory, Pasadena, California

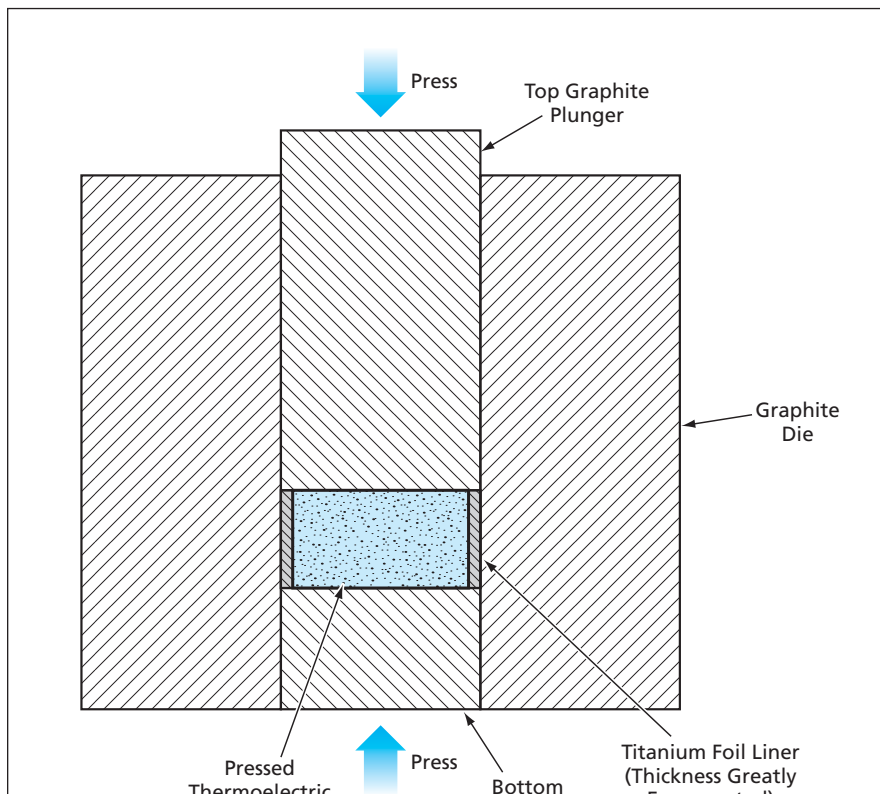
A technique for suppressing sublimation of key elements from skutterudite compounds in advanced thermoelectric devices has been demonstrated. The essence of the technique is to cover what would otherwise be the exposed skutterudite surface of such a device with a thin, continuous film of a chemically and physically compatible metal. Although similar to other sublimation-suppression techniques, this technique has been specifically tailored for application to skutterudite antimonides.

The primary cause of deterioration of most thermoelectric materials is thermal decomposition or sublimation—one or more elements sublime from the hot side of a thermoelectric couple, changing the stoichiometry of the device. Examples of elements that sublime from their respective thermoelectric materials

are Ge from SiGe, Te from Pb/Te, and now Sb from skutterudite antimonides. The skutterudite antimonides of primary interest are CoSb₃ [electron-donor (n) type] and CeFe_{3-x}Co_xSb₁₂ [electron-acceptor (p) type]. When these compounds are subjected to typical operating conditions [temperature of 700 °C and pressure $<10^{-5}$ torr (0.0013 Pa)], Sb sublimates from their surfaces, with the result that Sb depletion layers form and advance toward their interiors. As the depletion layer advances in a given device, the change in stoichiometry diminishes the thermal-to-electric conversion efficiency of the device.

The problem, then, is to prevent sublimation, or at least reduce it to an acceptably low level. In preparation for an experiment on suppression of sublimation, a specimen of CoSb₃ was tightly wrapped in

a foil of niobium, which was selected for its chemical stability. In the experiment, the wrapped specimen was heated to a temperature of 700 °C in a vacuum of residual pressure $<10^{-5}$ torr (0.0013 Pa), then cooled and sectioned. Examination of the sectioned specimen revealed that no depletion layer had formed, indicating the niobium foil prevented sublimation of antimony at 700 °C. This was a considerable improvement, considering that uncoated CoSb₃ had been found to decompose to form the lowest antimonide at the surface at only 600 °C. Evidently, because the mean free path of Sb at the given temperature and pressure was of the order of tens of centimeters, any barrier closer than tens of centimeters (as was the niobium foil) would have suppressed transport of Sb vapor, thereby suppressing sublimation of Sb.



In a Powder-Metallurgy Process used to fabricate a segment of a thermoelectric device, the particles of thermoelectric material are sintered by heat and pressure, which is also exploited to bond the sintered mass to the outer layer of titanium foil.

Guided by the aforementioned experiments, a powder-metallurgy process for fabricating skutterudite was modified to provide for covering the outer surfaces

of the segments with titanium foils. In the unmodified process, the thermoelectric material, in powder form, is hot-pressed in a graphite die, then removed,

then further processed. The combination of high temperature and pressure in the die acts to promote bonding between particles, and as such, is ideal as a means of adding an adherent sublimation-suppressing outer layer. Hence, the process is modified by simply lining the inner wall of the die with a foil of the barrier material before filling the die with the thermoelectric powder (see figure).

In preparation for further experiments, the modified process was used to fabricate specimens of n- and p-type skutterudites covered with adherent 25- μm -thick foils of titanium. In the experiments, these specimens were heated in a vacuum under the same conditions as in the experiments described above, then sectioned and examined. Like the niobium foils in those experiments, the titanium foil outer layers in these experiments were found to have suppressed sublimation of Sb.

This work was done by Jeffrey Sakamoto, Thierry Caillat, Jean-Pierre Fleurial, and G. Jeffrey Snyder of Caltech for NASA's Jet Propulsion Laboratory. Further information is contained in a TSP (see page 1).

This invention is owned by NASA, and a patent application has been filed. Inquiries concerning nonexclusive or exclusive license for its commercial development should be addressed to the Patent Counsel, NASA Management Office-JPL. Refer to NPO-40040.

Ultrahigh-Temperature Ceramics

Materials are being developed to withstand temperatures above 1,650 °C.

Ames Research Center, Moffett Field, California

Ultrahigh temperature ceramics (UHTCs) are a class of materials that include the diborides of metals such as hafnium and zirconium. The materials are of interest to NASA for their potential utility as sharp leading edges for hypersonic vehicles. Such an application requires that the materials be capable of operating at temperatures, often in excess of 2,000 °C. UHTCs are highly refractory and have high thermal conductivity, an advantage for this application. UHTCs are potentially applicable for other high-temperature processing applications, such as crucibles for molten-metal processing and high-temperature electrodes.

UHTCs were first studied in the 1960's by the U.S. Air Force. NASA's Ames Research Center concentrated on developing materials in the HfB_2/SiC

family for a leading-edge application. The work focused on developing a process to make uniform monolithic (2-phase) materials, and on the testing and design of these materials. Figure 1 shows arc-jet models made from UHTC materials fabricated at Ames. Figure 2 shows a cone being tested in the arc-jet. Other variations of these materials being investigated elsewhere include zirconium-based materials and fiber-reinforced composites.

Current UHTC work at Ames covers four broad topics: monoliths, coatings, composites, and processing. The goals include improving the fracture toughness, thermal conductivity and oxidation resistance of monolithic UHTCs and developing oxidation-resistant UHTC coatings for thermal-protection-system sub-



strates through novel coating methods.

Figure 1. Examples of UHTC Components are shown that have been tested in the NASA Ames Arc Jet facility to evaluate the materials response in a simulated reentry environment. The cone and wedge models are representative of the scale and geometries anticipated for use on UHTC sharp leading-edge vehicles.



Figure 2. A UHTC Cone is shown during testing in the NASA Ames Arc Jet facility. Surface temperatures on the tip of the cone model exceeded 2,000°C during this test.

As part of this effort, researchers are exploring compositions and processing changes that have yielded improvements in properties. Computational materials science and nanotechnology are being explored as approaches to reduce materials development time and improve and tailor properties.

This work was done by Sylvia M. Johnson, Donald T. Ellerby, Sarah E. Beckman, and Edward Irby of Ames Research Center and Matthew J. Gasch and Michael I. Gusman of ELORET. Further information is contained in a TSP (see page 1).

Inquiries concerning rights for the commercial use of this invention should be addressed to the Ames Technology Partnerships Division at (650) 604-2954. Refer to ARC-15258-1.

Improved C/SiC Ceramic Composites Made Using PIP

These materials are expected to remain strong for longer times at high temperatures.

Marshall Space Flight Center, Alabama

Improved carbon-fiber-reinforced SiC ceramic-matrix composite (C/SiC CMC) materials, suitable for fabrication of thick-section structural components, are producible by use of a combination of raw materials and processing conditions different from such combinations used in the prior art. In comparison with prior C/SiC CMC materials, these materials have more nearly uniform density, less porosity, and greater strength. The majority of raw-material/processing-condition combinations used in the prior art involve the use of chemical vapor infiltration (CVI) for densifying the matrix.

In contrast, in synthesizing a material of the present type, one uses a combination of infiltration with, and pyrolysis of, a pre-ceramic polymer [polymer infiltration followed by pyrolysis (PIP)]. PIP processing

is performed in repeated, tailored cycles of infiltration followed by pyrolysis. Densification by PIP processing takes less time and costs less than does densification by CVI. When one of these improved materials was tested by exposure to a high-temperature, inert-gas environment that caused prior C/SiC CMCs to lose strength, this material did not lose strength. (Information on the temperature and exposure time was not available at the time of writing this article.)

A material of the present improved type consists, more specifically, of (1) carbon fibers coated with an engineered fiber/matrix interface material and (2) a ceramic matrix, containing SiC, derived from a pre-ceramic polymer with ceramic powder additions. The enhancements of properties of these materials relative to

those of prior C/SiC CMC materials are attributable largely to engineering of the fiber/matrix interfacial material and the densification process.

The synthesis of a material of this type includes processing at an elevated temperature to a low level of open porosity. The approach followed in this processing allows one to fabricate not only simple plates but also more complexly shaped parts. The carbon fiber reinforcement in a material of this type can be in any of several alternative forms, including tow, fabric, or complex preforms containing fibers oriented in multiple directions.

This work was done by Timothy Easler of COI Ceramics Inc. (an Affiliate of ATK Space Systems) for Marshall Space Flight Center. Further information is contained in a TSP (see page 1). Refer to MFS-32384-1.

Coating Carbon Fibers With Platinum

Uniform coats are produced relatively inexpensively.

Marshall Space Flight Center, Alabama

A process for coating carbon fibers with platinum has been developed. The process may also be adaptable to coating carbon fibers with other noble and refractory metals, including rhenium and iridium. The coated carbon fibers would be used as ingredients of matrix/fiber composite materials that would resist ox-

idation at high temperatures. The metal coats would contribute to oxidation resistance by keeping atmospheric oxygen away from fibers when cracks form in the matrices.

Other processes that have been used to coat carbon fibers with metals have significant disadvantages:

- Metal-vapor deposition processes yield coats that are nonuniform along both the lengths and the circumferences of the fibers.
- The electrical resistivities of carbon fibers are too high to be compatible with electrolytic processes.
- Metal/organic vapor deposition en-

tails the use of expensive starting materials, it may be necessary to use a furnace, and the starting materials and/or materials generated in the process may be hazardous.

The present process does not have these disadvantages. It yields uniform, nonporous coats and is relatively inexpensive.

The process can be summarized as one of pretreatment followed by electrodeless deposition. The process consists of the following steps:

- The surfaces of the fiber are activated

by deposition of palladium crystallites from a solution.

- The surface-activated fibers are immersed in a solution that contains platinum.
- A reducing agent is used to supply electrons to effect a chemical reduction *in situ*.

The chemical reduction displaces the platinum from the solution. The displaced platinum becomes deposited on the fibers. Each platinum atom that has been deposited acts as a catalytic site for the deposition of another platinum

atom. Hence, the deposition process can also be characterized as autocatalytic. The thickness of the deposited metal can be tailored via the duration of immersion and the chemical activity of the solution.

This work was done by Michael R. Effinger of Marshall Space Flight Center, Peter Duncan and Duncan Coupland of Johnson-Matthey Noble Metals, and Mark J. Rigali of Advanced Ceramics Research. Further information is contained in a TSP (see page 1).

MFS-32021



Two-Band, Low-Loss Microwave Window

Microwave loss is only about 0.4 percent.

NASA's Jet Propulsion Laboratory, Pasadena, California

A window for a high-sensitivity microwave receiving system allows microwave radiation to pass through to a cryogenically cooled microwave feed system in a vacuum chamber, while keeping ambient air out of the chamber and helping to keep the interior of the chamber cold. The microwave feed system comprises a feed horn and a low-noise amplifier, both of which are required to be cooled to a temperature of 15 K during operation. The window is designed

to exhibit very little microwave attenuation in two frequency bands: 8 to 9 GHz and 30 to 40 GHz.

The window is 15 cm in diameter. It includes three layers (see figure):

- The outer layer is made of a poly(tetrafluoroethylene) film 0.025 mm thick. This layer serves primarily to reflect and absorb solar ultraviolet radiation to prolong the life of the underlying main window layer, which is made of a polyimide that becomes weakened when exposed

to ultraviolet. The poly(tetrafluoroethylene) layer also protects the main window layer against abrasion. Moreover, the inherent hydrophobicity of poly(tetrafluoroethylene) helps to prevent the highly undesirable accumulation of water on the outer surface.

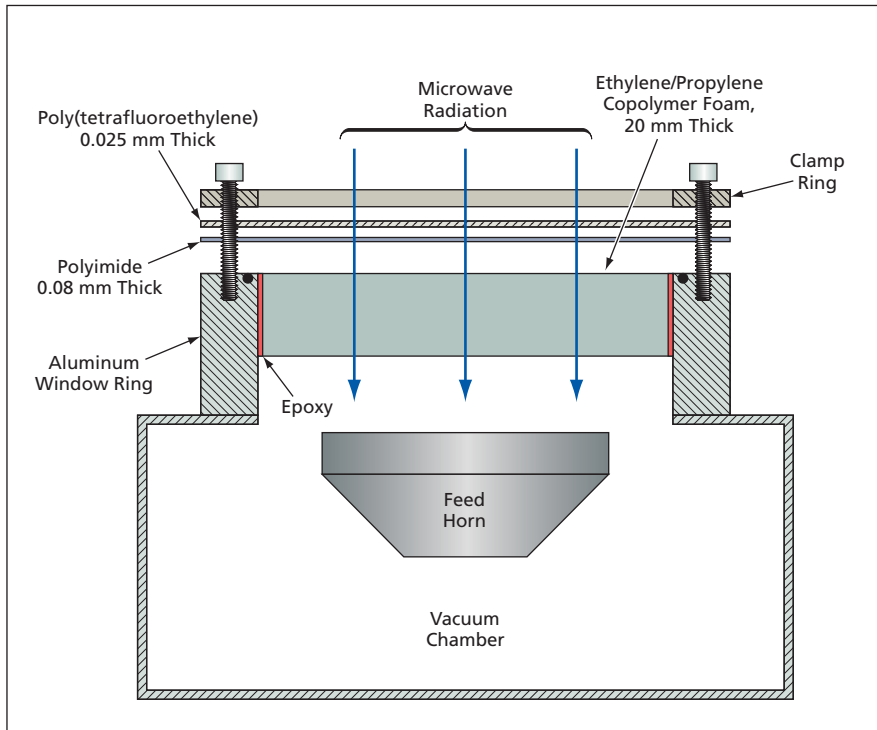
- The polyimide main window layer is 0.08 mm thick. This layer provides the vacuum seal for the window.
- A 20-mm-thick layer of ethylene/propylene copolymer foam underlies the main polyimide window layer. This foam layer acts partly as a thermal insulator: it limits radiational heating of the microwave feed horn and, concomitantly, limits radiational cooling of the window. This layer has high compressive strength and provides some mechanical support for the main window layer, reducing the strength required of the main window layer.

The ethylene/propylene copolymer foam layer is attached to an aluminum window ring by means of epoxy. The outer poly(tetrafluoroethylene) film and the main polyimide window layer are sandwiched together and pressed against the window ring by use of a bolted clamp ring.

The window has been found to introduce a microwave loss of only about 0.4 percent. The contribution of the window to the noise temperature of the microwave feed system has been found to be less than 1 K at 32 GHz and 0.2 K at 8.4 GHz.

This work was done by Michael Britcliffe and Manuel Franco of Caltech for NASA's Jet Propulsion Laboratory. Further information is contained in a TSP (see page 1).

NPO-40846



This Low-Loss Microwave Window is made from commercially available materials and is relatively inexpensive.

MCM Polarimetric Radiometers for Planar Arrays

In mass production, these would cost less than do traditional polarimetric radiometers.

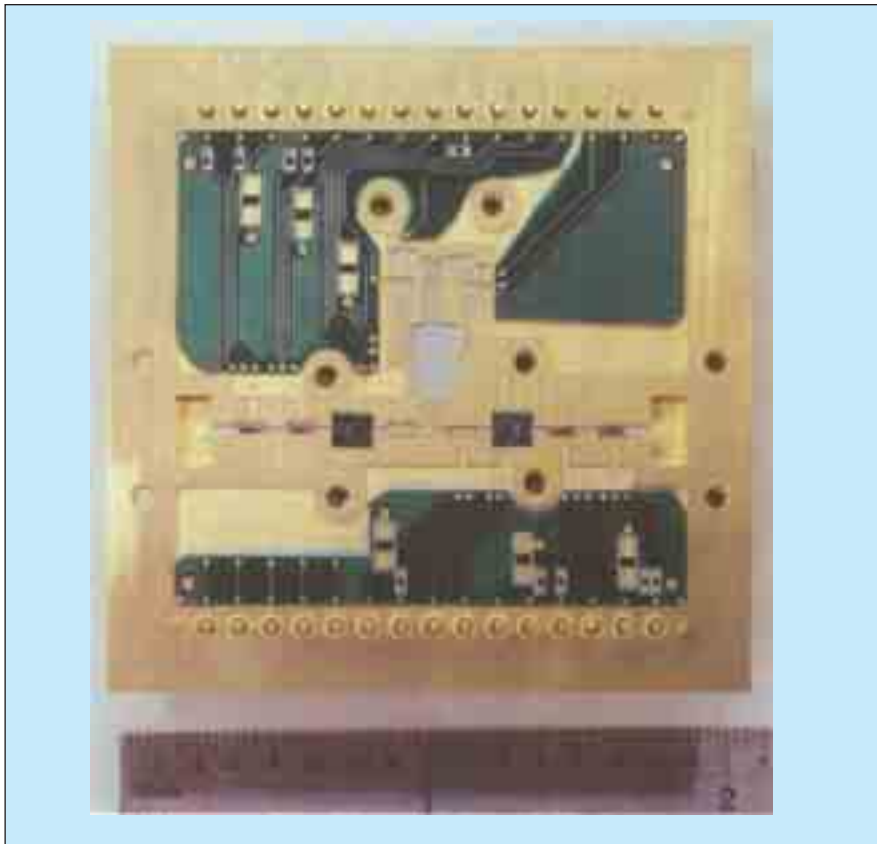
NASA's Jet Propulsion Laboratory, Pasadena, California

A polarimetric radiometer that operates at a frequency of 40 GHz has been designed and built as a prototype of multiple identical units that could be arranged in a planar array for scientific

measurements. Such an array is planned for use in studying the cosmic microwave background (CMB).

All of the subsystems and components of this polarimetric radiometer are inte-

grated into a single multi-chip module (MCM) of substantially planar geometry. In comparison with traditional designs of polarimetric radiometers, the MCM design is expected to greatly reduce the



The MCM performs all the microwave functions (other than initial reception and orthomode transduction) of a polarimetric microwave radiometer.

cost per unit in an array of many such units.

The design of the unit is dictated partly by a requirement, in the planned CMB application, to measure the Stokes parameters I , Q , and U of the CMB radiation with high sensitivity. (A complete definition of the Stokes pa-

rameters would exceed the scope of this article. In necessarily oversimplified terms, I is a measure of total intensity of radiation, while Q and U are measures of the relationships between the horizontally and vertically polarized components of radiation.) Because the sensitivity of a single polarimeter cannot be

increased significantly, the only way to satisfy the high-sensitivity requirement is to make a large array of polarimeters that operate in parallel.

The MCM includes contact pins that can be plugged into receptacles on a standard printed-circuit board (PCB). All of the required microwave functionality is implemented within the MCM; any required supporting non-microwave ("back-end") electronic functionality, including the provision of DC bias and control signals, can be implemented by standard PCB techniques.

On the way from a microwave antenna to the MCM, the incoming microwave signal passes through an orthomode transducer (OMT), which splits the radiation into an $h + iv$ beam and an $h - iv$ beam (where, using complex-number notation, h denotes the horizontal component, v denotes the vertical component, and $\pm i$ denotes a $\pm 90^\circ$ phase shift). Each of these beams enters the MCM through one of two WR-22 waveguide input terminals in the lid of the MCM. The $h + iv$ and $h - iv$ signals are amplified, then fed to a phase-discriminator hybrid designed specifically to fit the predominantly planar character of the MCM geometry and to enable determination of Q and U . The phase-discriminator hybrid generates four outputs, which are detected and used to calculate I , Q , and U .

*This work was done by Pekka Kangaslahti, Douglas Dawson, and Todd Gaier of Caltech for NASA's Jet Propulsion Laboratory. Further information is contained in a TSP (see page 1).
NPO-41335*

Aperture-Coupled Thin-Membrane L-Band Antenna

Two- and one-membrane designs offer advantages over prior three-membrane designs.

NASA's Jet Propulsion Laboratory, Pasadena, California

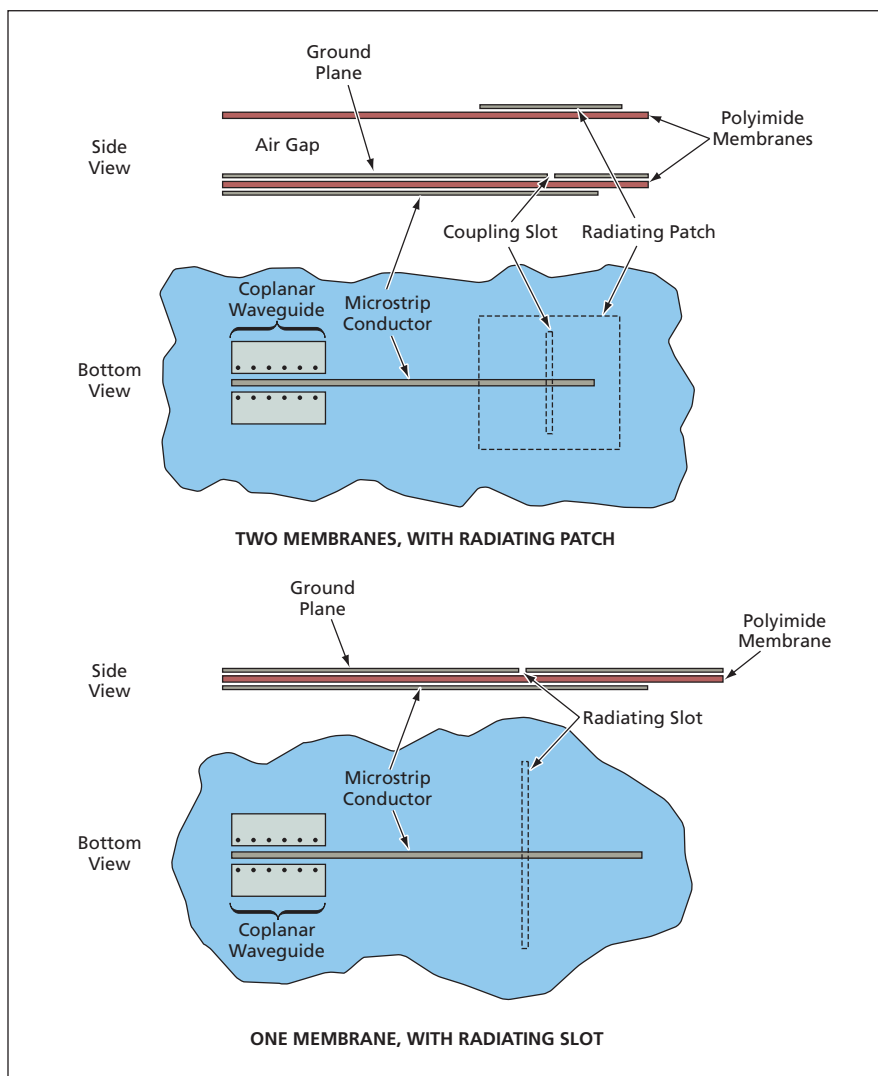
The upper part of the figure depicts an aperture-coupled L-band antenna comprising patterned metal conductor films supported on two thin polyimide membranes separated by an air gap. In this antenna, power is coupled from a microstrip line on the lower surface of the lower membrane, through a slot in a metal ground plane on the upper surface of the lower membrane, to a radiating metal patch on the upper surface of the upper membrane.

The two-membrane configuration of this antenna stands in contrast to a

three-membrane configuration heretofore considered as the basis for developing arrays of dual-polarization, wide-band microwave antennas that could be thin and could be, variously, incorporated into, or supported on, thin structures, including inflatable structures. By reducing the number of membranes from three to two, the present design simplifies the problems of designing and fabricating such antennas or arrays of such antennas, including the problems of integrating such antennas or arrays with thin-membrane-mounted trans-

mit/receive modules. In addition, the use of aperture (slot) coupling eliminates the need for rigid coaxial feed pins and associated solder connections on thin membranes, making this antenna more mechanically reliable, relative to antennas that include coaxial feed pins.

This antenna is designed for a nominal frequency of 1.26 GHz. The polyimide membranes are 0.05 mm thick and have a relative permittivity of 3.4. The radiating patch is square, 8.89 cm on each side. This radiating patch lies 1.27 cm above the ground plane. The feeding mi-



Aperture (Slot) Coupling is utilized in two- and one-membrane designs that are amenable to incorporation into thin structures and to integration with membrane-supported transmit/receive modules.

crostrip line is 0.12 mm wide and has a characteristic impedance of 50 Ω . The aperture-coupling slot, etched in the ground plane, is 0.48 mm wide and 79.5 mm long. In order to maximize coupling, the microstrip line is extended beyond the middle of the slot by a length of 36 mm, which corresponds to a transmission-line electrical length of about a quarter wavelength. The other end of the microstrip line is transformed to a 50- Ω coplanar waveguide line, which is used for connection to a transmit/receive module. Some plated-through vias are added to the outer conductors of the coplanar waveguide to suppress parallel-plate modes. The measured and calculated 10-dB-return-loss bandwidth of the antenna is 100 MHz.

By eliminating the radiating patch and the upper membrane that supports it, and performing two other simple modifications, one can convert the two-membrane antenna described above to a paper-thin single-membrane antenna, shown in the lower part of the figure. One modification is to increase the slot length to 104.95 mm; the other is to extend the microstrip to 36.68 mm past the middle of the slot. With these modifications, the slot now becomes a half-wavelength radiator with a nearly omnidirectional radiation pattern. In one potential use, such a paper-thin antenna could be pasted on an automobile window to enable omnidirectional communication.

This work was done by John Huang of Caltech for NASA's Jet Propulsion Laboratory. For further information contact iaoffice@jpl.nasa.gov. NPO-41416

WGM-Based Photonic Local Oscillators and Modulators

Efficient devices for detecting low-power terahertz radiation are proposed.

NASA's Jet Propulsion Laboratory, Pasadena, California

Photonic local oscillators and modulators that include whispering-gallery-mode (WGM) optical resonators have been proposed as power-efficient devices for generating and detecting radiation at frequencies of the order of a terahertz. These devices are intended especially to satisfy anticipated needs for receivers capable of detecting low-power, narrow-band terahertz signals to be used for sensing substances of interest in scientific and military applications. At present, available terahertz-signal detectors are power-inefficient and do not afford the spectral and ampli-

tude resolution needed for detecting such signals.

The proposed devices would not be designed according to the conventional approach of direct detection of terahertz radiation. Instead, terahertz radiation would first be up-converted into the optical domain, wherein signals could be processed efficiently by photonic means and detected by optical photodetectors, which are more efficient than are photodetectors used in conventional direct detection of terahertz radiation. The photonic devices used to effect the up-conversion would include a tunable

optical local oscillator and a novel electro-optical modulator.

A local oscillator according to the proposal would be a WGM-based mode-locked laser operating at a desired pulse-repetition rate of the order of a terahertz. The oscillator would include a terahertz optical filter based on a WGM microresonator, a fiber-optic delay line, an optical amplifier (which could be either a semiconductor optical amplifier or an erbium-doped optical fiber amplifier), and a WGM Ka-band modulator (see figure). The terahertz repetition rate would be obtained through har-

monic mode locking: for example, by modulating the light at a frequency of 33 GHz and locking each 33d optical mode, one would create a 1.089-THz pulse train. The high resonance quality factors (Q values) of WGM optical resonators should make it possible to decrease signal-generation threshold power levels significantly below those of other optical-signal-generation devices.

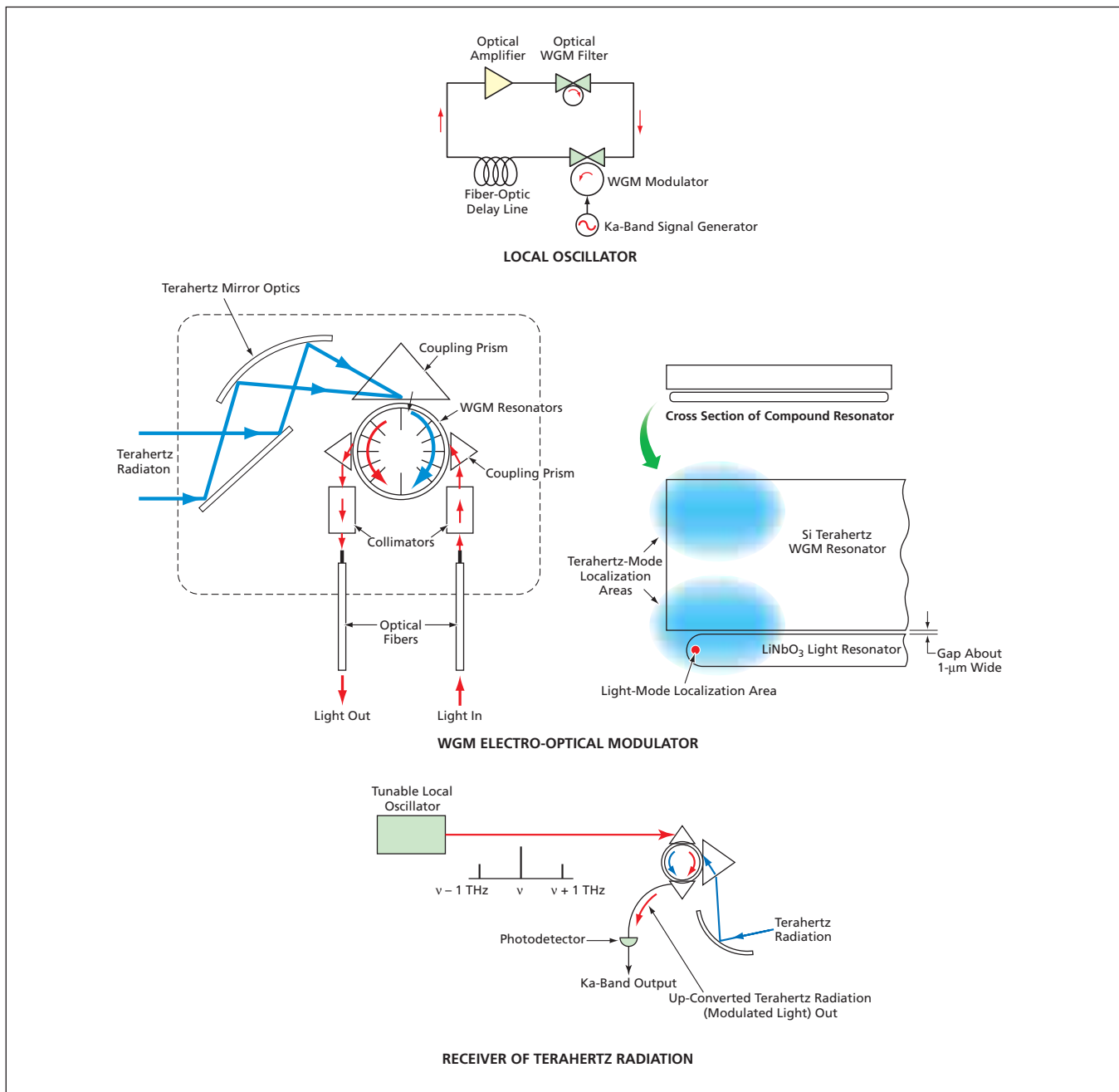
An electro-optical modulator as proposed would be a triply resonant compound WGM device. The modulator would comprise a periodically poled LiNbO_3 WGM optical resonator stacked almost in contact with an Si

WGM terahertz resonator. It would be necessary to use these two resonators because LiNbO_3 would afford the needed combination of high Q for the optical modes and enough nonlinearity for efficient interaction between light and terahertz radiation, while Si would afford the needed high Q for terahertz radiation.

Because Si absorbs light, it would be necessary to minimize penetration of light into the Si resonator. Because LiNbO_3 absorbs terahertz radiation more than Si does, the portion of the LiNbO_3 volume wherein the light and the terahertz radiation interact should be less

than the volume of the terahertz mode. These requirements would be satisfied by, among other things, positioning the two resonators with a gap of $\approx 1 \mu\text{m}$ between them and utilizing evanescent-field coupling between the light and the terahertz radiation. The periodicity of the poling of the LiNbO_3 would be chosen to ensure the required matching of phases between the light and the terahertz radiation.

This work was done by Andrey Matsko, Lute Maleki, Vladimir Ilchenko, and Anatoly Savchenkov of Caltech for NASA's Jet Propulsion Laboratory. Further information is contained in a TSP (see page 1). NPO-41139



A WGM-Based Local Oscillator and Electro-Optical Modulator would be components of a photonic receiver for detecting terahertz radiation.

Focal-Plane Arrays of Quantum-Dot Infrared Photodetectors

Electron-beam lithography would be used to make arrays sufficiently uniform.

NASA's Jet Propulsion Laboratory, Pasadena, California

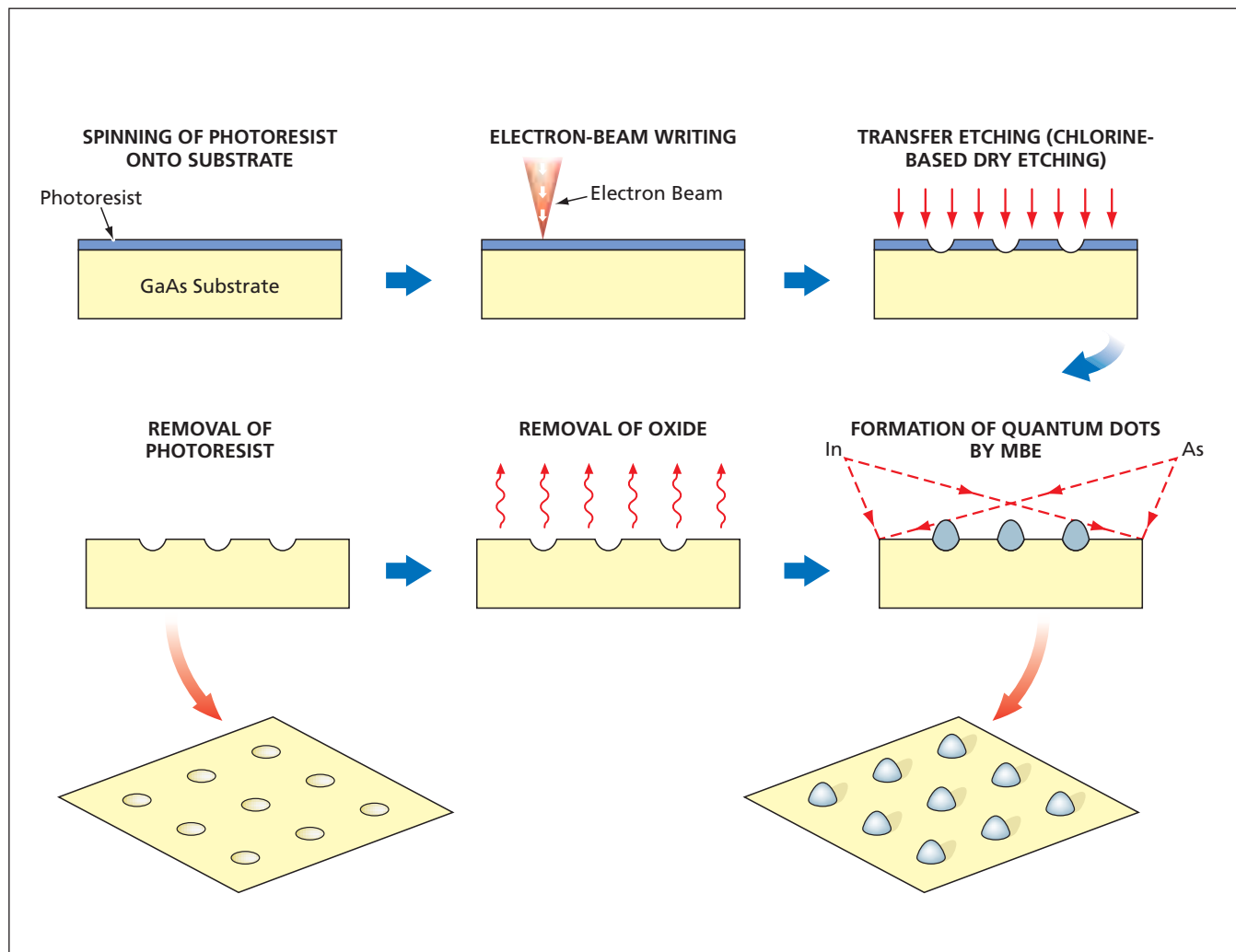
Focal-plane arrays of semiconductor quantum-dot infrared photodetectors (QDIPs) are being developed as superior alternatives to prior infrared imagers, including imagers based on HgCdTe devices and, especially, those based on quantum-well infrared photodetectors (QWIPs). HgCdTe devices and arrays thereof are difficult to fabricate and operate, and they exhibit large nonuniformities and high $1/f$ (where f signifies frequency) noise. QWIPs are easier to fabricate and operate, can be made nearly uniform, and exhibit lower $1/f$ noise, but they exhibit larger dark currents, and their quantization only along the growth direction prevents them from absorbing photons at normal incidence, thereby limiting their quantum efficiencies. Like QWIPs,

QDIPs offer the advantages of greater ease of operation, greater uniformity, and lower $1/f$ noise, but without the disadvantages: QDIPs exhibit lower dark currents, and quantum efficiencies of QDIPs are greater because the three-dimensional quantization of QDIPs is favorable to the absorption of photons at normal or oblique incidence. Moreover, QDIPs can be operated at higher temperatures (around 200 K) than are required for operation of QWIPs.

The main problem in the development of QDIP imagers is to fabricate quantum dots with the requisite uniformity of size and spacing. A promising approach to be tested soon involves the use of electron-beam lithography to define the locations and sizes of

quantum dots (see figure). A photoresist-covered GaAs substrate would be exposed to the beam generated by an advanced, high-precision electron-beam apparatus. The exposure pattern would consist of spots typically having a diameter of 4 nm and typically spaced 20 nm apart.

The exposed photoresist would be developed by either a high-contrast or a low-contrast method. In the high-contrast method, the spots would be etched in such a way as to form steep-wall holes all the way down to the substrate. The holes would be wider than the electron-beam spots — perhaps as wide as 15 to 20 nm, but may be sufficient to control the growth of the quantum dots. In the low-contrast method, the resist would be etched in such a way as to form dimples,



Electron-Beam Lithography and Molecular-Beam Epitaxy would be used to grow quantum dots with a relatively high degree of uniformity in size and spacing.

the shapes of which would mimic the electron-beam density profile. Then by use of a transfer etching process that etches the substrate faster than it etches the resist, either the pattern of holes or a pattern comprising the narrow, lowest portions of the dimples would be imparted to the substrate. Having been

thus patterned, the substrate would be cleaned. The resulting holes or dimples in the substrate would serve as nucleation sites for the growth of quantum dots of controlled size in the following steps. The substrate would be cleaned, then placed in a molecular-beam-epitaxy (MBE) chamber, where native

oxide would be thermally desorbed and the quantum dots would be grown.

This work was done by Sarath Gunapala, Daniel Wilson, Cory Hill, John Liu, Sumith Bandara, and David Ting of Caltech for NASA's Jet Propulsion Laboratory. Further information is contained in a TSP (see page 1). NPO-41236

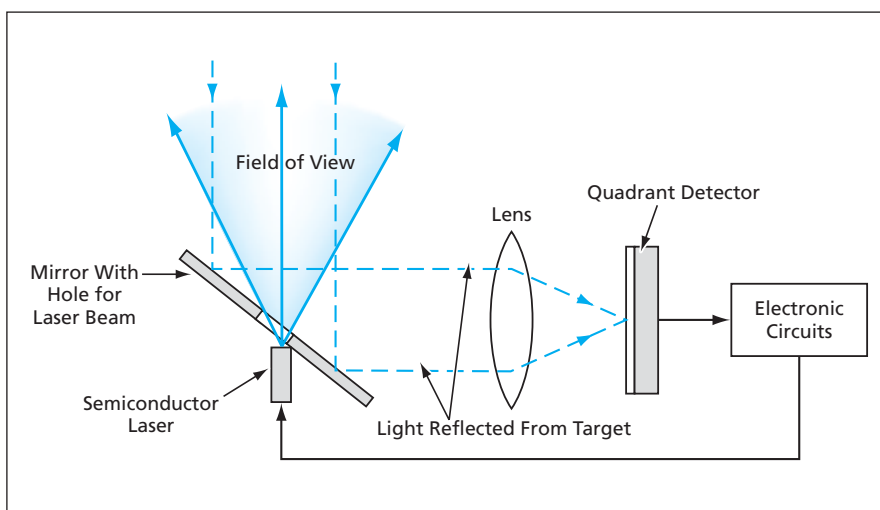
Laser Range and Bearing Finder With No Moving Parts

This instrument would locate a nearby target, without scanning.

Marshall Space Flight Center, Alabama

A proposed laser-based instrument would quickly measure the approximate distance and approximate direction to the closest target within its field of view. The instrument would not contain any moving parts and its mode of operation would not entail scanning over of its field of view. Typically, the instrument would be used to locate a target at a distance on the order of meters to kilometers. The instrument would be best suited for use in an uncluttered setting in which the target is the only or, at worst, the closest object in the vicinity; for example, it could be used aboard an aircraft to detect and track another aircraft flying nearby.

The proposed instrument would include a conventional time-of-flight or echo-phase-shift laser range finder, but unlike most other range finders, this one would not generate a narrow cylindrical laser beam; instead, it would generate a conical laser beam spanning the field of view (see figure). The instrument would also include a quadrant detector, optics to focus the light returning from the target onto the quadrant detector, and circuitry to synchronize the acquisition of the quadrant-detector output with the arrival of laser light returning from the



An Unusually Wide-Beam Laser Range Finder would be combined with a quadrant detector so that the distance and direction to a target could be measured simultaneously.

nearest target. A quadrant detector constantly gathers information from the entire field of view, without scanning; its output is a direct measure of the position of the target-return light spot on the focal plane and is thus a measure of the direction to the target.

The instrument should be able to operate at a repetition rate high enough to enable it to track a rapidly moving tar-

get. Of course, a target that is not sufficiently reflective could not be located by this instrument. Preferably, retroreflectors should be attached to the target to make it sufficiently reflective.

This work was done by Thomas C. Bryan, Richard T. Howard, and Michael L. Book of Marshall Space Flight Center. Further information is contained in a TSP (see page 1). MFS-31705

Microrectenna: A Terahertz Antenna and Rectifier on a Chip

Microscopic rectennas would supply DC power to microdevices.

NASA's Jet Propulsion Laboratory, Pasadena, California

A microrectenna that would operate at a frequency of 2.5 THz has been designed and partially fabricated. The circuit is intended to be a prototype of an extremely compact device that could be used to convert radio-beamed power to DC to drive microdevices (see Figure 1).

The microrectenna (see Figure 2) circuit consists of an antenna, a diode rectifier and a DC output port. The antenna consists of a twin slot array in a conducting ground plane (denoted the antenna ground plane) over an enclosed quarter-wavelength-thick resonant cavity (de-

noted the reflecting ground plane). The circuit also contains a planar high-frequency low-parasitic Schottky-barrier diode, a low-impedance microstrip transmission line, capacitors, and contact beam leads. The entire 3-D circuit is fabricated monolithically from a single



Figure 1. A Synthetic Image of the Microrectenna described in the text is here superimposed, to scale, on a real scanning electron micrograph of an insectlike microrobot. The underlying idea is to use the microrectenna to convert power from an incident 2.5-GHz radio beam to drive the robot and/or to charge its microbattery.

GaAs wafer. The resonant cavity renders the slot radiation pattern unidirectional with a half-power beam width of about 65°. A unique metal mesh on the rear of the wafer forms the backplate for the cavity but allows the GaAs to be wet etched from the rear surface of the twin slot antennas and ground plane. The beam leads protrude past the edge of the chip and are used both to mount the microrectenna and to make the DC electrical connection with external circuitry. The antenna ground plane and the components on top of it are formed on a 2- μm thick GaAs membrane that is grown in the initial wafer MBE (molecular beam epitaxy) process. The side walls of the antenna cavity are not metal coated and, hence, would cause some loss of power; however, the relatively high permittivity ($\epsilon=13$) of the GaAs keeps the cavity modes well confined, without the usual surface-wave losses associated with thick dielectric substrates.

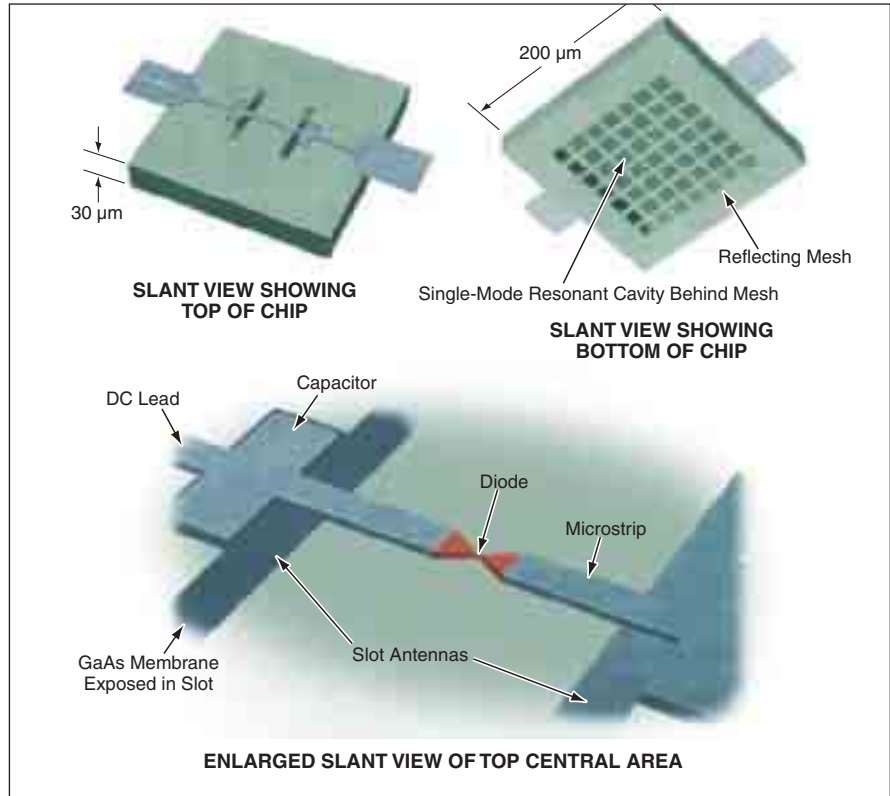


Figure 2. All RF and DC Components of the microrectenna would be fabricated together on a single GaAs chip.

The Schottky-barrier diode has the usual submicron dimensions associated with THz operation and is formed in a mesa process above the antenna ground plane. The diode is connected at the midpoint of a microstrip transmission line, which is formed on 1- μm -thick SiO (permittivity of 5) laid down on top of the GaAs membrane. The twin slots are fed in phase by this structure. To prevent radio-frequency (RF) leakage past the slot antennas, low-loss capacitors are integrated into the microstrip transmission line at the edges of the slots. The DC current-carrying lines extend from the outer

edges of the capacitors, widen approaching the edges of the chip, and continue past the edges of the chip to become the beam leads used in tacking down the devices. The structure provides a self-contained RF to DC converter that works in the THz range.

This work was done by Peter Siegel of Caltech for NASA's Jet Propulsion Laboratory.

This invention is owned by NASA, and a patent application has been filed. Inquiries concerning nonexclusive or exclusive license for its commercial development should be addressed to the Patent Counsel, NASA Management Office-JPL. Refer to NPO-30478.

Miniature L-Band Radar Transceiver

Numerous interdependent considerations are reflected in a compact, low-power, radiation-hard design.

NASA's Jet Propulsion Laboratory, Pasadena, California

A miniature L-band transceiver that operates at a carrier frequency of 1.25 GHz has been developed as part of a generic radar electronics module (REM) that would constitute one unit in an array of many identical units in a very-large-aperture phased-array antenna. NASA and the Department of Defense are considering the deploy-

ment of such antennas in outer space; the underlying principles of operation, and some of those of design, also are applicable on Earth. The large dimensions of the antennas make it advantageous to distribute radio-frequency electronic circuitry into elements of the arrays. The design of the REM is intended to implement the distribution.

The design also reflects a requirement to minimize the size and weight of the circuitry in order to minimize the weight of any such antenna. Other requirements include making the transceiver robust and radiation-hard and minimizing power demand.

Figure 1 depicts the functional blocks of the REM, including the L-band trans-

ceiver. The key functions of the REM include signal generation, frequency translation, amplification, detection, handling of data, and radar control and timing. An arbitrary-waveform generator that includes logic circuitry and a digital-to-analog converter (DAC) generates a linear-frequency-modulation chirp waveform. A frequency synthesizer produces local-oscillator signals used for frequency conversion and clock signals for the arbitrary-waveform generator, for a digitizer [that is, an analog-to-digital converter (ADC)], and for a control and timing unit. Digital functions include command, timing, telemetry, filtering, and high-rate framing and serialization of data for a high-speed scientific-data interface.

The aforementioned digital implementation of filtering is a key feature of the REM architecture. Digital filters, in contradistinction to analog ones, provide consistent and temperature-independent performance, which is particularly important when REMs are distributed throughout a large array. Digital filtering also enables selection among multiple filter parameters as required for different radar operating modes. After digital filtering, data are decimated appropriately in order to minimize the data rate out of an antenna panel.

The L-band transceiver (see Figure 2) includes a radio-frequency (RF)-to-baseband down-converter chain and an intermediate-frequency (IF)-to-RF up-con-

verter chain. Transmit/receive (T/R) switches enable the use of a single feed to the antenna for both transmission and reception. The T/R switches also afford a built-in test capability by enabling injection of a calibration signal into the receiver chain. In order of decreasing priority, components of the transceiver were selected according to requirements of radiation hardness, then compactness, then low power. All of the RF components are radiation-hard. The noise figure (NF) was optimized to the extent that (1) a low-noise amplifier (LNA) (characterized by $NF < 2$ dB) was selected but (2) the receiver front-end T/R switches were selected for a high degree of isolation and acceptably low loss, regardless of the requirement to minimize noise.

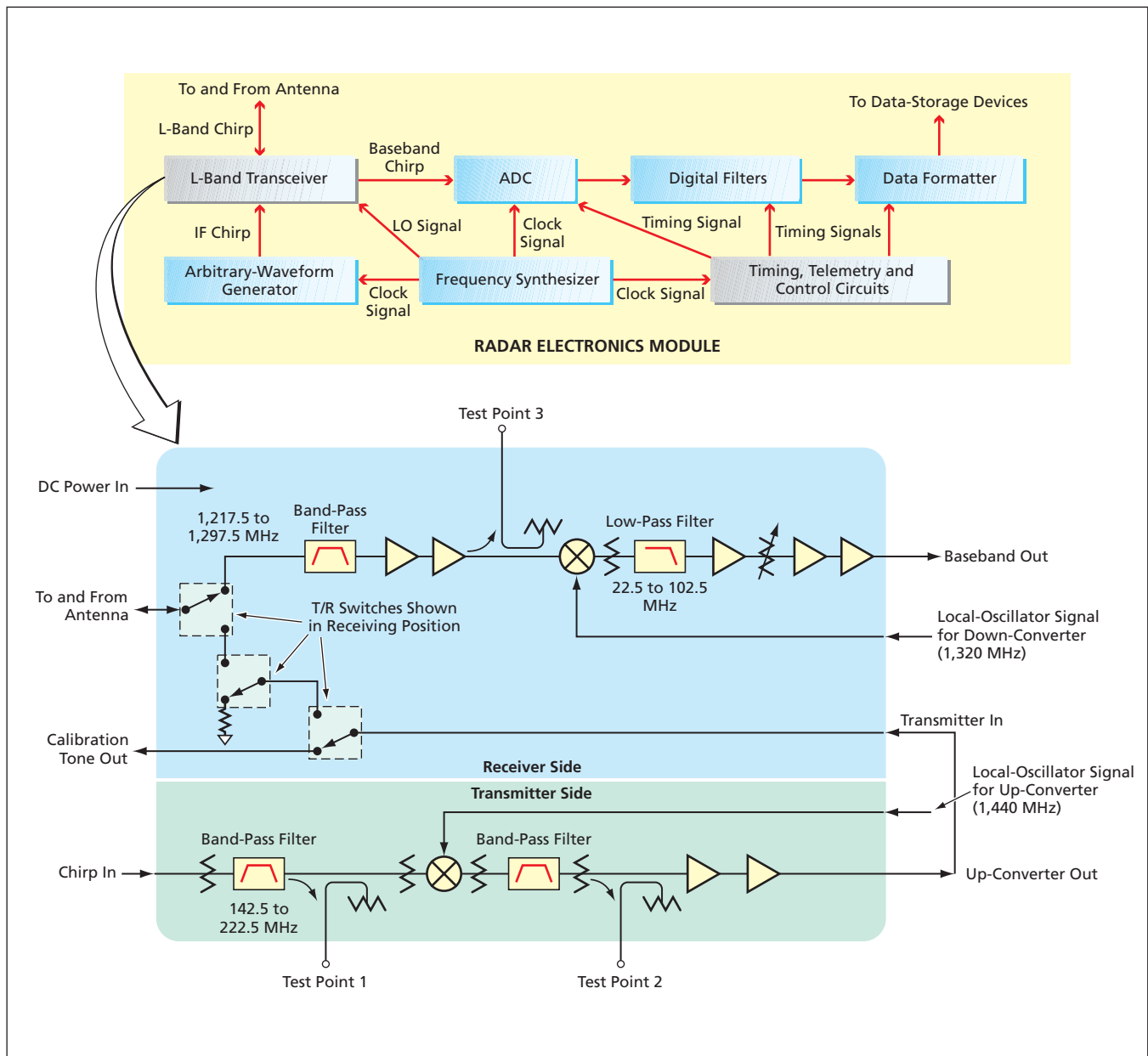


Figure 1. The Radar Electronics Module contains the miniature L-band transceiver.

The filter specifications were chosen to minimize the sizes of the filters, thereby placing the baseband higher in frequency than would otherwise be necessary. This is an acceptable trade-off inasmuch as (1) the consequent requisite digitizer bandwidth is still realizable by use of commercial devices and (2) the decimation performed by the digital filters eliminates excess bandwidth. The receiver band-pass filter (BPF) is placed in front of the LNA in order to limit radio-frequency interference. A programmable attenuator is included to provide adequate dynamic range in the event that the amplitude of the radar echo varies significantly. Care was taken to minimize cost by minimizing the number of parts and the number of different types of parts: in particular, the amplifiers and mixer used in the up-converter are also used in the down-converter.

The packaging of the L-band transceiver was designed in recognition that the different types of electronic devices used must be mounted and connected in different ways. The packaging approach was to place circuits that perform different functions in separate cavities in the module housing, coupling the DC signals through the walls by use of filtered connections only. This ap-

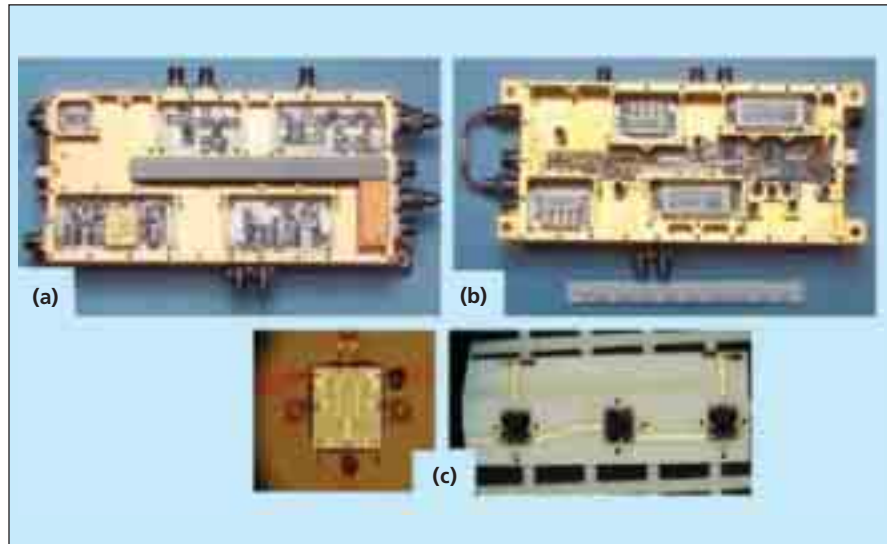


Figure 2. The Uncovered L-Band Transceiver Module shows the following: (a) top view (active components), (b) bottom view (filters and control), and (c) close-up views of packaging of individual switch die circuitry.

proach provides shielding from noise leakage. Thus, the down-converter (receiver) chain, the up-converter (transmitting) chain, and the control and power-supply circuitry are each located in separate cavities of the housing. The active RF components (e.g., amplifiers) are on one side of the module, while the passive RF components (e.g., attenuators and filters) and the control and

power circuits are on the opposite side. The RF functional blocks are further separated, according to frequency, onto individual substrates and into individual cavities.

This work was done by Dalia McWatters, Douglas Price, and Wendy Edelstein of Caltech for NASA's Jet Propulsion Laboratory. For more information, contact iaoffice@jpl.nasa.gov. NPO-41278

Robotic Vision-Based Localization in an Urban Environment

A probability distribution of location is superimposed on an approximate map.

NASA's Jet Propulsion Laboratory, Pasadena, California

A system of electronic hardware and software, now undergoing development, automatically estimates the location of a robotic land vehicle in an urban environment using a somewhat imprecise map, which has been generated in advance from aerial imagery. This system does not utilize the Global Positioning System and does not include any odometry, inertial measurement units, or any other sensors except a stereoscopic pair of black-and-white digital video cameras mounted on the vehicle. Of course, the system also includes a computer running software that processes the video image data.

The software consists mostly of three components corresponding to the three major image-data-processing functions:

- *Visual Odometry*

This component automatically tracks point features in the imagery and computes the relative motion of the cam-

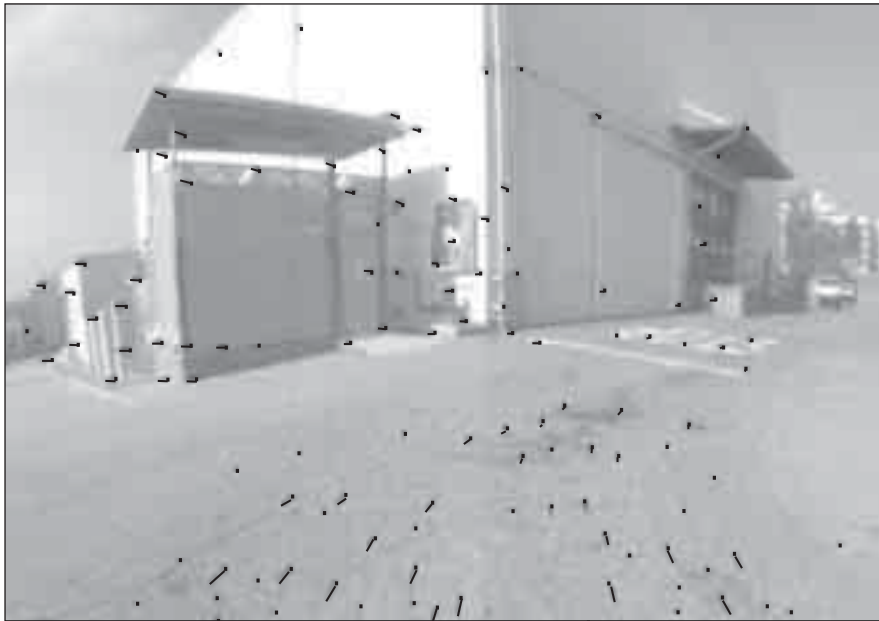
eras between sequential image frames. This component incorporates a modified version of a visual-odometry algorithm originally published in 1989. The algorithm selects point features, performs multiresolution area-correlation computations to match the features in stereoscopic images, tracks the features through the sequence of images, and uses the tracking results to estimate the six-degree-of-freedom motion of the camera between consecutive stereoscopic pairs of images (see figure).

- *Urban Feature Detection and Ranging*

Using the same data as those processed by the visual-odometry component, this component strives to determine the three-dimensional (3D) coordinates of vertical and horizontal lines that are likely to be parts of, or close to, the exterior surfaces of buildings. The basic sequence of processes performed by this component is the

following:

1. An edge-detection algorithm is applied, yielding a set of linked lists of edge pixels, a horizontal-gradient image, and a vertical-gradient image.
2. Straight-line segments of edges are extracted from the linked lists generated in step 1. Any straight-line segments longer than an arbitrary threshold (e.g., 30 pixels) are assumed to belong to buildings or other artificial objects.
3. A gradient-filter algorithm is used to test straight-line segments longer than the threshold to determine whether they represent edges of natural or artificial objects. In somewhat oversimplified terms, the test is based on the assumption that the gradient of image intensity varies little along a segment that represents the edge of an artificial object.



In this Example Showing Features Used in Visual Odometry, black lines superimposed on the image represent vectors proportional to displacement of features between sequential images.

4. A roof-line-detection algorithm identifies, as candidate roof lines, line segments (a) that exceed a threshold length and (b) above which there are no other such lines.
5. The 3D positions of line segments detected in the preceding steps are computed from either (a) ordinary stereoscopic imagery acquired simultaneously by the two cameras or (b) wide-baseline stereoscopic imagery synthesized from imagery acquired in two successive frames, using relative camera positions determined by visual odometry. The choice between (a) and (b) is made on the basis of which, given certain

parameters of the viewing geometry, is expected to enable a more accurate triangulation.

6. A heuristic pruning algorithm filters the remaining line segments: All lines that are not approximately vertical or horizontal are discarded, horizontal lines longer than 2 m are selected, vertical lines that extend above 2 m are selected, and sets of parallel lines are selected.

- *Particle-Filter-Based Localization*

The outputs of the visual-odometry and urban-feature-detection-and-ranging components are fed to this component, which implements a particle-filter-based localization algorithm. In

the theory of particle-filter-based robot localization, the key notion is that a particle filter produces an approximate probability density function for the position and heading of a robot by use of Monte Carlo techniques. This theory makes it possible to incorporate knowledge of measurement uncertainty in a rigorous manner. Because the open source particle-filter-based localization software (developed by Prof. Sebastian Thrun of Stanford University) used in a prototype of the system is based on a planar model, the input data fed to this component are preprocessed into simulated single-axis range data (in effect, simulated LIDAR range data) by projecting all 3D features onto a horizontal plane and sampling the field of view at small angular intervals (1°).

Notwithstanding the oversimplification inherent in this approach, success in localization has been achieved in initial experiments.

This work was done by Michael McHenry, Yang Cheng, and Larry Matthies of Caltech for NASA's Jet Propulsion Laboratory.

In accordance with Public Law 96-517, the contractor has elected to retain title to this invention. Inquiries concerning rights for its commercial use should be addressed to:

*Innovative Technology Assets Management
JPL*

*Mail Stop 202-233
4800 Oak Grove Drive
Pasadena, CA 91109-8099
(818) 354-2240*

E-mail: iaoffice@jpl.nasa.gov

Refer to NPO-41881, volume and number of this NASA Tech Briefs issue, and the page number.

Programs for Testing an SSME-Monitoring System

Marshall Space Flight Center, Alabama

A suite of computer programs has been developed for special test equipment (STE) that is used in verification testing of the Health Management Computer Integrated Rack Assembly (HMC-IRA), a ground-based system of analog and digital electronic hardware and software for "flight-like" testing for development of components of an advanced health-management system for the space shuttle main engine (SSME). HMC-IRA units are designed to be integrated into a test facility wherein they enable additional engine monitoring during SSME

hot-fire tests. Running on a control processor that is part of the STE, the STE software enables the STE to simulate the SSME Controller, the SSME itself, and interfaces between the SSME and the HMC-IRA.

The STE software enables the STE to simulate the analog input and the data flow of an SSME test firing from start to finish. The STE software also provides user interfaces, error injection, data storage, and board-level test routines. Accompanying the STE software is a suite of post-processing programs that

convert stored data from the HMC-IRA and STE to readable textual and graphical formats, extract timing and statistical data, and provide for calibration of analog circuit cards.

*These programs were written by Andre Lang, Jimmie Cecil, Ralph Heusinger, Kathleen Freestone, Lisa Blue, DeLisa Wilkerson, Leigh Anne McMahon, Richard B. Hall, Kosta Varnavas, Keary Smith, and Donna Kaukler of Marshall Space Flight Center and James Hall of Sverdrup Technology, Inc. Further information is contained in a TSP (see page 1).
MFS-32385-1.*

Cathodoluminescent Source of Intense White Light

This device is expected to have a long operational lifetime.

John H. Glenn Research Center, Cleveland, Ohio

The device shown in the figure exploits cathodoluminescence to generate intense light in the visible and near-infrared regions of the spectrum. This device is suitable for use as a source of white light for general illumination or microscopy or as a broad-band light

source for spectroscopy. Unlike incandescent lamps, which typically contain hot filaments, or high-pressure-gas electric-discharge lamps, this device would operate without exposing any of its components to high temperatures. Consequently, the lifetime of this device is ex-

pected to be considerably longer than the lifetimes of the aforementioned other light sources.

In general, cathodoluminescence occurs when a covalent or ionic material is exposed to a flux of energetic electrons. The emission of light is feeble when the kinetic energy of the incident electrons is low. One could increase the emission of light significantly by accelerating electrons to high kinetic energy (necessitating the use of high accelerating voltage). Alternatively, one could increase the luminescence by using moderately energetic electrons and taking measures to channel the electron flux appropriately. As described below, this alternative approach is taken in the design of the present device.

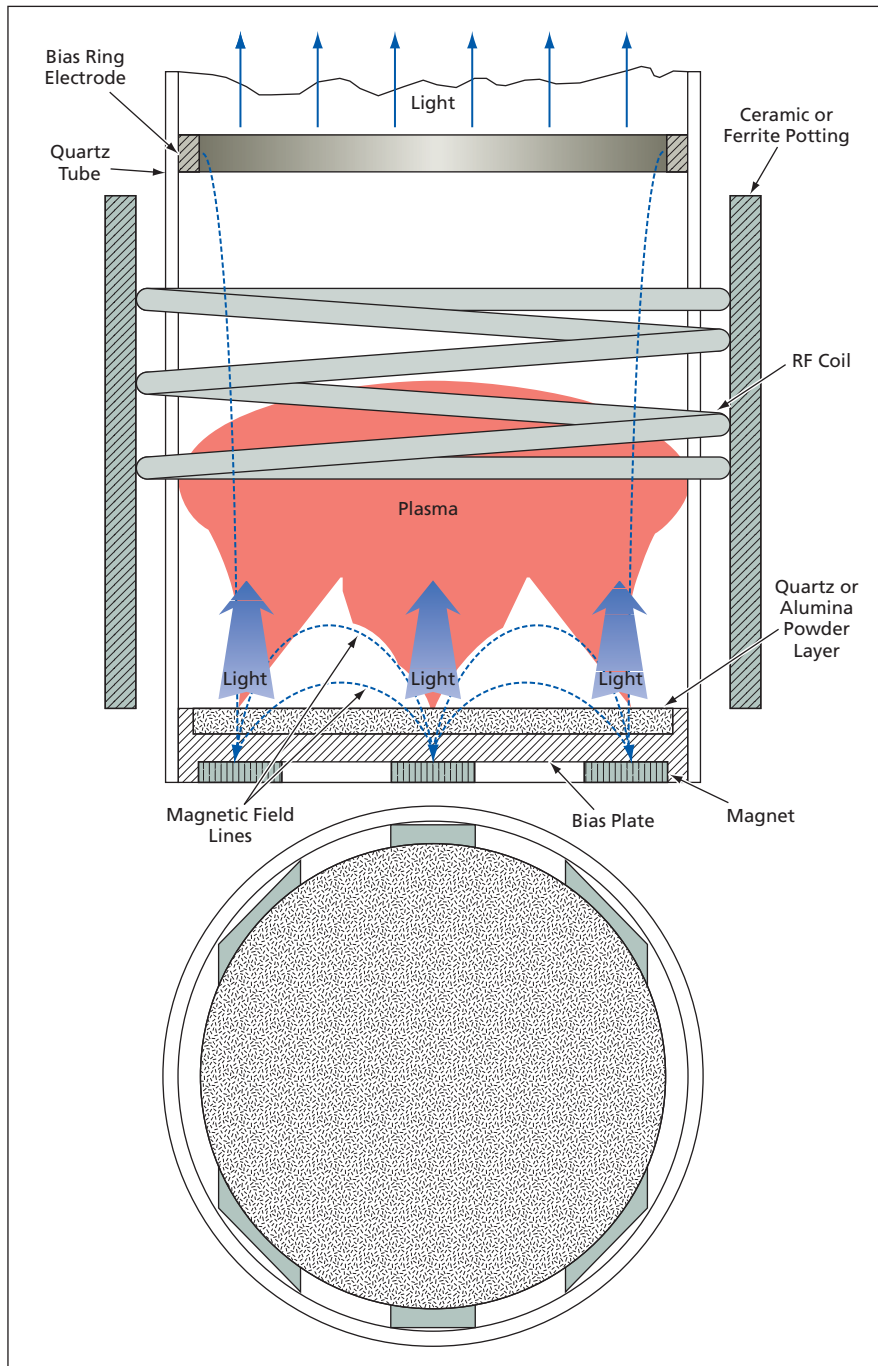
In this device, the material to be excited to luminescence is a layer of quartz or alumina powder on an electrically conductive plate exposed to a low-pressure plasma discharge. The plate is electrically biased positively to collect electron current.

The application of radio-frequency (RF) excitation via a coil that surrounds the quartz tube, shown in the figure, sustains the low-pressure plasma discharge. This plasma plays the role of a plasma cathode, which makes it possible to overcome the space-charge limitation encountered in the use of a hot-filament cathode or an electron gun. The electrons are extracted from the plasma via a plasma sheath at the surface of the powder-containing electrode.

The device utilizes magnets to form a cusped magnetic field that channels electrons into three areas on the layer of luminescent material. The luminescence from these areas is intense, even at bias potentials less than 1 kV. Moreover, though the emission is non-thermal, the effective blackbody temperature of the luminescence spectrum is well in excess of the blackbody temperatures of conventional incandescent-filament light sources.

This work was done by John E. Foster of Glenn Research Center. Further information is contained in a TSP (see page 1).

Inquiries concerning rights for the commercial use of this invention should be addressed to NASA Glenn Research Center, Innovative Partnerships Office, Attn: Steve Fedor, Mail Stop 4-8, 21000 Brookpark Road, Cleveland, Ohio 44135. Refer to LEW-17704-1.



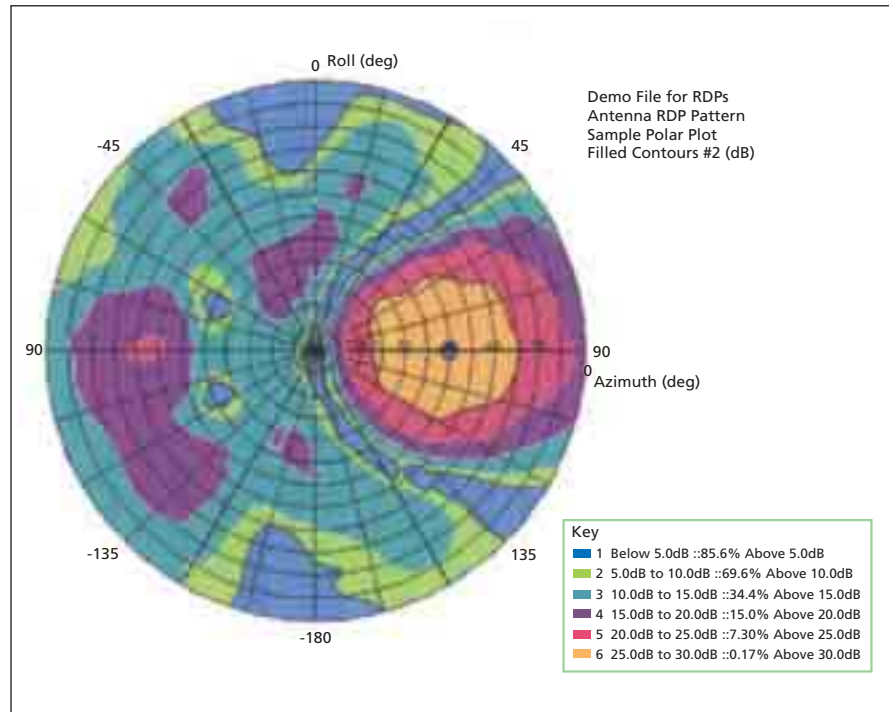
Electrons From the Plasma are channeled by the cusped magnetic field and accelerated toward the bias plate by the bias electric field. The impingement of the energetic electrons on the layer of quartz or alumina powder excites luminescence.

Displaying and Analyzing Antenna Radiation Patterns

Lyndon B. Johnson Space Center, Houston, Texas

Radiant Energy Display and Analysis Software Package (REDAP) is a computer program for processing antenna-radiation-pattern data that have been pre-processed by a data-collection program and stored in a spherical-coordinate format. REDAP is designed specifically for application to data generated in testing of antennas in an anechoic chamber at Johnson Space Center; parts of REDAP may be reusable for processing antenna-test data collected elsewhere. REDAP provides a graphical user interface (GUI) and executes mathematical and plotting routines on a personal computer. The routines include statistical calculations (e.g., maximum, minimum, 3-dB-falloff points, and percent coverage); addition and subtraction of offsets; multiplication and division by scaling factors; and computation of circular-polarization characteristics from linear-polarization measurement data.

REDAP can display radiation-pattern data in a variety of formats that include, for example, lines plotted on rectangular coordinates, images of radiation patterns in three-dimensional space, and contour plots on polar coordinates (see figure). All characteristics of a display, including contents of plots, coordinate axes, marks, colors, and the destination



A Sample Polar Plot illustrates one of the formats that can be generated from REDAP.

(e.g., printer or file) to which the display data are to be sent are controlled through a series of GUI dialog boxes.

This work was done by Jim Siekierski of

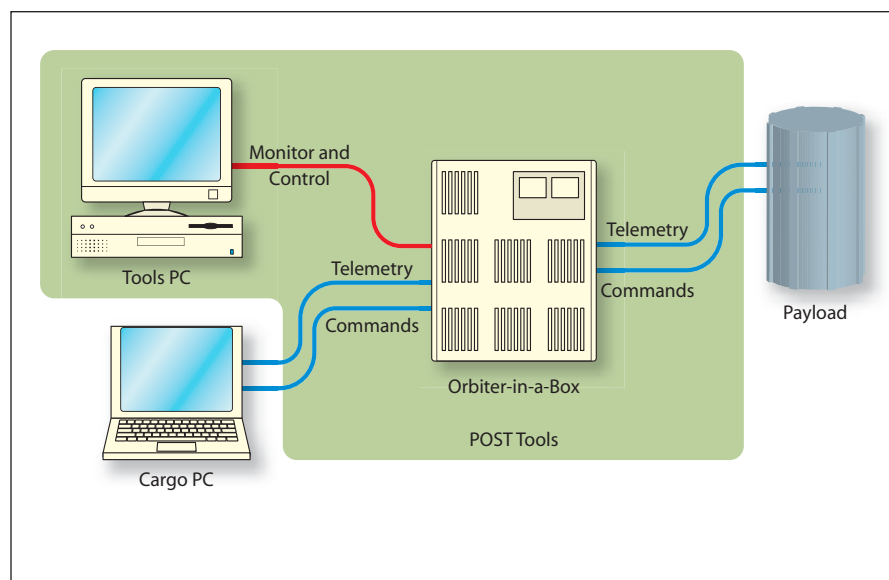
Johnson Space Center and Ash Henson of Lockheed Martin Corp. Further information is contained in a TSP (see page 1). MSC-23210-1

Payload Operations Support Team Tools

Lyndon B. Johnson Space Center, Houston, Texas

Payload Operations Support Team Tools is a software system that assists in (1) development and testing of software for payloads to be flown aboard the space shuttles and (2) training of payload customers, flight controllers, and flight crews in payload operations. POST Tools includes the following subsystems:

- The Orbiter-in-a-Box Tool is an embedded real-time operating-system model of the space-shuttle orbiter avionics. In conjunction with the Command and Data Tool described below, the Orbiter-in-a-Box Tool (see figure) enables testing of the application software of the Cargo PC, which is a computer through which a space-shuttle crew can monitor and control payloads.
- The Shuttle Mission Simulator (SMS) Model Tool is a suite of software tools that payload customers can use to cre-



An Orbiter-in-a-Box can be used to test the orbiter interface between the cargo PC and the payload.

ate mathematical models of payloads. These models will be used in the SMS to train flight controllers and flight crews on payload operations.

- The Mission Operations Tool provides a streamlined and simplified way to collect the payload-operations data to support the development of mission-operations documentation.
- The Command and Data Tool is a client-server database application program to be used to collect command and telemetry data for the Cargo PC.

This program was written by Bill Askew, Matthew Barry, Gary Burrows, Mike Casey, Joe Charles, Nicholas Downing, Monika Jain, Rebecca Leopold, Roger Luty, David McDill, Scott Mermelstein, Jon Morsics, Richard Osborne, Cindy Owens, Thomas Price, Ayman Quaddumi, Jim Thompson, and Patrick Walter of United Space Alliance, LLC; Melanie Vail of Raytheon Co.; and Richard Campbell and Mark Kelly of Systems Interface Software, Ltd. for Johnson Space Center. Further information is contained in a TSP (see page 1).

Title to this invention has been waived under the provisions of the National Aeronautics and Space Act (42 U.S.C. 2457(f)), to United Space Alliance, LLC. Inquiries concerning licenses for its commercial development should be addressed to:

*United Space Alliance, LLC
Flight Operations
600 Gemini
Houston, TX 77058-2777*

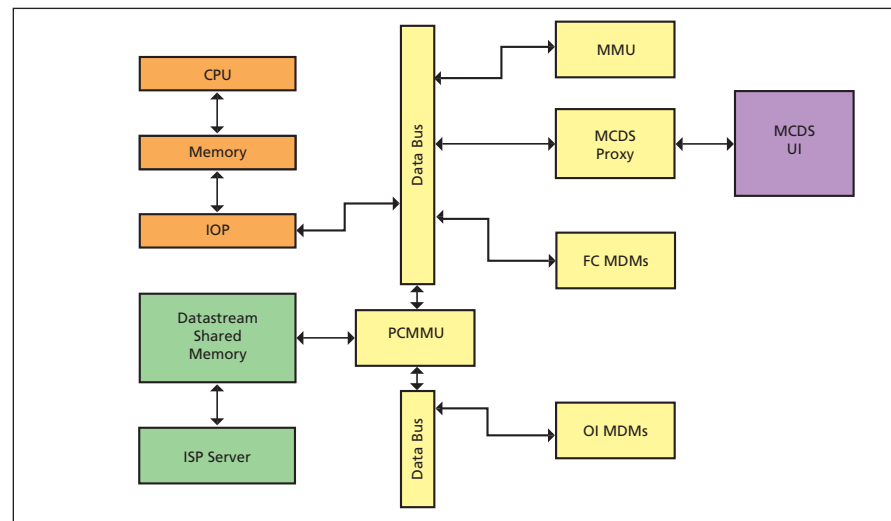
Refer to MSC-23419-1/20-1/1-1/2-1, volume and number of this NASA Tech Briefs issue, and the page number.

Space-Shuttle Emulator Software

Lyndon B. Johnson Space Center, Houston, Texas

A package of software has been developed to execute a raw binary image of the space shuttle flight software for simulation of the computational effects of operation of space shuttle avionics. This software can be run on inexpensive computer workstations. Heretofore, it was necessary to use real flight computers to perform such tests and simulations.

The package includes a program that emulates the space shuttle orbiter general-purpose computer (see figure) [consisting of a central processing unit (CPU), input/output processor (IOP), master sequence controller, and bus-control elements]; an emulator of the orbiter display electronics unit and models of the associated cathode-ray tubes, keyboards, and switch controls; computational models of the data-bus network; computational models of the multiplexer-demultiplexer components; an emulation of the pulse-code modulation master unit; an emulation of the payload data interleaver; a model of the master timing unit; a model of the mass memory unit; and a software component that ensures compatibility of telemetry and command services between the simulated space shuttle



A High-Level Schematic indicates the arrangement. (Note: CPU = central processing unit, IOP = input/output processor, ISP= information sharing protocol, PCMMU = pulse code modulation master unit, MCDS = multifunction CRT display system, MDMs = multiplexer/demultiplexers, FC = flight critical, OC = operational instrumentation, and UI = user interface.)

avionics and a mission control center. The software package is portable to several host platforms.

This program was written by Scott Arnold, Bill Askew, Matthew R. Barry, Agnes Leigh, Scott Mermelstein, James Owens, Dan Payne, Jim Pemble, John Sollinger, Hiram Thomp-

son, James C. Thompson, Patrick Walter, David Brummel and Steven P. Weismuller of United Space Alliance, LLC; and Ron Aadsen, Keith Hurley, and Chris Ruhle of Raytheon Co. for Johnson Space Center. Further information is contained in a TSP (see page 1). MSC-23289-1

Soft Real-Time PID Control on a VME Computer

NASA's Jet Propulsion Laboratory, Pasadena, California

microPID (μ PID) is a computer program for real-time proportional + integral + derivative (PID) control of a translation stage in a Fourier-transform ultraviolet spectrometer. μ PID implements a PID control loop over a position profile at sampling rate of 8 kHz (sampling period

125 μ s). The software runs in a stripped-down Linux operating system on a VersaModule Eurocard (VME) computer operating in real-time priority queue using an embedded controller, a 16-bit digital-to-analog converter (D/A) board, and a laser-positioning board (LPB).

μ PID consists of three main parts: (1) VME device-driver routines, (2) software that administers a custom protocol for serial communication with a control computer, and (3) a loop section that obtains the current position from an LPB-driver routine, calculates

the ideal position from the profile, and calculates a new voltage command by use of an embedded PID routine — all within each sampling period. The voltage command is sent to the D/A board to control the stage. μ PID uses special kernel headers to obtain microsecond

timing resolution. Inasmuch as μ PID implements a single-threaded process and all other processes are disabled, the Linux operating system acts as a soft real-time system.

This program was written by Vahag Karayan, Stanley Sander, and Richard

Cageo of Caltech for NASA's Jet Propulsion Laboratory. Further information is contained in a TSP (see page 1).

This software is available for commercial licensing. Please contact Karina Edmonds of the California Institute of Technology at (626) 395-2322. Refer to NPO-41107.

Analyzing Radio-Frequency Coverage for the ISS

Lyndon B. Johnson Space Center, Houston, Texas

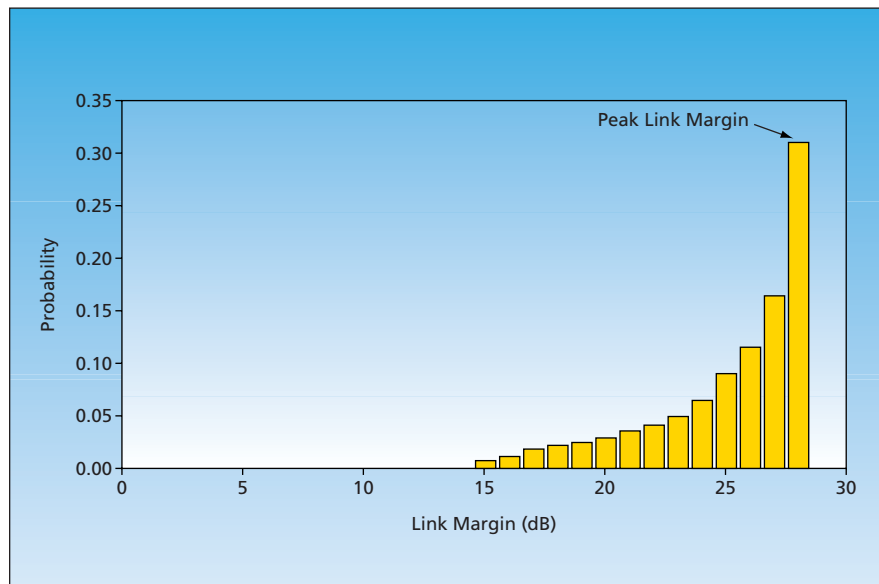
The Interactive Coverage Analysis Tool (iCAT) is an interactive desktop-computer program serving to (1) support planning of coverage, and management of usage of frequencies, of current

and proposed radio communication systems on and near the International Space Station (ISS) and (2) enable definition of requirements for development of future such systems. The iCAT can

also be used in design trade studies for other (both outer-space and terrestrial) communication systems.

A user can enter the parameters of a communication-system link budget in a table in a worksheet. The nominal (on-axis) link values for the bit-to-noise-energy ratio, received isotropic power (RIP), carrier-to-noise ratio (C/N), power flux density (PFD), and link margin (see figure) of the system are calculated and displayed in the table. Plots of field gradients for the RIP, C/N, PFD, and link margin are constructed in an ISS coordinate system, at a specified link range, for both the forward and return link parameters, and are displayed in worksheets. The forward and reverse link antenna gain patterns are also constructed and displayed. Line-of-sight (LOS) obstructions can be both incorporated into the gradient plots and displayed on separate plots.

This program was written by Steven M. Bolen and Catherine C. Sham of Johnson Space Center. Further information is contained in a TSP (see page 1). MSC-23536



This is the type of **Statistical Analysis** that can be made from the output of iCAT.



Nanorod-Based Fast-Response Pressure-Sensitive Paints

Improved, nanostructured coatings could be used to measure rapid pressure fluctuations.

John H. Glenn Research Center, Cleveland, Ohio

A proposed program of research and development would be devoted to exploitation of nanomaterials in pressure-sensitive paints (PSPs), which are used on wind-tunnel models for mapping surface pressures associated with flow fields. Heretofore, some success has been achieved in measuring steady-state pressures by use of PSPs, but success in measuring temporally varying pressures has been elusive because of the inherent slowness of the optical responses of these materials.

A PSP contains a dye that luminesces in a suitable wavelength range in response to photoexcitation in a shorter wavelength range. The luminescence is quenched by oxygen at a rate proportional to the partial pressure of oxygen and thus proportional to the pressure of air. As a result, the intensity of luminescence varies inversely with the pressure of air.

The major problem in developing a PSP that could be easily applied to a wind-tunnel model and could be useful for measuring rapidly varying pressure is to provide very high gas diffusivity for rapid, easy transport of oxygen to and from active dye molecules. Most PSPs include polymer-base binders, which limit the penetration of oxygen to dye mole-

cules, thereby reducing responses to pressure fluctuations. The proposed incorporation of nanomaterials (somewhat more specifically, nanorods) would result in paints having nanostructured surfaces that, relative to conventional PSP surfaces, would afford easier and more nearly complete access of oxygen molecules to dye molecules. One measure of greater access is effective surface area: For a typical PSP as proposed applied to a given solid surface, the nanometer-scale structural features would result in an exposed surface area more than 100 times that of a conventional PSP, and the mass of proposed PSP needed to cover the surface would be less than tenth of the mass of the conventional PSP.

One aspect of the proposed development would be to synthesize nanorods of Si/SiO₂, in both tangle-mat and regular-array forms, by use of chemical vapor deposition (CVD) and wet chemical processes, respectively. The rods would be coated with a PSP dye, and the resulting PSP signals would be compared with those obtained from PSP dye coats on conventional support materials.

Another aspect of the proposed development would be to seek to exploit the quan-

tum properties of nanorods of a suitable semiconductor (possibly GaN), which would be synthesized by CVD. These quantum properties of semiconductor nanorods include narrow-wavelength-band optical absorption and emission characteristics that vary with temperature. The temperature sensitivity might enable simultaneous measurement of fluctuating temperature and pressure and to provide a temperature correction for the PSP response. [The concept of such a temperature correction was described in "Temperature Correction for Pressure-Sensitive Paint" (LEW-16915), *NASA Tech Briefs*, Vol. 24, No. 1 (January 2000) page 50.]

This work was done by Timothy Bencic of Glenn Research Center and Randall L. VanderWal of the National Center For Space Exploration Research on Fluids and Combustion, formerly the National Center for Microgravity Research on Fluids and Combustion. Further information is contained in a TSP (see page 1).

Inquiries concerning rights for the commercial use of this invention should be addressed to NASA Glenn Research Center, Innovative Partnerships Office, Attn: Steve Fedor, Mail Stop 4-8, 21000 Brookpark Road, Cleveland, Ohio 44135. Refer to LEW-17827-1.



Capacitors Would Help Protect Against Hypervelocity Impacts

Marshall Space Flight Center, Alabama

A proposal investigates alternatives to the present "bumper" method of protecting spacecraft against impacts of meteoroids and orbital debris. The proposed method is based on a British high-voltage-capacitance technique for protecting armored vehicles against shaped-charge warheads.

A shield, according to the proposal, would include a bare metal outer layer separated by a gap from an inner metal layer covered with an electrically insulating material. The metal layers would constitute electrodes of a capacitor. A

bias potential would be applied between the metal layers. A particle impacting at hypervelocity on the outer metal layer would break apart into a debris cloud that would penetrate the electrical insulation on the inner metal layer. The cloud would form a path along which electric current could flow between the metal layers, thereby causing the capacitor to discharge. With proper design, the discharge current would be large enough to vaporize the particles in the debris cloud to prevent penetration of the spacecraft.

The shield design can be mass optimized to be competitive with existing bumper designs. Parametric studies were proposed to determine optimum correction between bias voltage, impacting particle velocity, gap space, and insulating material required to prevent spacecraft penetration.

This work was done by David Edwards, Whitney Hubbs, and Mary Hovater of Marshall Space Flight Center. Further information is contained in a TSP (see page 1).

MFS-31995-1

Diaphragm Pump With Resonant Piezoelectric Drive

Resonance is used to amplify the stroke and thus the flow rate.

Lyndon B. Johnson Space Center, Houston, Texas

A diaphragm pump driven by a piezoelectric actuator is undergoing development. This pump is intended to be a prototype of lightweight, highly reliable pumps for circulating cooling liquids in protective garments and high-power electronic circuits, and perhaps for some medical applications. The pump would be highly reliable because it would contain no sliding seals or bearings that could wear, the only parts subject to wear would be two check valves, and the diaphragm and other flexing parts could be designed, by use of proven methods, for extremely long life. Because the pump would be capable of a large volumetric flow rate and would have only a small dead volume, its operation would not be disrupted by ingestion of gas, and it could be started reliably under all conditions.

The prior art includes a number piezoelectrically actuated diaphragm pumps. Because of the smallness of the motions of piezoelectric actuators (typical maximum strains only about 0.001), the volumetric flow rates of those pumps are much too small for typical cooling applications. In the pump now undergoing development, mechanical resonance would be utilized to amplify the motion generated by the piezoelectric actuator and

thereby multiply the volumetric flow rate.

The prime mover in this pump would be a stack of piezoelectric ceramic actuators, one end of which would be connected to a spring that would be part of a spring-and-mass resonator structure. The "mass" part of the resonator struc-

ture would include the pump diaphragm (see Figure 1). Contraction of the spring would draw the diaphragm to the left, causing the volume of the fluid chamber to increase and thereby causing fluid to flow into the chamber. Subsequent expansion of the spring would

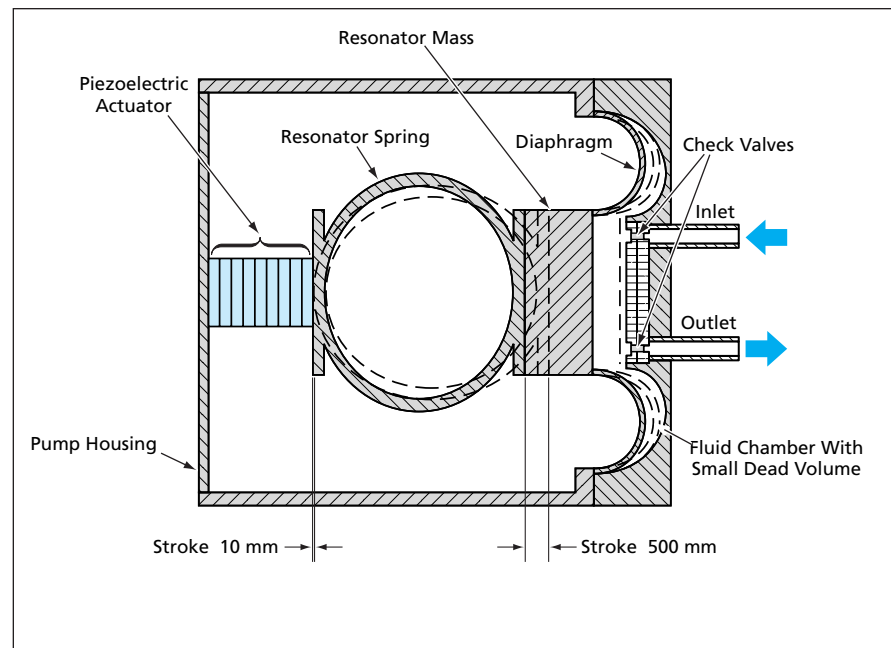


Figure 1. The Spring-and-Mass Resonator, if properly designed and constructed, would amplify the stroke of the piezoelectric stack by a factor of the order of 20.

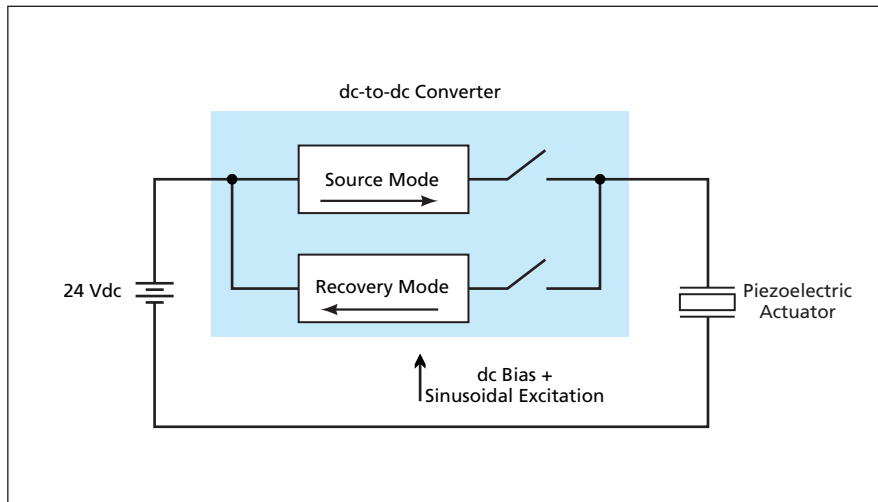


Figure 2. This Circuit Would Recover Energy returned by the piezoelectric actuator during each cycle of oscillation, thereby minimizing the power demand of the pump.

push the diaphragm to the right, causing the volume of the fluid chamber to decrease, and thereby expelling fluid from the chamber. The fluid would enter and leave the chamber through check valves.

The piezoelectric stack would be driven electrically to make it oscillate at the resonance frequency of the spring-and-mass structure. This frequency could be made high enough (of the order of 400 Hz) that the masses of all components could be made conve-

niently small. The resonance would amplify the relatively small motion of the piezoelectric stack (a stroke of the order of 10 μm) to a diaphragm stroke of the order of 0.5 mm. The exact amplification factor would depend on the rate of damping of oscillations; this, in turn, would depend on details of design and operation, including (but not limited to) the desired pressure rise and volumetric flow rate. In order to obtain resonance with large displacement, the damping rate must be low enough that

the energy imparted to the pumped fluid on each stroke is much less than the kinetic and potential energy exchanged between the mass and spring during each cycle of oscillation.

To minimize the power demand of the pump, a highly efficient drive circuit would be used to excite the piezoelectric stack. This circuit (see Figure 2) would amount to a special-purpose regenerative, switching power supply that would operate in a power-source mode during the part of an oscillation cycle when the excitation waveform was positive and in a power-recovery mode during the part of the cycle when the excitation waveform was negative. The circuit would include a voltage-boosting dc-to-dc converter that would convert between a supply potential of 24 Vdc and the high voltage needed to drive the piezoelectric stack. Because of the power-recovery feature, the circuit would consume little power. It should be possible to build the circuit as a compact unit, using readily available components.

This work was done by Michael G. Izenson, Robert J. Kline-Schoder, and Martin A. Shimko of Creare, Inc. for Johnson Space Center. For further information, contact the Johnson Commercial Technology Office at (281) 483-3809. MSC-23112

Improved Quick-Release Pin Mechanism

Lyndon B. Johnson Space Center, Houston, Texas

An improved quick-release pin mechanism supplants a prior such mechanism in which the pin bears a shear load to hold two objects together. The prior mechanism, of a ball-locking design, can fail when vibrations cause balls to fall out. The load-bearing pin is an outer tube with a handle at one end (hereafter denoted the near end). Within the outer tube is a spring-loaded inner tube that includes a handle at its near end and a

pivoting tab at its far end. The pin is inserted through holes in the objects to be retained and the inner tube is pushed against an offset pivot inside the outer tube to make the tab rotate outward so that it protrudes past the outer diameter of the outer tube, and the spring load maintains this configuration so that the pin cannot be withdrawn through the holes. Pushing the handles together against the spring load moves the lock-

ing tab out far enough that the tab becomes free to rotate inward. Then releasing the inner-tube handle causes the tab to be pulled into a resting position inside the outer tube. The pin can then be pulled out through the holes.

This work was done by Jay M. Wright of Johnson Space Center. For further information, contact the Johnson Innovative Partnerships Office at (281) 483-3809. MSC-23298

Designing Rolling-Element Bearings

Marshall Space Flight Center, Alabama

Bearing Analysis Tool (BAT) is a computer program for designing rolling-element bearings for cryogenic turbomachines. BAT provides a graphical user interface (GUI) that guides the entry of data to develop mathematical models

of bearings. The GUI breaks model data into logical subsets that are entered through logic-driven input screens. The software generates a three-dimensional graphical model of a bearing as the data are entered. Most data-

entry errors become immediately obvious in the graphical model. BAT provides for storage of all the data on a shaft/bearing system, enabling the creation of a library of proven designs. Data from the library can be trans-

ferred to subsequent projects by use of simple cut-and-paste routines.

BAT includes a library of temperature-dependent cryogenic bearing-material properties for use in the mathematical models. BAT implements algorithms that (1) enable the user to

select combinations of design and/or operating-condition parameters, and then (2) automatically optimize the design by performing trade studies over all of the parameter combinations. This feature enables optimization over a large trade space in a fraction of the

time taken when using prior bearing-model software.

This program was written by James D. Moore, Jr., and Ed Troy of SRS Technologies for Marshall Space Flight Center. Further information is contained in a TSP (see page 1). MFS-31864-1.

Reverse-Tangent Injection in a Centrifugal Compressor

The compressor flow can be stabilized against stall and surge.

John H. Glenn Research Center, Cleveland, Ohio

Injection of working fluid into a centrifugal compressor in the reverse tangent direction has been invented as a way of preventing flow instabilities (stall and surge) or restoring stability when stall or surge has already commenced. If not suppressed, such instabilities interrupt the smooth flow of the working fluid and, in severe cases of surge, give rise to pressure and flow oscillations that can be strong enough to damage the compressor and adjacent equipment.

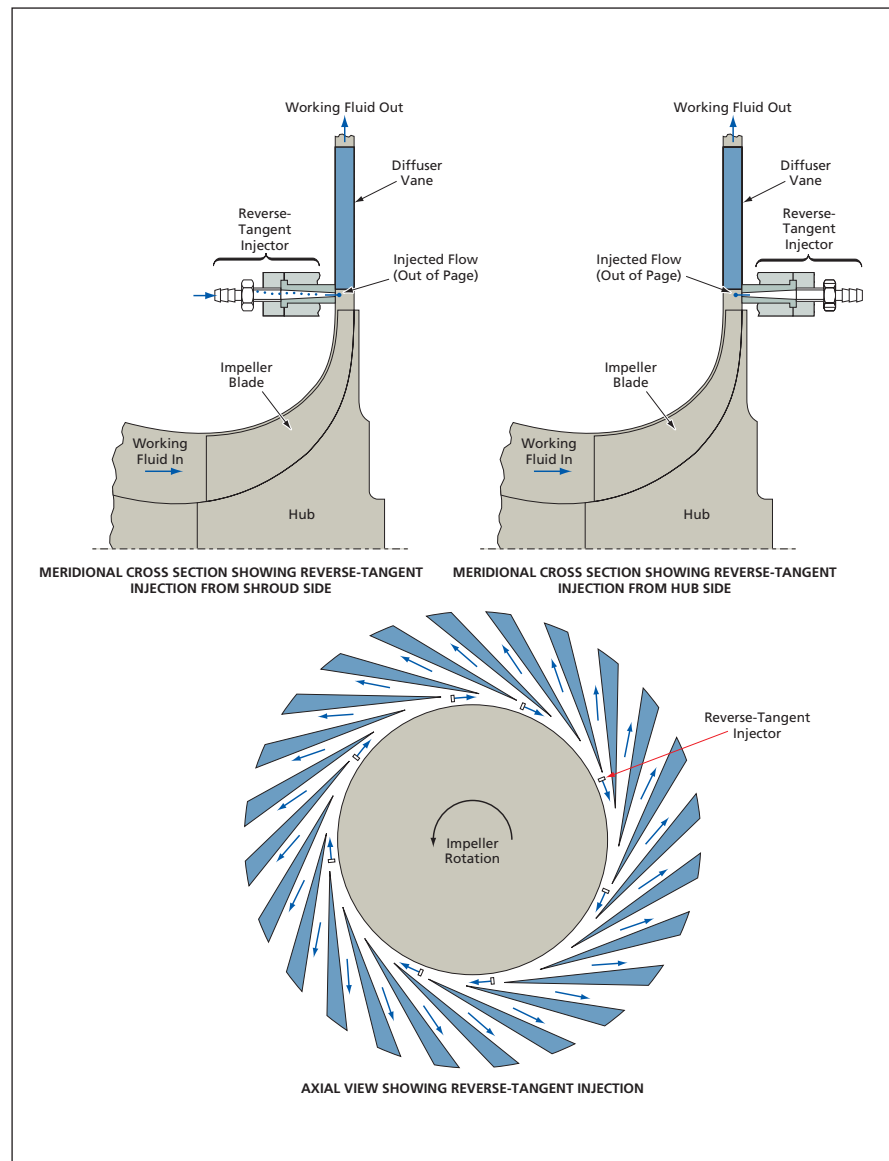
The invention applies, in particular, to a centrifugal compressor, the diffuser of which contains vanes that divide the flow into channels oriented partly radially and partly tangentially. In reverse-tangent injection, a stream or jet of the working fluid (the fluid that is compressed) is injected into the vaneless annular region between the blades of the impeller and the vanes of the diffuser (see figure). As used here, "reverse" signifies that the injected flow opposes (and thereby reduces) the tangential component of the velocity of the impeller discharge. At the same time, the injected jet acts to increase the radial component of the velocity of the impeller discharge. The net effect is to turn the impeller discharge flow toward a more radial direction; in other words, to reduce the flow angle of fluid entering the vaned diffuser passage, thereby reducing diffusion ahead of the passage throat, reducing the pressure load and the incidence of flow on the leading edges of the vanes. The reduction of the flow angle also changes the dynamic coupling between the impeller and diffuser in such a way as to prevent the development of certain instability modes in the diffuser.

The number and distribution of reverse-tangent injectors can be tailored to match the expected stall/surge characteristics of the compressor and the space available for installation. Reverse-tangent injection can be implemented in

any of three operating modes:

1. Continuous operation, in which the working fluid is injected continuously;
2. Open-loop operation, in which injection

is initiated by on-off valves upon detection of compressor instability or conditions known to precede compressor instability and the injection is



Working Fluid Is Injected in the direction opposing the tangential component of impeller discharge velocity at multiple points (eight in this example) in the vaneless region between the impeller blades and the diffuser vanes.

- terminated when stable compressor operation returns; or
3. Closed-loop or feedback-controlled operation, in which compressor stability is monitored and the number of active injectors and the injection rate are continually adjusted, using a dynamic control model and controlled valves.

In each of these operating modes, the injected working fluid can be supplied from an external source or from a downstream compressor stage where the total pressure is sufficient to produce the injected stream(s).

This work was done by Gary J. Skoch of the U.S. Army Research Laboratory for Glenn Re-

search Center. Further information is contained in a TSP (see page 1).

Inquiries concerning rights for the commercial use of this invention should be addressed to NASA Glenn Research Center, Commercial Technology Office, Attn: Steve Fedor, Mail Stop 4-8, 21000 Brookpark Road, Cleveland, Ohio 44135. Refer to LEW-17560-1.

✿ Inertial Measurements for Aero-assisted Navigation (IMAN)

NASA's Jet Propulsion Laboratory, Pasadena, California

IMAN is a Python tool that provides inertial sensor-based estimates of spacecraft trajectories within an atmospheric influence. It provides Kalman filter-derived spacecraft state estimates based upon data collected onboard, and is shown to perform at a level comparable to the conventional methods of spacecraft navigation in terms of accuracy and at a higher level with regard to the availability of results immediately after completion of an atmospheric drag pass. A benefit of this architecture is that this technology is conducive to onboard data processing and estimation and thus can compute near real-time spacecraft state estimates making it suitable for autonomous operations and/or closed-loop guidance, navigation, and control strategies.

This tool can be used to reliably predict subsequent periapsis times and locations over all aerobraking regimes. It also yields accurate peak dynamic pressure and heating rates, which are critical for a successful corridor control strategy. These data are comparable to radiometric-based navigation team reconstructed values. IMAN also provides the first instance of the use of the Unscented Kalman Filter (UKF) for the purpose of estimating an actual spacecraft trajectory arc about another planet. A significant advantage to the implementation of this type of filter is that the UKF is a non-linear filter and thus accurate to at least second order. It provides more meaningful and realistic covariances and has been shown to be robust in the presence of sparse data sets.

Currently, IMAN is being used in an experiment to demonstrate Inertial Measurement Unit (IMU)-based aerobraking navigation for the Mars Reconnaissance Orbiter (MRO). It also can be used in other operational missions such as those using the atmosphere for entry-descent-landing or solar sail missions that experience significant solar radiation pressure for propulsion.

This program was written by Moriba Jah, Michael Lisano, and George Hockney of Caltech for NASA's Jet Propulsion Laboratory. Further information is contained in a TSP (see page 1).

This software is available for commercial licensing. Please contact Karina Edmonds of the California Institute of Technology at (626) 395-2322. Refer to NPO-43677.

✿ Analysis of Complex Valve and Feed Systems

Stennis Space Center, Mississippi

A numerical framework for analysis of complex valve systems supports testing of propulsive systems by simulating key valve and control system components in the test loop. In particular, it is designed to enhance the analysis capability in terms of identifying system transients and quantifying the valve response to these transients. This system has analysis capability for simulating valve motion in complex systems operating in diverse flow regimes ranging from compressible gases to cryogenic liquids. A key feature is the hybrid, unstructured framework with sub-models for grid movement and phase change including cryogenic cavitations.

The multi-element unstructured framework offers improved predictions of valve performance characteristics under steady conditions for structurally complex valves such as pressure regulator valve. Unsteady simulations of valve motion using this computational approach have been car-

ried out for various valves in operation at Stennis Space Center such as the split-body valve and the 10-in. (≈ 25.4 -cm) LOX (liquid oxygen) valve and the 4-in. (≈ 10 cm) Y-pattern valve (liquid nitrogen). Such simulations make use of variable grid topologies, thereby permitting solution accuracy and resolving important flow physics in the seat region of the moving valve.

An advantage to this software includes possible reduction in testing costs incurred due to disruptions relating to unexpected flow transients or functioning of valve/flow control systems. Prediction of the flow anomalies leading to system vibrations, flow resonance, and valve stall can help in valve scheduling and significantly reduce the need for activation tests. This framework has been evaluated for its ability to predict performance metrics like flow coefficient for cavitating venturis and valve coefficient curves, and could be a valuable tool in predicting and under-

standing anomalous behavior of system components at rocket propulsion testing and design sites.

This program was written by Vineet Ahuja, Ashvin Hosangadi, Jeremy Shipman, Peter Cavallo, and Sanford Dash of Combustion Research and Flow Technology (CRAFT), Inc. for Stennis Space Center.

In accordance with Public Law 96-517, the contractor has elected to retain title to this invention. Inquiries concerning rights for its commercial use should be addressed to:

*Dr. Vineet Ahuja
Combustion Research and Flow Technology (CRAFT Tech), Inc.
6210 Keller's Church Road
Pipersville, PA 18947-1020
Phone No.: (215) 766-1520
Fax: (215) 766-1524
E-mail: vineet@craft-tech.com*

Refer to SSC-00245, volume and number of this NASA Tech Briefs issue, and the page number.

⚙ Improved Path Planning Onboard the Mars Exploration Rovers

NASA's Jet Propulsion Laboratory, Pasadena, California

A revised version of the AutoNav (autonomous navigation with hazard avoidance) software running onboard each Mars Exploration Rover (MER) affords better obstacle avoidance than does the previous version. Both versions include GESTALT (Grid-based Estimation of Surface Traversability Applied to Local Terrain), a navigation program that generates local-terrain models from stereoscopic image pairs captured by onboard rover cameras; uses this information to evaluate candidate arcs that extend across the terrain from the current rover location; ranks the arcs with respect to hazard avoidance, minimization of steering time, and the direction towards the goal; and combines the rankings in a weighted vote to select an arc, along which the rover is then driven.

GESTALT works well in navigating around small isolated obstacles, but

tends to fail when the goal is on the other side of a large obstacle or multiple closely spaced small obstacles. When that occurs, the goal seeking votes and hazard avoidance votes conflict severely. The hazard avoidance votes will not allow the rover to drive through the unsafe area, and the waypoint votes will not allow enough deviation from the straight-line path for the rover to get around the hazard. The rover becomes stuck and is unable to reach the goal.

The revised version of AutoNav utilizes a global path-planning program, Field D*, to evaluate the cost of traveling from the end of each GESTALT arc to the goal. In the voting process, Field D* arc votes supplant GESTALT goal-seeking arc votes. Hazard avoidance, steering bias, and Field D* votes are merged and the rover is driven a preset distance along the arc with the highest

vote. Then new images are acquired and the process as described is repeated until the goal is reached. This new technology allows the rovers to autonomously navigate around much more complex obstacle arrangements than was previously possible. In addition, this improved autonomy enables longer traverses per Sol (a day on Mars), and can make planning drives easier for operators on Earth.

The Field D algorithm was developed and configured for MER by Anthony Stentz and David Ferguson of Carnegie Mellon University and integrated into MER flight software by Joseph Carsten and Arturo Rankin of Caltech for NASA's Jet Propulsion Laboratory.*

The software used in this innovation is available for commercial licensing. Please contact Karina Edmonds of the California Institute of Technology at (626) 395-2322. Refer to NPO-44504.

⚙ Robust, Flexible Motion Control for the Mars Explorer Rovers

NASA's Jet Propulsion Laboratory, Pasadena, California

The Mobility Flight Software, running on computers aboard the Mars Explorer Rover (MER) robotic vehicles Spirit and Opportunity, affords the robustness and flexibility of control to enable safe and effective operation of these vehicles in traversing natural terrain. It can make the vehicles perform specific maneuvers commanded from Earth, and/or can autonomously administer multiple aspects of mobility, including choice of motion, measurement of actual motion, and even selection of targets to be approached. Mo-

tion of a vehicle can be commanded by use of multiple layers of control, ranging from motor control at a low level, direct drive operations (e.g., motion along a circular arc, motion along a straight line, or turn in place) at an intermediate level to goal-position driving (that is, driving to a specified location) at a high level.

The software can also perform high-level assessment of terrain and selection of safe paths across the terrain: this involves processing of the digital equivalent of a local traversability map gener-

ated from images acquired by stereoscopic pairs of cameras aboard the vehicles. Other functions of the software include interacting with the rest of the MER flight software and performing safety checks.

This program was written by Mark Maimone and Jeffrey Biesiadecki of Caltech for NASA's Jet Propulsion Laboratory.

This software is available for commercial licensing. Please contact Karina Edmonds of the California Institute of Technology at (626) 395-2322. Refer to NPO-41261.

⚙ Solar Sail Spaceflight Simulation

NASA's Jet Propulsion Laboratory, Pasadena, California

The Solar Sail Spaceflight Simulation Software (S5) toolkit provides solar-sail designers with an integrated environment for designing optimal solar-sail trajectories, and then studying the attitude dynamics/control, navigation, and trajectory control/correction of sails during realistic mission

simulations. Unique features include a high-fidelity solar radiation pressure model suitable for arbitrarily-shaped solar sails, a solar-sail trajectory optimizer, capability to develop solar-sail navigation filter simulations, solar-sail attitude control models, and solar-sail high-fidelity force models.

The integration of heliocentric or planetocentric trajectory design and optimization, with attitude control modeling, and navigation filter modeling, using a high-fidelity, arbitrary-shape sail model is new for solar-sail software. The present-day, state-of-the-art in solar-sail dynamics tools for analy-

sis are stand-alone tools for trajectory optimization, which generally use a very simple sail force model and stand-alone attitude control modeling. The current version, v2.1, is an update to a previous beta version.

This program was written by Michael Lisano, James Evans, and Jordan Ellis of Caltech; John Schimmels and Timothy Roberts of Raytheon ITSS; Leonel Rios-Reyes and Daniel Scheeres of the University of Michigan; Jeff Bladt of Ball Aerospace; Dale Lawrence of the University of

Colorado; and Scott Piggott of Odyssey Aerospace Corp. for NASA's Jet Propulsion Laboratory.

This software is available for commercial licensing. Please contact Karina Edmonds of the California Institute of Technology at (626) 395-2322. Refer to NPO-43641.



Fluorine-Based DRIE of Fused Silica

A suitable choice of process parameters enables etching of vertical side walls.

NASA's Jet Propulsion Laboratory, Pasadena, California

A process of deep reactive-ion etching (DRIE) using a fluorine-based gas mixture enhanced by induction-coupled plasma (ICP) has been demonstrated to be effective in forming high-aspect-ratio three-dimensional patterns in fused silica. The patterns are defined in part by an etch mask in the form of a thick, high-quality aluminum film. The process was developed to satisfy a need to fabricate high-aspect-ratio fused-silica resonators for vibratory microscopes, and could be used to satisfy similar requirements for fabricating other fused-silica components.

The development of the process involved manipulation of some process parameters, including the selection of gases, the mixture ratios of the gases, the process pressure, and power of the radio-frequency signal used to excite the

ICP. It was found that polymeric materials that contained silicon and/or fluorine were formed on the side walls during etching and were subsequently etched away, resulting in anisotropic etching. It was also found that helium added to gas mixtures contributes to cooling of substrates and thereby helps in forming vertical side-wall patterns.

One version of the process was found to effect etching of vertical side walls in 100- μm -deep fused silica at a rate of about 0.4 $\mu\text{m}/\text{min}$. Some of the parameters of this version of the process were the following:

- ICP power 1.2 kW;
- Reactive-ion etching power 0.5 kW;
- Process pressure 6 mtorr (≈ 0.8 Pa);
- Gas mixture of 1 part C_4F_8 to 1.6 parts of H_2 ; and
- Thickness of aluminum mask 5 μm .

The rate of etching of the fused silica was found to be about 5 times the rate of etching of the aluminum.

This work was done by Karl Yee, Kirill Shcheglov, Jian Li, and Daniel Choi of Caltech for NASA's Jet Propulsion Laboratory.

In accordance with Public Law 96-517, the contractor has elected to retain title to this invention. Inquiries concerning rights for its commercial use should be addressed to:

Innovative Technology Assets Management

JPL

Mail Stop 202-233

4800 Oak Grove Drive

Pasadena, CA 91109-8099

(818) 354-2240

E-mail: iaoffice@jpl.nasa.gov

Refer to NPO-43837, volume and number of this NASA Tech Briefs issue, and the page number.

Mechanical Alloying for Making Thermoelectric Compounds

Constituents are ball-milled into a powder, which is then hot pressed.

NASA's Jet Propulsion Laboratory, Pasadena, California

An economical room-temperature mechanical alloying process has been shown to be an effective means of making a homogeneous powder that can be hot-pressed to synthesize a thermoelectric material having reproducible chemical composition. The thermoelectric materials to which the technique has thus far been applied with success include rare-earth chalcogenides [$\text{La}_{3-x}\text{Te}_4$ ($0 < x < 0.33$) and $\text{La}_{3-x}\text{Yb}_y\text{Te}_4$ ($0 < x < 1, 0 < y < 1$)] and Zintl compounds (including $\text{Yb}_{14}\text{MnSb}_{11}$ and $\text{Yb}_{14}\text{BiSb}_{11}$). The synthesis of a given material consists of the room-temperature thermomechanical-alloying process followed by a hot-pressing process. Relative to synthesis of nominally the same material by a traditional process that includes hot melting, this synthesis is simpler and yields a material having superior thermoelectric properties.

The room-temperature mechanical alloying process is, more specifically, a

ball-milling process. It begins inside an argon-filled glove box, wherein elemental constituents in amounts corresponding to their desired proportions in the thermoelectric material to be synthesized are loaded into a vial that contains milling balls. The vial and milling balls are made of a material compatible with the material to be synthesized. (For synthesizing $\text{Yb}_{14}\text{MnSb}_{11}$, one uses a vial and balls made of tungsten carbide; for synthesizing $\text{La}_{3-x}\text{Te}_4$ or $\text{La}_{3-x}\text{Yb}_y\text{Te}_4$, one uses a vial and balls made of stainless steel.) Next, the filled vial is removed from the glove box and clamped onto a commercially available mixer/mill machine, which is used to shake the vial for as long as 40 hours to effect ball milling.

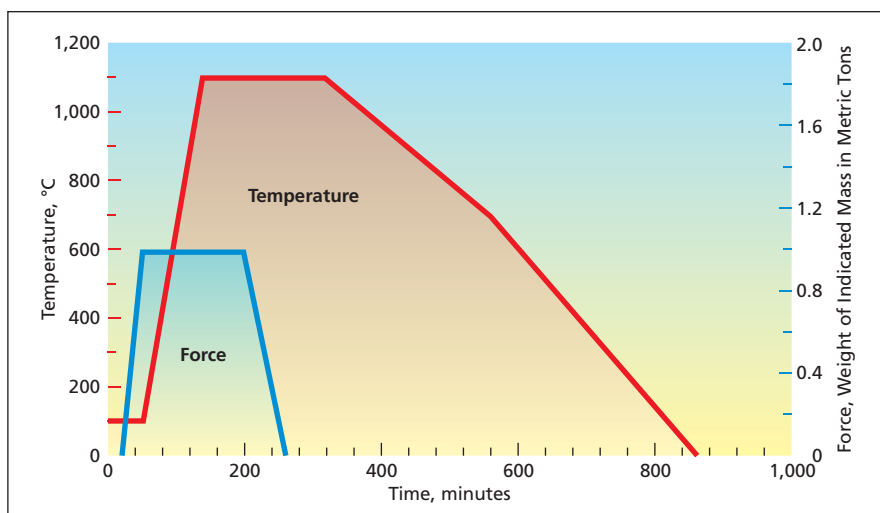
After ball milling, the vial is returned to the glove box, wherein the powder produced by the ball milling is loaded into a graphite die for hot pressing.

- In the case of $\text{Yb}_{14}\text{MnSb}_{11}$, it is neces-

sary to sandwich the powder between two graphite foil layers at each end. In ascending order, the resulting assembly inside the die consists of one or more spacer(s), two graphite foil layers, the powder, two more graphite foil layers, and a plunger that presses down on the aforementioned components.

- In the case of $\text{La}_{3-x}\text{Te}_4$ or $\text{La}_{3-x}\text{Yb}_y\text{Te}_4$, the plunger is made of graphite, the inside of the die is lined with graphite foil, and the powder touches the top and bottom spacers, which are coated with boron nitride to prevent adhesion.

The die and its contents are then placed in a hot press, wherein the powder is subjected to a temperature-vs.-time and a pressure- (or force)-vs.-time profile, specified for the material to be synthesized (for example, see figure), to consolidate the powder into a solid mass of requisite density. After this hot pressing, the mass is removed from the die. In the case of $\text{La}_{3-x}\text{Te}_4$ or $\text{La}_{3-x}\text{Yb}_y\text{Te}_4$, the



These **Temperature and Force Schedules** are followed in hot pressing of $\text{La}_{3-x}\text{Te}_4$ or $\text{La}_{3-x}\text{Yb}_x\text{Te}_4$ powder to consolidate it into a solid mass having superior thermoelectric properties. The force indicated here is calculated to yield a specified pressure when exerted over an area slightly more than 12 mm in diameter.

mass is sanded to remove graphite foil and boron nitride from its surface.

This work was done by Chen-Kuo Huang, Jean-Pierre Fleurial, G. Jeffrey Snyder, Richard Blair, and Andrew May of Caltech for NASA's Jet Propulsion Laboratory. Further information is contained in a TSP (see page 1).

In accordance with Public Law 96-517, the contractor has elected to retain title to this invention. Inquiries concerning rights for its commercial use should be addressed to:

Innovative Technology Assets Management
JPL

Mail Stop 202-233

4800 Oak Grove Drive

Pasadena, CA 91109-8099

(818) 354-2240

E-mail: iaoffice@jpl.nasa.gov

Refer to NPO-44356, volume and number of this NASA Tech Briefs issue, and the page number.

Process for High-Rate Fabrication of Alumina Nanotemplates

Approximately regular hexagonal arrays of holes are formed in an anodizing process.

NASA's Jet Propulsion Laboratory, Pasadena, California

An anodizing process, at an early stage of development at the time of reporting the information for this article, has shown promise as a means of fabricating alumina nanotemplates integrated with silicon wafers. Alumina nanotemplates are basically layers of alumina, typically several microns thick, in which are formed approximately regular hexagonal arrays of holes having typical diameters of the order of 10 to 100 nm. Interest in alumina nanotemplates has grown in recent years because they have been found to be useful as templates in the fabrication of nanoscale magnetic, electronic, optoelectronic, and other devices. The present anodizing process is attractive for the fabrication of alumina nanotemplates integrated with silicon wafers in two respects: (1) the process involves self-ordering of the holes; that is, the holes as formed by the process are spontaneously arranged in approximately regular hexagonal arrays; and (2) the rates of growth (that is, elongation) of the holes are high enough to make the process compatible with other processes used in the mass production of integrated circuits.

In preparation for fabrication of alumina nanotemplates in this process, one first uses electron-beam evaporation to deposit thin films of titanium, followed by thin films of aluminum, on silicon

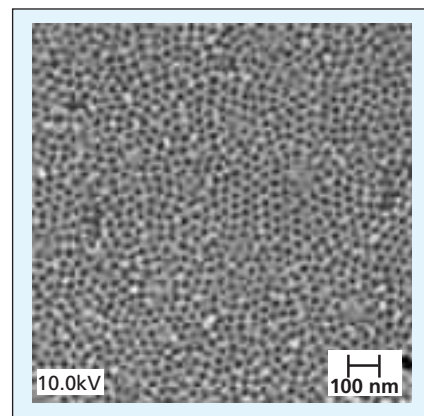
wafers. Then the alumina nanotemplates are formed by anodizing the aluminum layers, as described below.

In experiments in which the process was partially developed, the titanium films were 200 Å thick and the aluminum films were 5 µm thick. The aluminum films were oxidized to alumina, and the arrays of holes were formed by anodizing the aluminum in aqueous solutions of sulfuric and/or oxalic acid at room temperature (see figure). The diameters, spacings, and rates of growth of the holes were found to depend, variously, on the composition of the anodizing solution, the applied current, or the applied potential, as follows:

- In galvanostatically controlled anodizing, regardless of the chemical composition of the solution, relatively high current densities (50 to 100 mA/cm²) resulted in arrays of holes that were more nearly regular than were those formed at lower current densities.
- The rates of elongation of the holes were found to depend linearly on the applied current density: the observed factor of proportionality was 1.2 (µm/h)/(mA/cm²).
- For a given fixed current density and room temperature, the hole diameters were found to depend mainly on the chemical compositions of the anodizing

solutions. The holes produced in sulfuric acid solutions were smaller than those produced in oxalic acid solutions.

- The arrays of holes produced in sulfuric acid were more ordered than were those produced in oxalic acid.
- The breakdown voltage was found to decrease logarithmically with increasing concentration of sulfuric acid.
- The breakdown voltage was also found to decrease with temperature and to be accompanied by a decrease in hole diameter.
- The hole diameter was found to vary linearly with applied potential, with a



This **Alumina Nanotemplate** was made by room-temperature anodizing in an aqueous solution of 40 volume percent sulfuric acid at a current density of 50 mA/cm². The hole diameter is 17 nm and the porosity is 16 percent.

slope of 2.1 nm/V. This slope differs from slopes (2.2 and 2.77 nm/V) reported for similar prior measurements on nanotemplates made from bulk aluminum. The differences among these slopes may be attributable to differences among impurities and defects in

bulk and electron-beam-evaporated aluminum specimens.

This work was done by Nosang Myung, Jean-Pierre Fleurial, Minhee Yun, William West, and Daniel Choi of Caltech for NASA's Jet Propulsion Laboratory. Further information is contained in a TSP (see page 1).

This invention is owned by NASA, and a patent application has been filed. Inquiries concerning nonexclusive or exclusive license for its commercial development should be addressed to the Patent Counsel, NASA Management Office-JPL. Refer to NPO-40070.

Electroform/Plasma-Spray Laminates for X-Ray Optics

Properties of lightweight components can be optimized.

Goddard Space Flight Center, Greenbelt, Maryland

Electroform/plasma-spray laminates have shown promise as lightweight, strong, low-thermal-expansion components for x-ray optics. The basic idea is to exploit both (1) the well-established art of fabrication of optical components by replication and (2) plasma spraying as a means of reinforcing a thin replica optic with one or more backing layer(s) having tailorable thermomechanical properties. In x-ray optics as in other applications, replication reduces the time and cost of fabrication because grinding and polishing can be limited to a few thick masters, from which many lightweight replicas can thereafter be made.

The first step in the fabrication of a component of the type in question is to make a replica optic by electroforming a thin layer of nickel on a master. Through proper control of the electro-

forming process conditions, it is possible to minimize residual stress and, hence, to minimize distortion in the replica. Next, a powder comprising ceramic particles coated with a metal compatible with the electroformed nickel is plasma-sprayed onto the backside of the nickel replica. Then through several repetitions and variations of the preceding steps or perhaps a small compressive stress, alternating layers of electroformed nickel and plasma-sprayed metal-coated ceramic powder are deposited.

The thicknesses of the layers and the composition of the metal-coated ceramic powder are chosen to optimize the strength, areal mass density, and toughness of the finished component. An important benefit of using both elec-

troforming and plasma spraying is the possibility of balancing stresses to a minimum level, which could be zero or perhaps a small net compressive stress designed to enhance the function of the component in its intended application.

This work was done by Melville P. Ulmer, Michael Graham, and Semyon Vaynman of Northwestern University for Goddard Space Flight Center.

In accordance with Public Law 96-517, the contractor has elected to retain title to this invention. Inquiries concerning rights for its commercial use should be addressed to:

*Northwestern University
1880 Oak Avenue, Suite 100
Evanston, IL 60201*

Refer to GSC-14977-1, volume and number of this NASA Tech Briefs issue, and the page number.



An Automated Flying-Insect Detection System

Real-time monitoring and early detection networks detect harmful flying insects.

Stennis Space Center, Mississippi

An automated flying-insect detection system (AFIDS) was developed as a proof-of-concept instrument for real-time detection and identification of flying insects. This type of system has use in public health and homeland-security decision support, agriculture and military pest management, and/or entomological research.

As shown in Figure 1 (top panel), insects are first lured into the AFIDS integrated sphere by insect attractants. Once inside the sphere, the insect's wing beats cause alterations in light intensity that is detected by a photoelectric sensor. Following detection, the insects are encouraged (with the use of a small fan) to move out of the

sphere and into a designated insect trap where they are held for taxonomic identification or serological testing. The acquired electronic wing-beat signatures are pre-processed (Fourier transformed) in real-time to display a periodic signal. These signals are sent to the end user where they are graphically displayed as shown in Figure 1

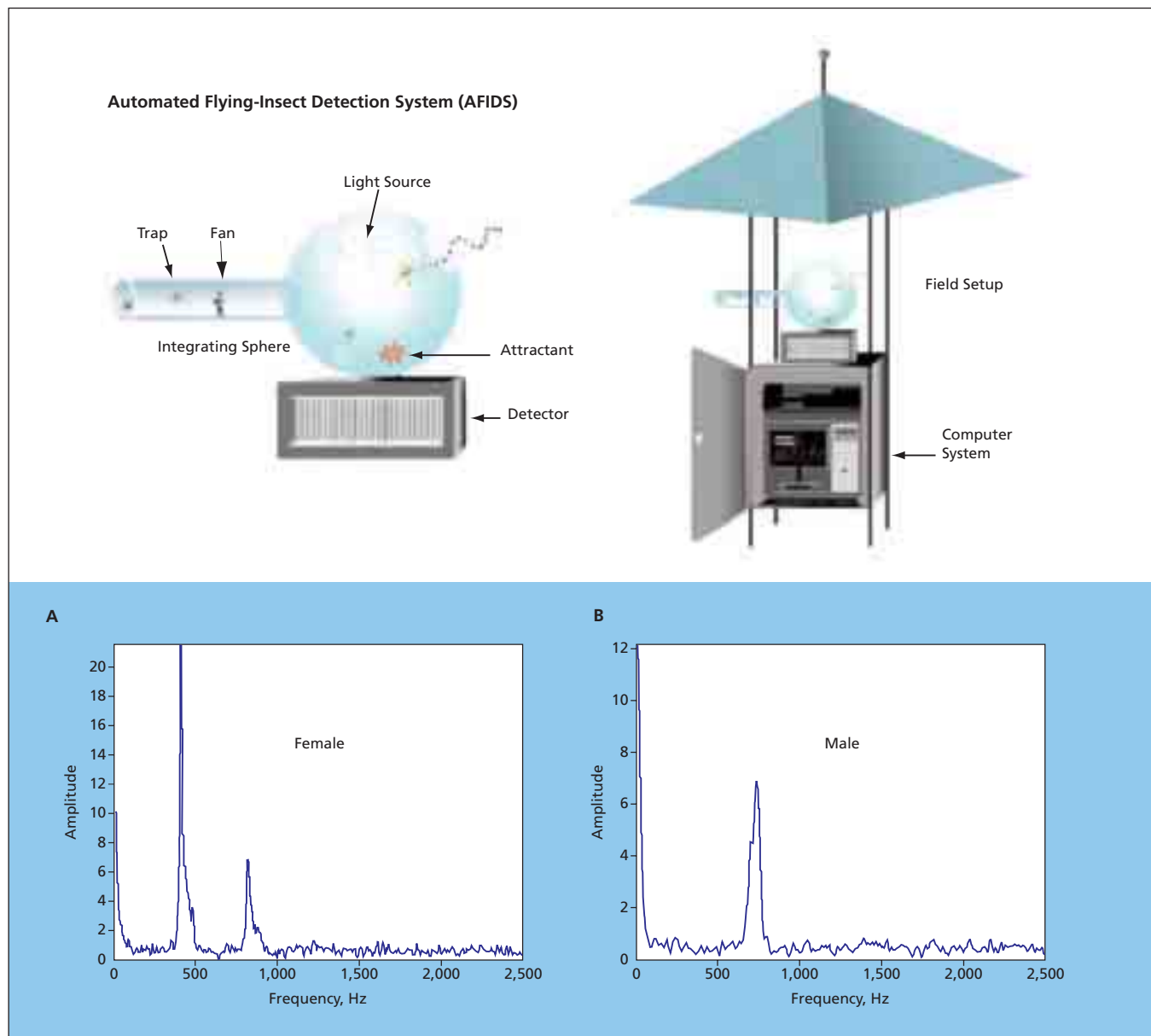


Figure 1. AFIDS is deployed as shown in the top panel. The bottom panel shows spectral plots of AFIDS acquired wing-beat signatures. The differences between female (plot A, 409 Hz) and male (plot B, 737 Hz) *Aedes albopictus* mosquitoes are apparent.

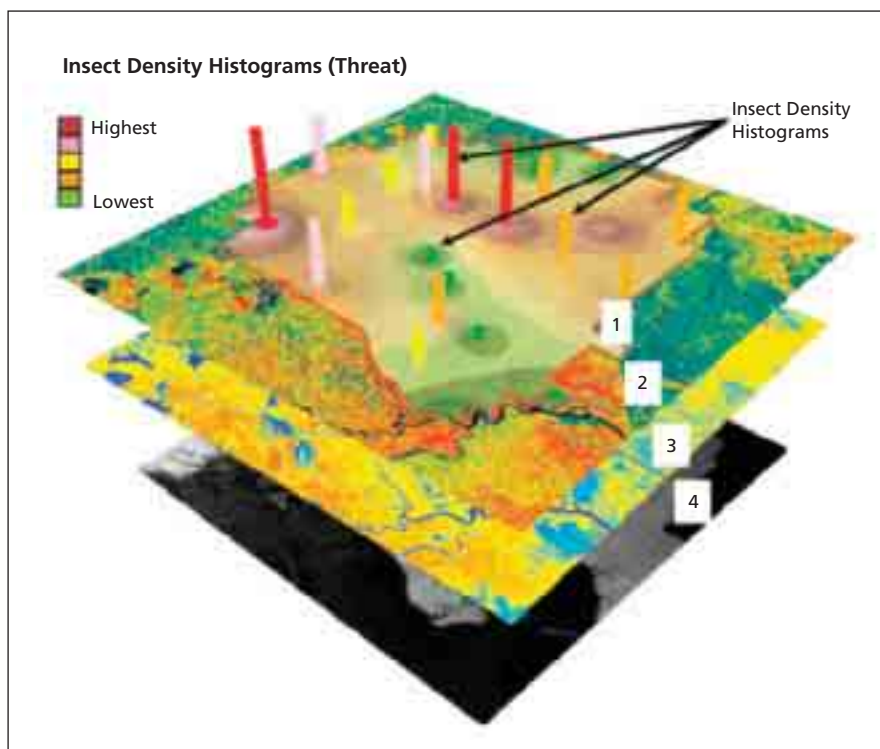


Figure 2. Integration of AFIDS and GIS Data Layers is illustrated for hypothetical military, civilian, or agricultural pest management. Data layers are as follows: (1) Hypothetical AFIDS insect density contours (histograms = threat intensity); (2) STAR-3i radar imagery; (3) ASTER Normalized Difference Vegetative Index; and (4) LIDAR digital terrain.

(bottom panel). All AFIDS data are pre-processed in the field with the use of a laptop computer equipped with LabVIEW™. The AFIDS software can be programmed to run continuously or at specific time intervals when insects are prevalent.

A special DC-restored transimpedance amplifier reduces the contribu-

tions of low-frequency background light signals, and affords approximately two orders of magnitude greater AC gain than conventional amplifiers. This greatly increases the signal-to-noise ratio and enables the detection of small changes in light intensity. The AFIDS light source consists of high-intensity Al-

GaInP light-emitting diodes (LEDs). The AFIDS circuitry minimizes brightness fluctuations in the LEDs and when integrated with an integrating sphere, creates a diffuse uniform light field. The insect wing beats isotropically scatter the diffuse light in the sphere and create wing-beat signatures that are detected by the sensor. This configuration minimizes variations in signal associated with insect flight orientation.

Preliminary data indicate that AFIDS has sufficient sensitivity and frequency-measuring capability to differentiate between male and female mosquitoes (Figure 1, bottom panel) and fruit flies (data not shown). Similar studies show that AFIDS can be utilized to detect discrete differences between two mosquito species, *Aedes aegypti* and *Aedes albopictus*.

When fully deployable, a wireless network of AFIDS monitors could be used in combination with other remotely sensed data and visually displayed in a geographic information system (GIS) to provide real-time surveillance (see Figure 2). More accurate and sensitive insect population forecasts and effective rapid response and mitigation of insect issues would then be possible.

This work was done by Timi Vann of Stennis Space Center and Jane C. Andrews, Dane Howell, and Robert Ryan of Lockheed Martin Corp.

Inquiries concerning rights for the commercial use of this invention should be addressed to the Intellectual Property Manager, Stennis Space Center, (228) 688-1929. Refer to SSC-00192.

Calligraphic Poling of Ferroelectric Material

Arbitrary patterns can be written relatively easily and inexpensively.

NASA's Jet Propulsion Laboratory, Pasadena, California

Calligraphic poling is a technique for generating an arbitrary, possibly complex pattern of localized reversal in the direction of permanent polarization in a wafer of LiNbO₃ or other ferroelectric material. The technique is so named because it involves a writing process in which a sharp electrode tip is moved across a surface of the wafer to expose the wafer to a polarizing electric field in the desired pattern. The technique is implemented by use of an apparatus, denoted a calligraphic poling machine (CPM), that includes the electrode and other components as described in more detail below.

A capability for forming poling patterns is needed for research on, and development of, photonic devices that exploit the nonlinear optical properties of ferroelectric crystals. Specific poling structures in ferroelectric crystals can be engineered to variously amplify or suppress these nonlinear optical properties to effect such useful functions as optical switching, modulation, frequency conversion, and frequency filtering.

Outside of industry, poling machines have been available to only a few research laboratories and have been typified by high costs and limited flexibility. Prior poling techniques and machines

are suitable for generating relatively simple patterns (e.g., straight lines) but are not suitable for generating the arbitrary patterns required in some applications. Each of the prior techniques involves one or more of the following: expensive fabrication of electrically conductive masks, expensive holograms, a cleanroom, high vacuum, and high temperature. In contrast, a CPM operates in air at room temperature with equipment readily available in a typical laboratory; hence, calligraphic poling costs less than does poling by the prior techniques.

In a CPM (see figure), the wafer to be poled is placed in the x - y (horizontal)

plane on a smooth, flat substrate that serves as a lower electrode. Typically, the wafer is a crystal of LiNbO_3 or other ferroelectric material that is z-cut. [In this case, “z-cut” signifies that the polarization axis of the wafer is perpendicular to its broad faces and thus coincides with the z (vertical) axis when the wafer is placed on the substrate]. A thin layer of saltwater is placed between the substrate and the wafer to ensure electrical contact between the nominally planar wafer and substrate surfaces. The thin layer of saltwater also serves to mechanically bind the wafer temporarily to the substrate. The electrode has a tungsten tip $0.5 \mu\text{m}$ wide and is biased at a suitable potential with respect to the substrate (typically, $\approx 1.5 \text{ kV}$ for a $100\text{-}\mu\text{m}$ -thick LiNbO_3 crystal). The writing electrode is mounted on an x-y translation stage, which is used to move the electrode across the wafer surface in the desired pattern.

By varying the magnitude and dura-

tion of the applied voltage in conjunction with the motion or stationarity of the electrode, one can exert some control over the sizes and shapes of the ferroelectric domains. For example, it was

found that smooth lines having widths of the order of a few microns could be formed by applying potentials between 0.8 and 1.8 kV for times of the order of 10 s while the pen was moving, as illus-

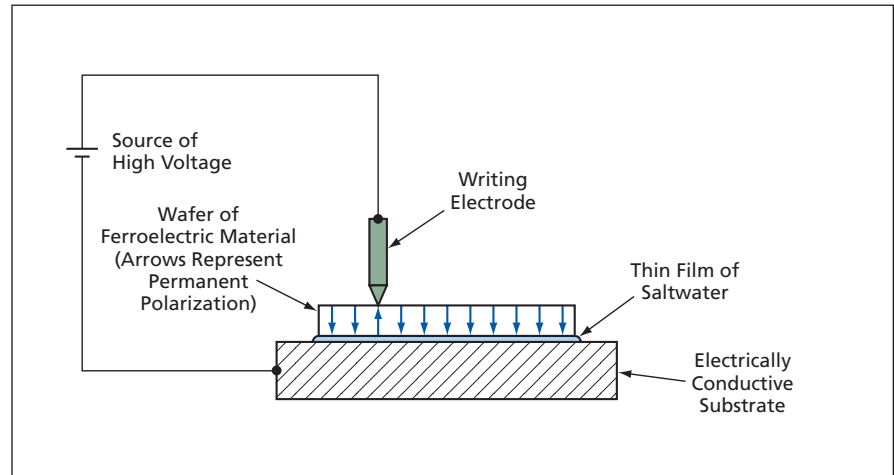


Figure 1. A **Sharp Electrode** applies a strong electric field to effect localized poling of the wafer. Used like a pen, the electrode is moved across the wafer to write a poling pattern.

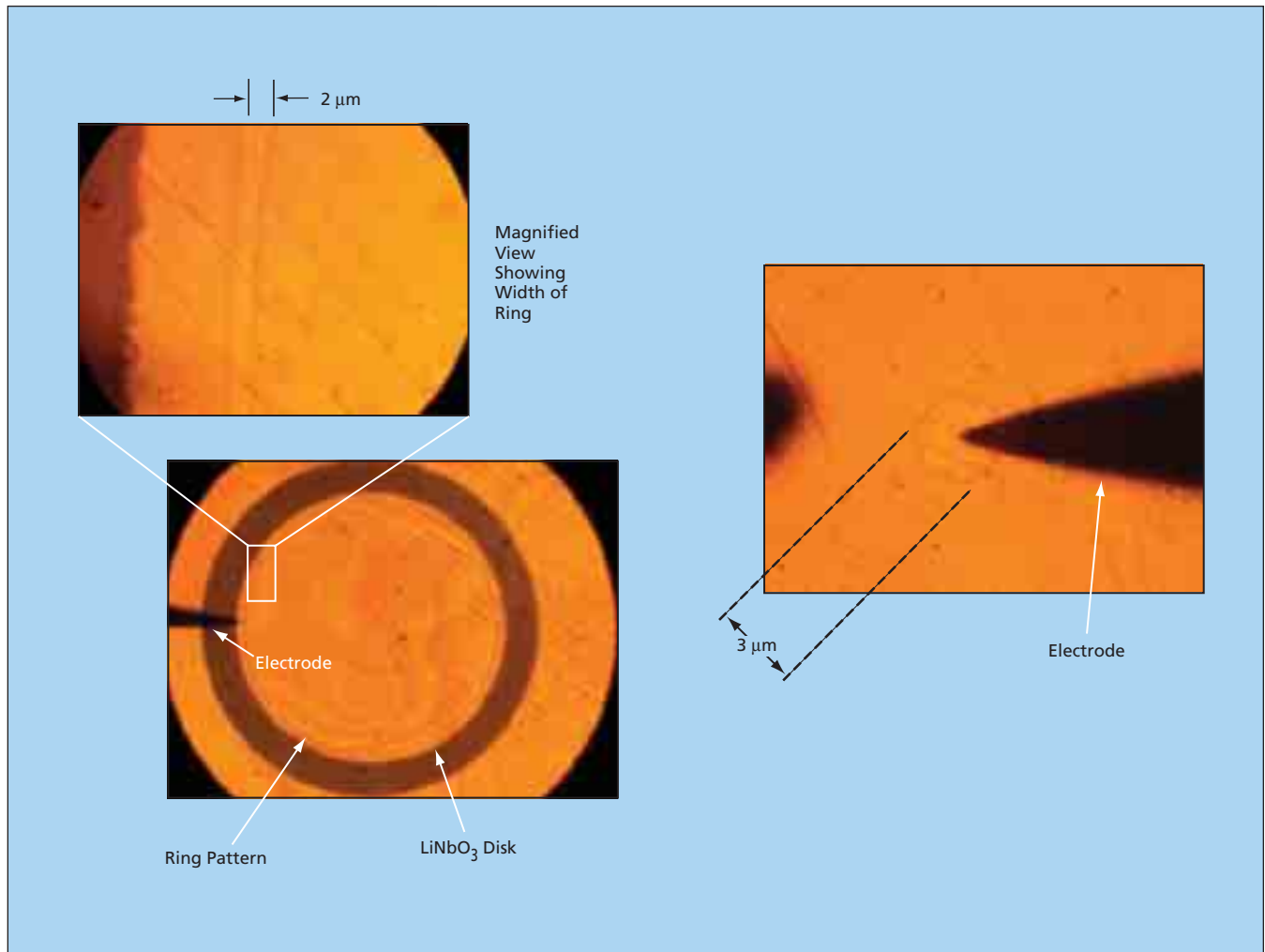


Figure 2. **These Are Two Examples** of patterns made by calligraphic poling. The images at the left show a $2\text{-}\mu\text{m}$ -wide ring formed on a $100\text{-}\mu\text{m}$ -thick LiNbO_3 disk at a potential of 1.8 kV applied during a writing time of 10 s . The image at the right shows a $3\text{-}\mu\text{m}$ -wide hexagonal domain formed on a $120\text{-}\mu\text{m}$ -thick LiNbO_3 crystal by use of a 2.5-kV bias applied to a stationary electrode for 1.5 s .

trated in the left part of the figure. For another example, it was found that potentials between 2 and 3 kV applied for times <2 s while the electrode was held stationary yield hexagons (a consequence of the crystalline structure of LiNbO_3), as illustrated in the right part of Figure 2.

Among the advantages of calligraphic poling is that it is possible to visually observe the domains in ordinary (that is, non-polarized) light as they are being formed. Light incident from above along the z-axis travels through the wafer and is reflected from its bottom surface. The poling electric field magni-

fies the gradient in the index of refraction between a +z and -z-poled region to such an extent as to give rise to a dark outline, coinciding with the boundary between the regions, that is visible in the reflected light when viewed from above through a conventional optical microscope. In addition, it is possible to view the domains nondestructively after they have been formed, because a potential sufficient to generate the dark outline (typically 200 V) is much smaller than the domain-reversal potential.

This work was done by Makan Mohageg, Dmitry Strelakov, Anatoliy Savchenkov, Adrey Matsko, Lute Maleki, and Vladimir

Ilchenko of Caltech for NASA's Jet Propulsion Laboratory.

In accordance with Public Law 96-517, the contractor has elected to retain title to this invention. Inquiries concerning rights for its commercial use should be addressed to:

*Innovative Technology Assets Management
JPL*

*Mail Stop 202-233
4800 Oak Grove Drive
Pasadena, CA 91109-8099
(818) 354-2240*

E-mail: iaoffice@jpl.nasa.gov

Refer to NPO-41566, volume and number of this NASA Tech Briefs issue, and the page number.

Blackbody Cavity for Calibrations at 200 to 273 K

Care must be taken to ensure high emissivity to minimize error.

Stennis Space Center, Mississippi

A laboratory blackbody cavity has been designed and built for calibrating infrared radiometers used to measure radiant temperatures in the range from about 200 to about 273 K. In this below-room-temperature range, scattering of background infrared radiation from room-temperature surfaces could, potentially, contribute significantly to the spectral radiance of the blackbody cavity, thereby contributing a significant error to the radiant temperature used as the calibration value. The spectral radiance error at wavelength λ is given by

$$[1 - \epsilon(\lambda)][B(T_c, \lambda) + B(T_a, \lambda)],$$

where $\epsilon(\lambda)$ is the effective spectral emissivity of the cavity, $B(T, \lambda)$ is the ideal spectral radiance of a body at absolute temperature T according to Planck's radiation law, T_c is

the temperature in the cavity, and T_a is the ambient temperature. Examining the above expression shows that by making $\epsilon(\lambda)$ as close as possible to unity, one can minimize the spectral-radiance error and the associated radiant-temperature error. For example, it has been calculated that to obtain a radiant-temperature error of 1 K or less at a cavity temperature of 200 K, ambient temperature of 300 K, and wavelength of 6 μm , one has $\epsilon(\lambda) > 0.999$ (see Figure 1). A 1 K radiant-temperature error is more than sufficient for atmospheric and cloud studies, which is a common application of infrared radiometers.

The present blackbody cavity is of an established type in which multiple

reflections from a combination of conical and cylindrical black-coated walls (see Figure 2) are exploited to obtain an effective emissivity greater than the emissivity value of the coating material on a flat exposed surface. The coating material in this case is a flat black paint that has an emissivity of approximately 0.91 in the thermal spectral range and was selected over other, higher-emissivity materials because of its ability to withstand thermal cycling. We found many black coatings cracked and flaked after thermal cycling due to differences in the coefficient of expansion. On the basis of theoretical calculations, the effective emissivity is expected to approach 0.999.

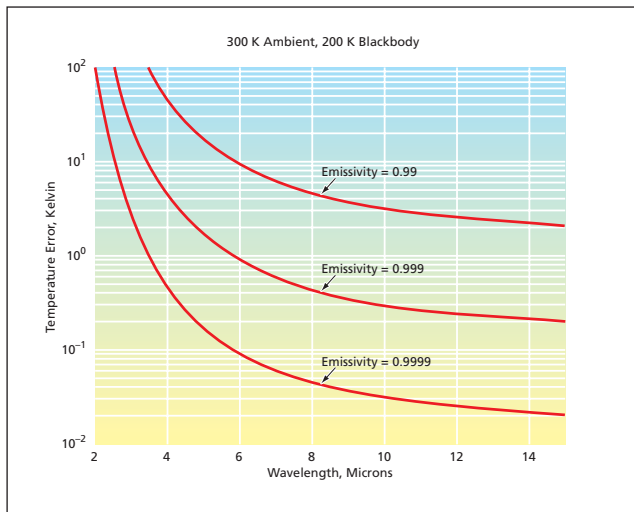


Figure 1. The Error in the Radiant Temperature as a function of wavelength was calculated for three different emissivity values for a cavity temperature of 200 K and ambient temperature of 300 K.

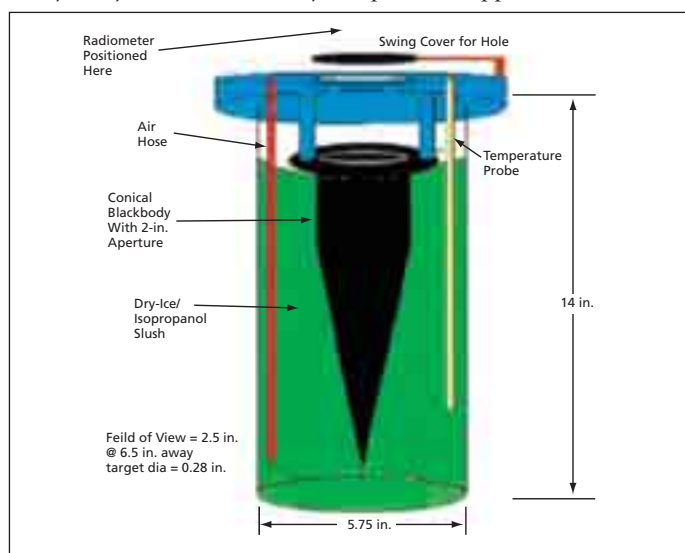


Figure 2. The Blackbody Cavity has a shape and size chosen as a compromise among maximizing the number of internal reflections, maximizing effective emissivity out to an acceptably large radius, and keeping the cone short enough to fit in a Dewar flask, as shown.

The cylindrical/conical shell enclosing the cavity is machined from copper, which is chosen for its high thermal conductivity. In use, the shell is oriented vertically, open end facing up, and inserted in a Dewar flask filled with isopropyl alcohol/dry-ice slush. A flange at the open end of the shell is supported by a thermally insulating ring on the lip of the Dewar flask. The slush cools the shell (and thus the blackbody cavity) to the desired temperature. Typically, the slush starts at a

temperature of about 194 K. The slush is stirred and warmed by bubbling dry air or nitrogen through it, thereby gradually increasing the temperature through the aforementioned calibration range during an interval of several hours. The temperature of the slush is monitored by use of a precise thermocouple probe. A comparison with an independently calibrated commercial radiometer with a thermocouple demonstrated less than a 1 K difference between a thermocouple in the slush

and the radiometer's output. The flow of dry air also acts as a purge to prevent airborne water vapor from frosting the conical and cylindrical cavity surfaces.

This work was done by Dane Howell, Robert Ryan, Jim Ryan, Dane Howell, Doug Henderson, and Larry Clayton of Stennis Space Center.

Inquiries concerning rights for the commercial use of this invention should be addressed to the Intellectual Property Manager, Stennis Space Center, (228) 688-1929. Refer to SSC-00193.

KML Super Overlay to WMS Translator

NASA's Jet Propulsion Laboratory, Pasadena, California

This translator is a server-based application that automatically generates KML super overlay configuration files required by Google Earth for map data access via the Open Geospatial Consortium WMS (Web Map Service) standard. The translator uses a set of URL parameters that mirror the WMS parameters as much as possible, and it also can generate a super overlay subdivision of any given area that is only loaded when needed, enabling very large areas of coverage at very high resolutions. It can

make almost any dataset available as a WMS service visible and usable in any KML application, without the need to reformat the data.

With the proper configuration, very large datasets that exist in WMS can become layers in a KML-enabled client. For example, Google Earth natively uses KML for data access and is both popular and available. This KML to WMS translator makes Google Earth act as a WMS client and can be used to make NASA remote sensing data more accessible, thus

enabling exploration, collaboration, and education efforts. Simulated or modeled data available in WMS can become available in KML. This tool can be used for remote imagery of other planets, the Moon, and Earth.

This program was written by Lucian Plesea of Caltech for NASA's Jet Propulsion Laboratory.

This software is available for commercial licensing. Please contact Karina Edmonds of the California Institute of Technology at (626) 395-2322. Refer to NPO-44684.

High-Performance Tiled WMS and KML Web Server

NASA's Jet Propulsion Laboratory, Pasadena, California

This software is an Apache 2.0 module implementing a high-performance map server to support interactive map viewers and virtual planet client software. It can be used in applications that require access to very-high-resolution geolocated images, such as GIS, virtual planet applications, and flight simulators. It serves Web Map Service (WMS) requests that comply with a given request grid from an existing tile dataset. It also generates

the KML super-overlay configuration files required to access the WMS image tiles. This server can sustain extremely high request rates with very short request latencies in both WMS and KML protocols. It does not require significant computer resources and can operate from read-only media.

This server makes it possible to support very demanding interactive or immersive applications that require geo-

graphically located data. It has direct applications for making NASA data such as remote sensing and modeled or simulated data available to applications like WorldWind or Google Earth.

This program was written by Lucian Plesea of Caltech for NASA's Jet Propulsion Laboratory.

This software is available for commercial licensing. Please contact Karina Edmonds of the California Institute of Technology at (626) 395-2322. Refer to NPO-44685.

Modeling of Radiative Transfer in Protostellar Disks

NASA's Jet Propulsion Laboratory, Pasadena, California

This program implements a spectral line, radiative transfer tool for interpreting Spitzer Space Telescope observations by matching them with models of

protostellar disks for improved understanding of planet and star formation. The Spitzer Space Telescope detects gas-phase molecules in the infrared spectra

of protostellar disks, with spectral lines carrying information on the chemical composition of the material from which planets form. Input to the software in-

cludes chemical models developed at JPL. The products are synthetic images and spectra for comparison with Spitzer measurements.

Radiative transfer in a protostellar disk is primarily affected by absorption and emission processes in the dust and in molecular gases such as H₂, CO, and HCO. The magnitude of the optical absorption and emission is determined by the population of the electronic, vibrational, and rotational energy levels. The population of the molecular level is in turn determined by the intensity of the

radiation field. Therefore, the intensity of the radiation field and the population of the molecular levels are interdependent quantities.

To meet the computational challenges of solving for the coupled radiation field and electronic level populations in disks having wide ranges of optical depths and spatial scales, the tool runs in parallel on the JPL Dell Cluster supercomputer with C++ and Fortran compiler with a Message Passing Interface. Because this software has been developed on a distributed com-

puting platform, the modeling of systems previously beyond the reach of available computational resources is possible.

This program was written by Paul Von Allmen and Neal Turner of Caltech for NASA's Jet Propulsion Laboratory. Further information is contained in a TSP (see page 1).

The software used in this innovation is available for commercial licensing. Please contact Karina Edmonds of the California Institute of Technology at (626) 395-2322. Refer to NPO-44467.

Composite Pulse Tube

Axial leakage of heat is reduced.

Lyndon B. Johnson Space Center, Houston, Texas

A modification of the design of the pulse tube in a pulse-tube cryocooler reduces axial thermal conductance while preserving radial thermal conductance. It is desirable to minimize axial thermal conductance in the pulse-tube wall to minimize leakage of heat between the warm and cold ends of the pulse tube. At the same time, it is desirable to maximize radial thermal conductance at the cold end of the pulse tube to ensure adequate thermal contact between (1) a heat exchanger in the form of a stack of copper screens inside the pulse tube at the cold end and (2) the remainder of the cold tip, which is the object to which the heat load is applied and from which heat must be removed. The modified design yields a low-heat-leak pulse tube that can be easily integrated with a cold tip.

A typical pulse tube of prior design is either a thin-walled metal tube or a metal tube with a nonmetallic lining. It

is desirable that the outer surface of a pulse tube be cylindrical (in contradistinction to tapered) to simplify the design of a regenerator that is also part of the cryocooler. Under some conditions, it is desirable to taper the inner surface of the pulse tube to reduce acoustic streaming. The combination of a cylindrical outer surface and a tapered inner surface can lead to unacceptably large axial conduction if the pulse tube is made entirely of metal. Making the pulse-tube wall of a nonmetallic, low-thermal-conductivity material would not solve the problem because the wall would not afford the needed thermal contact for the stack of screens in the cold end.

The modified design calls for fabricating the pulse tube in two parts: a longer, nonmetallic part that is tapered on the inside and cylindrical on the outside and a shorter, metallic part that is cylindrical on both the inside and the

outside. The nonmetallic part can be made from G-10 fiberglass-reinforced epoxy or other low-thermal-conductivity, cryogenically compatible material. The metallic part must have high thermal conductivity in the cryogenic temperature range and would typically be made of pure copper to satisfy this requirement. The metallic part is bonded to the nonmetallic part with epoxy. Copper screens are inserted in the metallic part to form the cold-end heat exchanger, then the assembled pulse tube is inserted in the cold tip.

This work was done by Jerry L. Martin and Jason H. Cloyd of Mesoscopic Devices, LLC for Johnson Space Center. For further information, contact:

*Jerry L. Martin
Mesoscopic Devices, LLC
510 Compton Street, Suite 106
Broomfield, CO 80020
Phone No.: (303) 466-6968
Refer to MSC-23522*

Photometric Calibration of Consumer Video Cameras

In imaging of point sources, dynamic ranges can be extended beyond saturation levels.

Marshall Space Flight Center, Alabama

Equipment and techniques have been developed to implement a method of photometric calibration of consumer video cameras for imaging of objects that are sufficiently narrow or sufficiently distant to be optically equivalent to point or line sources. Heretofore, it has been difficult to calibrate consumer video cameras,

especially in cases of image saturation, because they exhibit nonlinear responses with dynamic ranges much smaller than those of scientific-grade video cameras. The present method not only takes this difficulty in stride but also makes it possible to extend effective dynamic ranges to several powers of ten beyond saturation

levels. The method will likely be primarily useful in astronomical photometry. There are also potential commercial applications in medical and industrial imaging of point or line sources in the presence of saturation.

This development was prompted by the need to measure brightnesses of de-

bris in amateur video images of the breakup of the Space Shuttle Columbia. The purpose of these measurements is to use the brightness values to estimate relative masses of debris objects. In most of the images, the brightness of the main body of Columbia was found to exceed the dynamic ranges of the cameras. A similar problem arose a few years ago in the analysis of video images of Leonid meteors. The present method is a refined version of the calibration method developed to solve the Leonid calibration problem.

In this method, one performs an end-to-end calibration of the entire imaging system, including not only the imaging optics and imaging photodetector array but also analog tape recording and play-

back equipment (if used) and any frame grabber or other analog-to-digital converter (if used). To automatically incorporate the effects of nonlinearity and any other distortions into the calibration, the calibration images are processed in precisely the same manner as are the images of meteors, space-shuttle debris, or other objects that one seeks to analyze.

The light source used to generate the calibration images is an artificial variable star comprising a Newtonian collimator illuminated by a light source modulated by a rotating variable neutral-density filter. This source acts as a point source, the brightness of which varies at a known rate. A video camera to be calibrated is aimed at this source.

Fixed neutral-density filters are inserted in or removed from the light path as needed to make the video image of the source appear to fluctuate between dark and saturated bright. The resulting video-image data are analyzed by use of custom software that determines the integrated signal in each video frame and determines the system response curve (measured output signal versus input brightness). These determinations constitute the calibration, which is thereafter used in automatic, frame-by-frame processing of the data from the video images to be analyzed.

This work was done by Robert Suggs of Marshall Space Flight Center and Wesley Swift, Jr., of Raytheon Co. Further information is contained in a TSP (see page 1). MFS-32090-1

Criterion for Identifying Vortices in High-Pressure Flows

This criterion could enable appropriate comparisons between experiments and simulations.

NASA's Jet Propulsion Laboratory, Pasadena, California

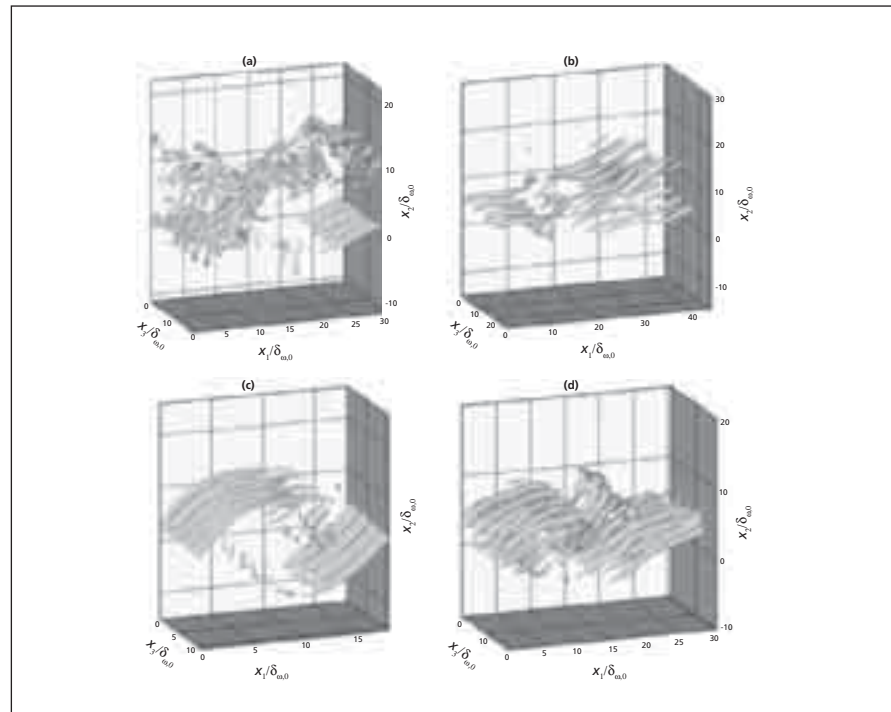
A study of four previously published computational criteria for identifying vortices in high-pressure flows has led to the selection of one of them as the best. This development can be expected to contribute to understanding of high-pressure flows, which occur in diverse settings, including diesel, gas turbine, and rocket engines and the atmospheres of Jupiter and other large gaseous planets.

Information on the atmospheres of gaseous planets consists mainly of visual and thermal images of the flows over the planets. Also, validation of recently proposed computational models of high-pressure flows entails comparison with measurements, which are mainly of visual nature. Heretofore, the interpretation of images of high-pressure flows to identify vortices has been based on experience with low-pressure flows. However, high-pressure flows have features distinct from those of low-pressure flows, particularly in regions of high pressure gradient magnitude caused by dynamic turbulent effects and by thermodynamic mixing of chemical species. Therefore, interpretations based on low-pressure behavior may lead to misidentification of vortices and other flow structures in high-pressure flows. The study reported here was performed in recognition of the need for one or more quantitative criteria for identifying coherent flow structures — especially vortices — from

previously generated flow-field data, to complement or supersede the determination of flow structures by visual inspection of instantaneous fields or flow animations. The focus in the study was on correlating visible images of flow features with various quantities computed from flow-field data.

The quantities involved in the four criteria considered in the study are the following:

- The discriminant of the deformation tensor;
- The second invariant of the deformation tensor;
- The intermediate eigenvalue of the



These Plots of Isosurfaces of positive values of the second invariant were generated from numerical simulations of two high-pressure mixing flows of heptane/nitrogen, (a) and (c), and two high-pressure mixing flows of oxygen/hydrogen (b) and (d).

symmetric tensor representing the sum of the square power of the strain-rate tensor and the square power of the rotation tensor; and

- The magnitude of the vorticity vector.

The criteria associated with the first three quantities are those inside a vortex core, the discriminant is positive, the second invariant is positive, and the intermediate eigenvalue is negative, respectively. The fourth criterion — taking magnitude of the vorticity as an indication of vortical activity — might intuitively seem to be a good choice, but it is subjective rather than objective because it entails subjective

selection of a threshold magnitude value for isolating flow structures of interest in high-vorticity regions.

These criteria were tested by use of a database generated in direct numerical simulations of high-pressure, binary-species-mixing flows undergoing transitions to turbulence. The quantities involved in the criteria were computed from the database, isosurfaces of these quantities were plotted, and plots were assessed with respect to utility in demarcating flow structures. Of the four criteria, that based on the second invariant was found to yield the most realistic plots of flow structures and to

capture structures in all regions of the flow.

The figure presents plots of the second invariant isosurfaces showing vortical features from four of the simulations. The diversity of the features is noticeable and has been interpreted as boding well for the extraction of vortical features from visual data and enabling appropriate comparisons between experimental and computationally simulated flows.

This work was done by Josette Bellan and Nora Okong'o of Caltech for NASA's Jet Propulsion Laboratory. For more information, contact iaoffice@jpl.nasa.gov NPO-41932

Amplified Thermionic Cooling Using Arrays of Nanowires

Cooling devices could be highly miniaturized.

NASA's Jet Propulsion Laboratory, Pasadena, California

A class of proposed thermionic cooling devices would incorporate precise arrays of metal nanowires as electron emitters. The proposed devices could be highly miniaturized, enabling removal of heat from locations, very close to electronic devices, that have previously been inaccessible for heat-removal purposes. The resulting enhancement of removal of heat would enable operation of the devices at higher power levels and higher clock speeds. Moreover, the mass, complexity, and bulk of electronic circuitry incorporating these highly miniaturized cooling devices could be considerably reduced, relative to otherwise equivalent circuitry cooled by conventional electromechanical, thermoelectric, and fluidic means.

In thermionic cooling, one exploits the fact that because only the highest-energy

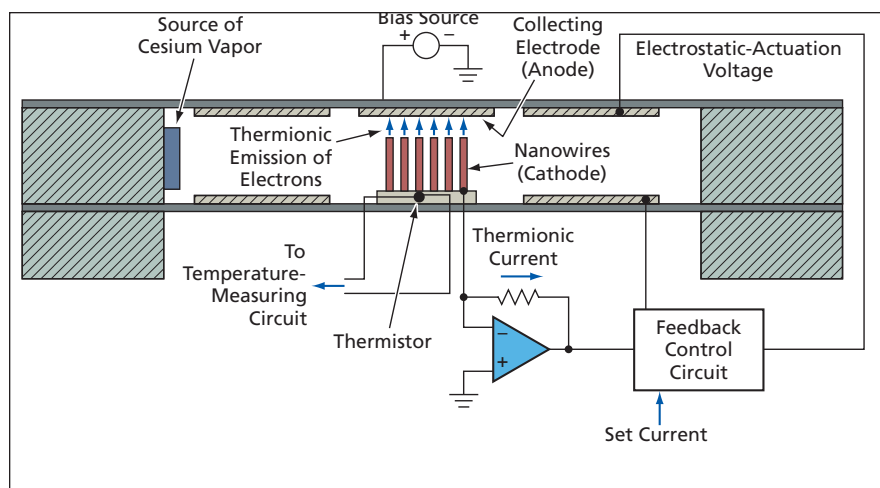
electrons are thermionically emitted, collecting those electrons to prevent their return to the emitting electrode results in the net removal of heat from that electrode. Collection is effected by applying an appropriate positive bias potential to another electrode placed near the emitting electrode.

The concept underlying the proposal is that the thermionic-emission current and, hence, the cooling effect attainable by use of an array of nanowires could be significantly greater than that attainable by use of a single emitting electrode or other electron-emitting surface. The wires in an array according to the proposal would protrude perpendicularly from a planar surface and their heights would be made uniform to within a sub-nanometer level of precision.

A process of growing metal nanotubes in alumina nanopores has already been demonstrated and would be incorporated into the following process for fabricating an array according to the proposal:

1. An aluminum layer would be deposited on a silicon nitride membrane mesh substrate, the central portion of which would be covered with a silicon island.
2. The aluminum layer would be oxidized to grow an alumina nanopore template on the silicon-island portion.
3. Metal nanowires would be grown inside the nanopores of the template by electrodeposition.
4. The exposed surface of the template and nanowires would be subjected to chemical-mechanical polishing.
5. The template would be etched away to expose the array of metal nanowires centered on the silicon island on the nitride membrane mesh substrate.

An experimental prototype array fabricated as described above would be further processed and tested as follows: A thermistor would be embedded in the island. The resulting assembly would be mounted in a vacuum chamber with electrical contacts to the array and the thermistor (see figure). In the vacuum chamber, cesium and/or other alkali metal(s) would be deposited on the nanowires to reduce their work function. The chamber would contain an upper membrane with metal-coated areas that would serve, respectively, as a collecting electrode (anode) and electrostatic-attraction electrodes. By means of electrostatic attraction with feedback



An Array of Nanowires would be coated with cesium and tested for effectiveness in thermionic cooling by use of an apparatus shown here in simplified schematic form.

control, this membrane would be pulled down to maintain a gap of the order of nanometers between the tips of the nanowires and the anode.

The bias potential would be applied to the anode and the temperature of the array (the cathode) would be measured by the thermistor. Because of the thermionic reduction of temperature is expected to be small in initial experiments, the sensitivity of measurement of this reduction would be enhanced by

use of a lock-in technique in which the bias potential would be modulated and the variation in temperature measured at the modulation frequency.

This work was done by Eui-Hyeok Yang, Daniel Choi, Kirill Shcheglov, and Yoshikazu Hishinuma of Caltech for NASA's Jet Propulsion Laboratory. Further information is contained in a TSP (see page 1).

In accordance with Public Law 96-517, the contractor has elected to retain title to this invention. Inquiries concerning rights

for its commercial use should be addressed to:

*Innovative Technology Assets Management
JPL*

Mail Stop 202-233

4800 Oak Grove Drive

Pasadena, CA 91109-8099

(818) 354-2240

E-mail: iaoffice@jpl.nasa.gov

Refer to NPO-42101, volume and number of this NASA Tech Briefs issue, and the page number.

Delamination-Indicating Thermal Barrier Coatings

Luminescent sublayers reveal previously hidden coating damage.

John H. Glenn Research Center, Cleveland, Ohio

The risk of premature failure of thermal barrier coatings (TBCs), typically composed of yttria-stabilized zirconia (YSZ), compromises the reliability of TBCs used to provide thermal protection for turbine engine components. Unfortunately, TBC delamination proceeds well beneath the TBC surface and cannot be monitored by visible inspection. Nondestructive diagnostic tools that could reliably probe the subsurface damage state of TBCs would alleviate the risk of TBC premature failure by indicating when the TBC needs to be replaced before the level of TBC damage threatens engine performance or safety. To meet this need, a new coating design for thermal barrier coatings (TBCs) that are self-indicating for delamination has been successfully implemented by incorporating a europium-doped luminescent sublayer at the base of a TBC composed of YSZ. The luminescent sublayer has the same YSZ composition as the rest of the TBC except for the addition of low-level europium doping and therefore does not alter TBC performance.

The strategy for producing delamination-indicating TBCs relies on the enhanced luminescence produced by regions of the TBC where subsurface cracks are propagating. This enhanced luminescence is due to a large fraction of the excited luminescence that is incident upon the crack at an angle beyond the angle for total internal reflection. Deposition of 125- μm thick TBCs above a 7- μm thick europium-doped layer was performed in collaboration with Penn State University. These self-indicating TBCs were deposited by multiple-ingot electron-beam physical-vapor deposition without disrupting TBC growth so as not

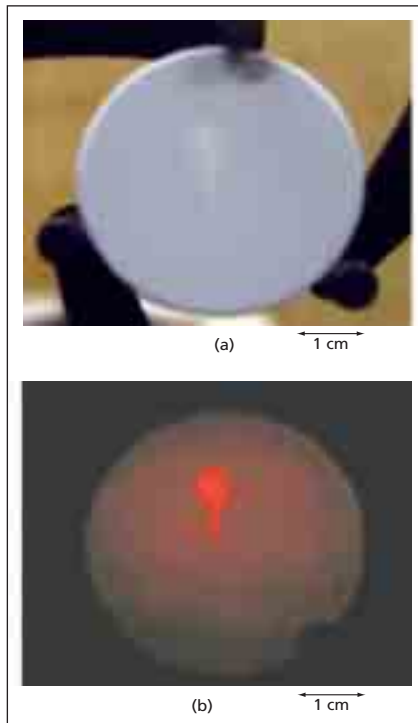
to alter the usual columnar growth that gives these TBCs many of their desirable properties. To demonstrate delamination indication, localized TBC delamination was induced by scratching the coating with a stylus.

While the delaminated region can be faintly discriminated in a standard white-light image [part (a) in the figure], the delaminated region stands out strongly in a luminescence image due to the greatly enhanced red emission originating from that area [part (b) in the fig-

ure]. The enhanced luminescence from the europium-doped sublayer was caused by total internal reflection of a large fraction of both the 532-nm excitation and the 606-nm emission wavelengths at the TBC/crack interface. Typically, luminescence is enhanced from delaminated regions by about a factor of three for electron-beam physical vapor deposited TBCs and by an incredible factor of about 100 for plasma-sprayed TBCs. Luminescence imaging was very simple to implement and can be achieved using only light-emitting-diode illumination source and a camera with a band-pass filter. High-resolution luminescence images were obtained within a few seconds that immediately identified regions of TBC delamination that would otherwise be difficult to detect, thereby showing great promise for routine inspection of TBCs.

Future work will concentrate on developing delamination-indicating TBCs with near-infrared-luminescent sublayers. Because TBCs are much more transparent at near-infrared wavelengths than at visible wavelengths, luminescence can then be detected with less attenuation and from much greater coating depths. The prime candidate dopants for near-infrared luminescence are erbium and neodymium, which luminesce at 1.55- and 1.06- μm wavelength, respectively.

This work was done by Jeffrey I. Eldridge of Glenn Research Center. Further information is contained in a TSP (see page 1). Inquiries concerning rights for the commercial use of this invention should be addressed to NASA Glenn Research Center, Innovative Partnerships Office, Attn: Steve Fedor, Mail Stop 4-8, 21000 Brookpark Road, Cleveland, Ohio 44135. Refer to LEW-17929-1/30-1.



Delamination-Indicating Thermal Barrier Coating is examined as (a) white-light image and (b) Eu^{3+} luminescence image. Enhanced Eu^{3+} 606 nm (red) luminescence detected from scratched region of TBC readily reveals subsurface delamination.



Preventing Raman Lasing in High-*Q* WGM Resonators

Raman-lasing threshold power is increased through suitable choice of dimensions.

NASA's Jet Propulsion Laboratory, Pasadena, California

A generic design has been conceived to suppress the Raman effect in whispering-gallery-mode (WGM) optical resonators that have high values of the resonance quality factor (*Q*). Although it is possible to exploit the Raman effect (even striving to maximize the Raman gain to obtain Raman lasing), the present innovation is intended to satisfy a need that arises in applications in which the Raman effect inhibits the realization of the full potential of WGM resonators as frequency-selection components. Heretofore, in such applications, it has been necessary to operate high-*Q* WGM resonators at unattractively low power levels to prevent Raman lasing. (The Raman-lasing thresholds of WGM optical resonators are very low and are approximately proportional to Q^{-2} .)

Heretofore, two ways of preventing Raman lasing at high power levels have been known, but both entail significant disadvantages:

- A resonator can be designed so that the optical field is spread over a relatively large mode volume to bring the power density below the threshold. For any given combination of *Q* and power level, there is certain mode volume wherein Raman lasing does not start. Unfortunately, a resonator that has a large mode volume also has a high spectral density, which is undesirable in a typical photonic application.
- A resonator can be cooled to the tem-

perature of liquid helium, where the Raman spectrum is narrower and, therefore, the Raman gain is lower. However, liquid-helium cooling is inconvenient.

The present design overcomes these disadvantages, making it possible to operate a low-spectral-density (even a single-mode) WGM resonator at a relatively high power level at room temperature, without risk of Raman lasing.

The present design exploits the following two physical principles:

- There is a wavelength interval between the optical pump signal (in this case, the optical signal at the desired resonance frequency) and the Raman signal emitted by the resonator material in response to the pump signal. For a CaF₂ resonator, this wavelength interval is ≈80 nm; for a diamond resonator, this wavelength interval is ≈400 nm.
- In a single-mode resonator, there is a cutoff frequency — a minimum frequency at which the optical mode is still confined and has high material-limited value of *Q*. At lower frequency, *Q* is limited by leakage of the partially confined mode to the environment.

The essence of the present design is to choose the dimensions of a single-mode WGM resonator to place the cutoff frequency between the pump and Raman frequencies. For example, if the resonator is to be made of diamond and to

have a resonance wavelength of 1,550 nm, then its dimensions should be chosen to place the cutoff wavelength between 1,550 nm and the Raman wavelength of 1,550 + 400 = 1,950 nm. Preferably, the cutoff wavelength should be set at or near 1,750 nm. The basic inequality that expresses the required relationship among the wavelengths and dimensions for a WGM resonator like the one in the figure is

$$\lambda_p < 2L(2\epsilon h/R)^{1/2} < \lambda_R,$$

where λ_p is the pump wavelength, *L* is the axial length of the resonator, ϵ is the relative permittivity of the resonator material, *h* is the radial depth of the groove that separates the resonator from the rest of the rod of resonator material, *R* is the radius of the rod, and λ_R is the Raman wavelength.

In a resonator designed in this way, the value of *Q* at the Raman lasing wavelength is a fraction, $1/\rho$, of the value of *Q* in an otherwise identical WGM resonator that has not been designed to place the cutoff wavelength between the pump and Raman wavelengths. Consequently, the Raman-lasing threshold power is about ρ^2 times as high as it is in the absence of this innovation.

This work was done by Anatoliy Savchenkov, Andrey Matsko, Dmitry Strekalov, and Lute Maleki of Caltech for NASA's Jet Propulsion Laboratory. Further information is contained in a TSP (see page 1). NPO-43334



Procedures for Tuning a Multiresonator Photonic Filter

A desired high-order filter function can be established and maintained.

NASA's Jet Propulsion Laboratory, Pasadena, California

Two procedures have been devised for tuning a photonic filter that comprises multiple whispering-gallery-mode (WGM) disk resonators. As used here, "tuning" signifies locking the filter to a specific laser frequency and configuring the filter to obtain a desired high-order transfer function.

The main problem in tuning such a filter is how to select the correct relative loading of the resonators to realize a prescribed filter function. The first of the two procedures solves this problem.

As temperature gradients develop during operation, the spectra of individual resonators tend to drift, primarily because of the thermorefractive effect. Thus, there arises the additional problem of how to adjust the tuning during operation to maintain the desired transfer function. The second of the two procedures solves this problem.

To implement the procedures, it is necessary to incorporate the resonators into an apparatus like that of Figure 1. In this apparatus, the spectrum of each

resonator can be adjusted individually, via the electro-optical effect, by adjusting a bias voltage applied to that resonator. In addition, the positions of the coupling prisms and resonators can be adjusted to increase or reduce the gaps between them, thereby reducing or increasing, respectively, the optical coupling between them. The optical power (P_i) in resonator *i* is monitored by use of a tracking photodiode. Another tracking diode monitors the power reflected from the input terminal (P_r),

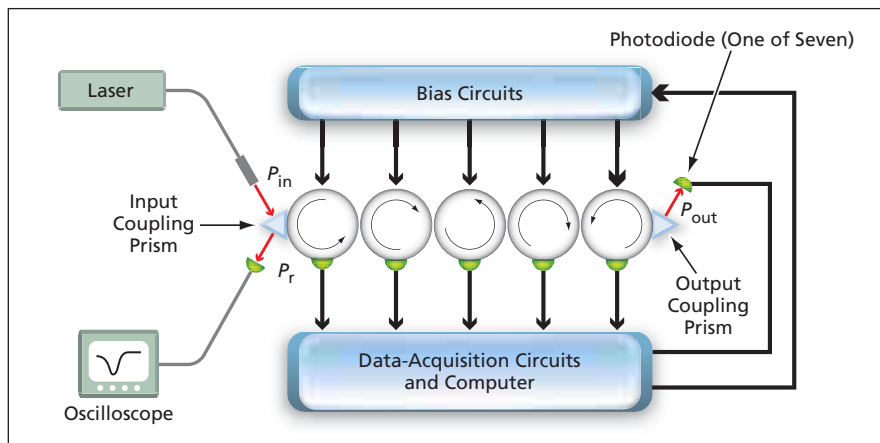


Figure 1. Five WGM Resonators are arranged to form a filter chain. Through adjustment of gaps and voltages, guided by monitoring of optical power levels, desired transfer function (P_{out}/P_{in} versus frequency detuning) can be obtained. The underlying principles of design and operation are also applicable to a chain of more or fewer than five WGM resonators.

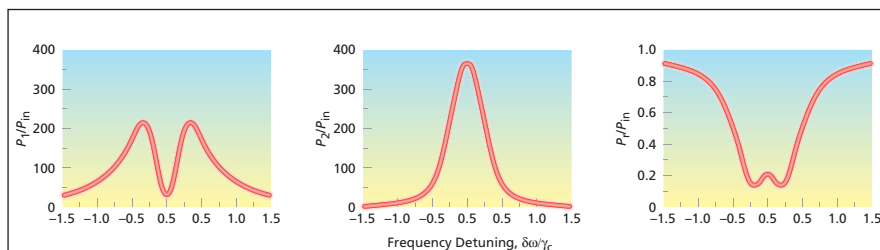


Figure 2. These Curves Represent Optimal Coupling of the first two resonators in an intermediate step toward realizing a fifth-order Butterworth filter. On the abscissa, $\delta\omega$ denotes the frequency detuning and γ_c denotes the full frequency width of the resonance spectral peak at half maximum in the fully loaded condition.

and still others monitor the input power (P_{in}) and output power (P_o). The readings of these photodiodes are used to guide the tuning adjustments described below.

The steps of the first procedure are the following:

1. Uncouple all the resonators and prisms by increasing all the gaps.
2. Overload resonator 1 with the input coupling prism, then measure the input power (P_{in}), reflected power (P_r), and the power in resonator 1 (P_1) as functions of frequency detuning from resonance, and use the measure-

ment data to determine the resonance quality factor (Q).

3. Couple resonator 2 to resonator 1, then measure P_{in} , P_r , P_1 , and P_2 as functions of frequency detuning from resonance. Adjust the gap between resonators 1 and 2 until P_r/P_{in} , P_1/P_{in} , and P_2/P_{in} as functions of frequency detuning match a set of theoretical template functions (see Figure 2) calculated to contribute to the desired high-order transfer function.
4. Couple resonator 3 to resonator 2, then measure P_{in} , P_r , P_1 , P_2 , and P_3 as functions of frequency detuning from reso-

nance. Adjust the gap between resonators 2 and 3 until P_r/P_{in} , P_1/P_{in} , and P_2/P_{in} as functions of frequency detuning match a different set of theoretical template functions calculated to contribute to the desired high-order transfer function.

5. Repeat step 4, each time adding the next resonator (and then adding the output coupling prism after the last resonator has been added) and adjusting the gaps to obtain the desired responses.

The steps of the second procedure are the following:

1. Measure and tabulate the dependence of each resonance frequency of each resonator on the bias voltage applied to that resonator.
2. Introduce, into the filter operation, "dark" periods, during which the laser and the resonators are scanned over some finite frequency band.
3. During a dark period, apply a specified voltage to resonator 1 to shift its resonance frequency by some amount. Measure the shift, then compensate it by applying another voltage to shift the resonance to the middle of the scan of the laser frequency.
4. Repeat step 3 for resonator 2 and subsequent resonators except the last one.
5. Adjust the voltage on the last resonator to scan its frequency until the filter exhibits maximum transmission, at which point the desired high-order transfer function has been restored.

This work was done by Andrey Matsko, Anatoliy Savchenkov, Dmitry Strelakov, and Lute Maleki of Caltech for NASA's Jet Propulsion Laboratory. Further information is contained in a TSP (see page 1).

The software used in this innovation is available for commercial licensing. Please contact Karina Edmonds of the California Institute of Technology at (626) 395-2322. Refer to NPO-43872.

Robust Mapping of Incoherent Fiber-Optic Bundles

Images scrambled by the bundles can be unscrambled.

Marshall Space Flight Center, Alabama

A method and apparatus for mapping between the positions of fibers at opposite ends of incoherent fiber-optic bundles have been invented to enable the use of such bundles to transmit images in visible or infrared light. The method is robust in the sense that it provides useful mapping even for a bundle that contains thousands

of narrow, irregularly packed fibers, some of which may be defective.

In a coherent fiber-optic bundle, the input and output ends of each fiber lie at identical positions in the input and output planes; therefore, the bundle can be used to transmit images without further modification. Unfortunately, the

fabrication of coherent fiber-optic bundles is too labor-intensive and expensive for many applications. An incoherent fiber-optic bundle can be fabricated more easily and at lower cost, but it produces a scrambled image because the position of the end of each fiber in the input plane is generally different from

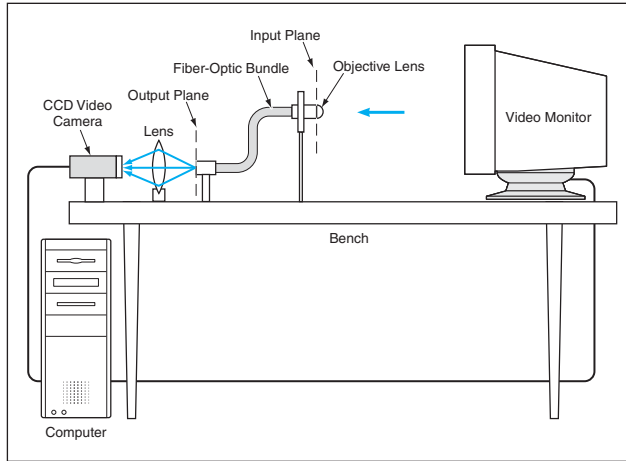


Figure 1. Test Patterns Are Generated on the video monitor and imaged onto the input end of the fiber-optic bundle. The resulting scrambled images that appear on the output end of the bundle are analyzed to determine a mapping between the input and output fiber ends.

the end of the same fiber in the output plane. However, the image transmitted by an incoherent fiber-optic bundle can be unscrambled (or, from a different perspective, decoded) by digital processing of the output image if the mapping between the input and output fiber-end positions is known. Thus, the present invention enables the use of relatively inexpensive fiber-optic bundles to transmit images.

The invention calls for a two-part calibration or mapping process. Part 1 of the process (ordinarily performed by the fiber-bundle supplier) takes place on the apparatus depicted in Figure 1. A computer that controls the apparatus and processes its measurement causes a video monitor to generate a test pattern described below. The input end of the fiber-optic bundle is equipped with an objective lens and is positioned so that the test pattern on the video monitor is focused onto the input plane. Another lens focuses the image from the output plane onto a charge-coupled-device (CCD) video camera. The output of the camera is digitized and fed to a frame grabber in the computer.

At first, the test pattern is a solid bright screen, so that the output ends of all the fibers (except the defective ones) appear bright. The digitized image of the output plane is subjected to a sequence of digital processing steps in which the centroids of the output-fiber-end subimages are computed, as illustrated in the upper part of Figure 2. Thereafter, these centroids are deemed to be the positions of the output fiber ends for the purpose of mapping.

As shown in the lower part of Figure 2, a test pattern in the form of a bright horizontal line is then swept vertically across the input end, in increments correspon-

ding to one pixel of the CCD; at each increment of position, the brightness at each pixel location on the CCD is recorded. Next, the same thing is done with a test pattern in the form of a bright vertical line swept horizontally. On the basis of the brightness-vs.-pixel-position data from the horizontal and vertical sweeps, the horizontal and vertical line positions that result in maximum brightnesses at the

previously determined centroids are computed. These horizontal and vertical line positions are converted to coordinates of fiber ends on the input plane. Thus, the relationship between the coordinates of the input and output ends of each and every fiber (not including defective fibers) is established. This relationship, which is the desired mapping, is recorded in a lookup table (LUT). Each fiber-optic bundle is characterized by a unique LUT.

The mapping as determined thus far is unique to the pixel coordinate system and the setup of the mapping apparatus; as such, the mapping is subject to change along with changes in magnification, translation, and rotation of images when the fiber bundle is removed from the mapping apparatus and installed in another apparatus in which it

is to be used to transmit images. The mapping as determined thus far is also subject to change associated with focus adjustments, change of the CCD camera, or insertion or removal of an infrared or visible-light filter in the image-transmission system.

Part 2 of the calibration process involves a partial remapping to compensate for such changes. Part 2 (ordinarily performed by the end user) takes place once the fiber-optic bundle has been installed in the imaging system. The input end of the bundle is illuminated with a solid bright test pattern and the user visually compares the video image of the output end with the corresponding image recorded previously in the first step of Part 1. The user identifies the ends of four fibers in the two images for use as fiducial points. Then software computes a preliminary new LUT based on the previous LUT and the coordinates of the fiducial points in the previous and present coordinate systems. The new LUT can be tested visually by computing the output fiber centroids and overlaying them on the video image. If necessary, the transformation coefficients can be modified in an iterative subprocess until the fiber centroids computed by use of the new LUT appear to lie at the centers of the fibers in the video image.

This work was done by Harry E. Roberts, Brent E. Deason, Charles P. DePlachett, Robert A. Pilgrim, and Harold S. Sanford of SRS Technologies for Marshall Space Flight Center. Further information is contained in a TSP (see page 1). MFS-31520

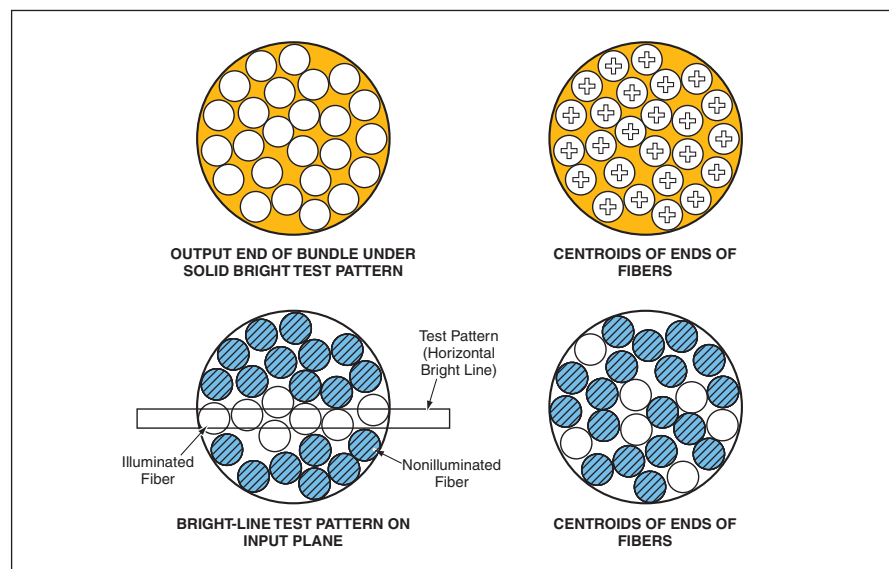


Figure 2. Centroids of Output Fiber Ends are computed in the first step of part 1 of the calibration procedure. The relationship between coordinates of input and output ends is determined from image data acquired in sweeps of horizontal and vertical bright lines across the input plane.

Extended-Range Ultrarefractive 1D Photonic Crystal Prisms

Practical applications could include miniature spectrometers and wavelength-division multiplexers.

NASA's Jet Propulsion Laboratory, Pasadena, California

A proposal has been made to exploit the special wavelength-dispersive characteristics of devices of the type described in "One-Dimensional Photonic Crystal Superprisms" (NPO-30232) *NASA Tech Briefs*, Vol. 29, No. 4 (April 2005), page 10a. A photonic crystal is an optical component that has a periodic structure comprising two dielectric materials with high dielectric contrast (e.g., a semiconductor and air), with geometrical feature sizes comparable to or smaller than light wavelengths of interest.

Experimental superprisms have been realized as photonic crystals having three-dimensional (3D) structures comprising regions of amorphous Si alternating with regions of SiO₂, fabricated in a complex process that included sputtering. A photonic crystal of the type to be exploited according to the present proposal is said to be one-dimensional (1D) because its contrasting dielectric materials would be stacked in parallel planar layers; in other words, there would be spatial periodicity in one dimension only. The processes of designing and fabricating 1D photonic crystal superprisms would be simpler and, hence, would cost less than do those for 3D photonic crystal superprisms. As in 3D structures, 1D photonic crystals may be used in applications such as wavelength-division multiplexing. In the extended-range configuration (see Figure 1), it is also suitable for spectrometry applications.

As an engineered structure or artificially engineered material, a photonic crystal can exhibit optical properties not commonly found in natural substances. Prior research had revealed several classes of photonic crystal structures for which the propagation of electromagnetic radiation is forbidden in certain frequency ranges, denoted photonic bandgaps. It had also been found that in narrow frequency bands just outside the photonic bandgaps, the angular wavelength dispersion of electromagnetic waves propagating in photonic crystal superprisms is much stronger than is the angular wavelength dispersion obtained by use of conventional prisms and diffraction gratings and is highly nonlinear.

In recent theoretical calculations leading to the present proposal, it was

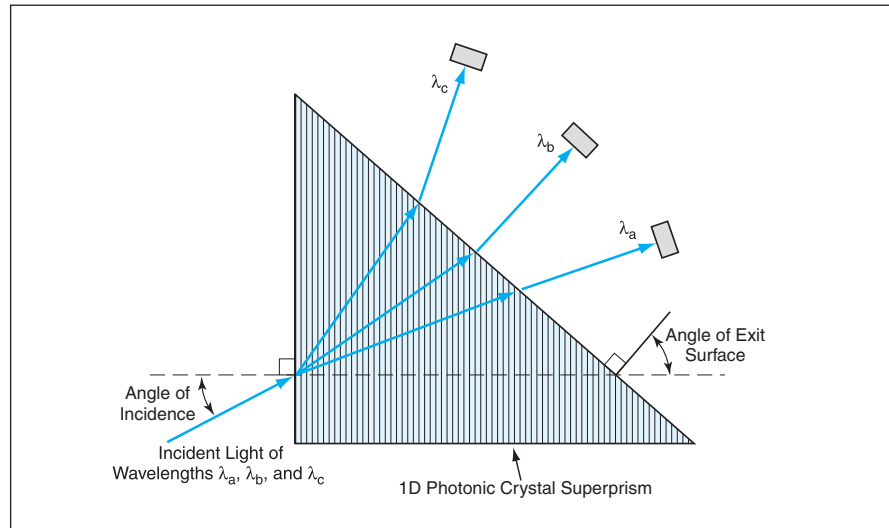


Figure 1. A **Miniature Spectrometer** could be constructed by combining a 1D photonic crystal superprism with suitably positioned photodetectors. The 1D photonic crystal superprism would function somewhat like a conventional glass prism, but the degree of its wavelength dispersion would be much greater and its design could be tailored to obtain unusual dispersive characteristics.

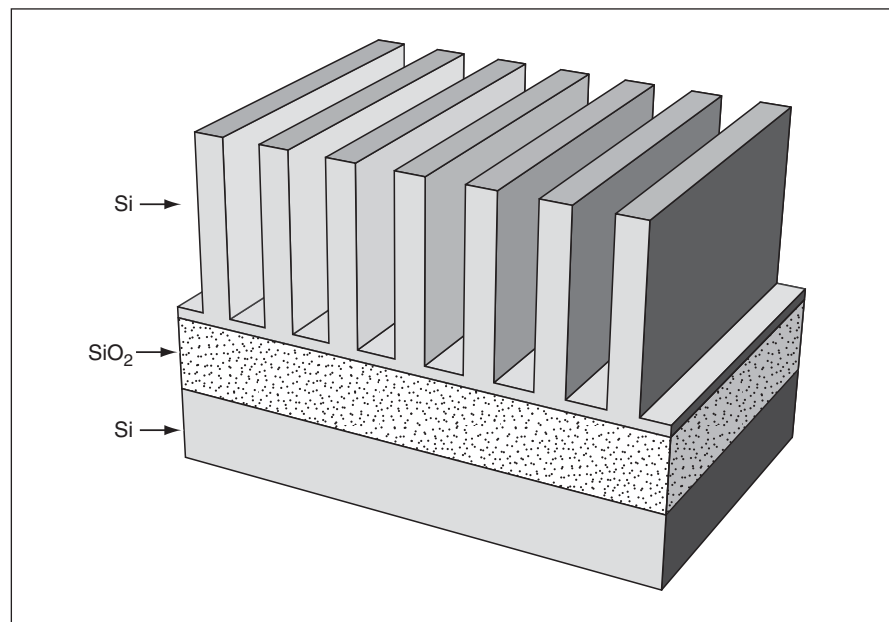


Figure 2. A **1D Photonic Crystal**, made of alternating layers of silicon and air, could be fabricated on a silicon-on-insulator substrate.

found that in the extended-range configurations, the 1D photonic crystal prism exhibits very strong wavelength dispersion properties over wavelength ranges covering entire photonic bands, rather than at the band edges only. The dependence of angular dispersion as a function of wavelength is also found to be less non-linear. While the

wavelength dispersing capability in the extended-range configuration is not as dramatic as in the narrow-range (band-edge only) ultra-refractive configuration, it is still calculated to be over one order of magnitude stronger than that of the conventional prism.

Hence, in designing photonic crystal superprisms to effect wavelength disper-

sion of polychromatic light, it would be possible to utilize broader wavelength ranges, maintain high transmissivity through use of wavelengths farther from the edges of the photonic bandgaps, take advantage of the reduction in non-linearity to simplify the positioning of optical components, and take advantage of larger crystal spatial periods to further simplify fabrication. The design parameters that could be varied to obtain the desired properties include the angle

of incidence, the angle of the exit surface, and the thicknesses of the layers.

One-dimensional photonic crystal superprisms for visible and infrared wavelengths could be fabricated on semiconductor wafers and, hence, could be integrated monolithically with other miniature optical components. In one example of this approach, a 1D photonic crystal superprism would be fabricated by patterning and anisotropic etching of one of two silicon layers of a silicon-on-in-

ulator substrate (see Figure 2). In this case, the insulator (SiO_2) would not only provide structural support, because the index of refraction of SiO_2 is lower than that of Si, the SiO_2 layer would also act as an optical cladding layer to confine light to the 1D photonic crystal.

This work was done by David Z. Ting of Caltech for NASA's Jet Propulsion Laboratory. Further information is contained in a TSP (see page 1). NPO-30594

Rapid Analysis of Mass Distribution of Radiation Shielding

Lyndon B. Johnson Space Center, Houston, Texas

Radiation Shielding Evaluation Toolset (RADSET) is a computer program that rapidly calculates the spatial distribution of mass of an arbitrary structure for use in ray-tracing analysis of the radiation-shielding properties of the structure. RADSET was written to be used in conjunction with unmodified commercial computer-aided design

(CAD) software that provides access to data on the structure and generates selected three-dimensional-appearing views of the structure. RADSET obtains raw geometric, material, and mass data on the structure from the CAD software. From these data, RADSET calculates the distribution(s) of the masses of specific materials about any user-specified

point(s). The results of these mass-distribution calculations are imported back into the CAD computing environment, wherein the radiation-shielding calculations are performed.

This program was written by Edward Zapp of Lockheed Martin Corp. for Johnson Space Center. Further information is contained in a TSP (see page 1). MSC-23935

Modeling Magnetic Properties in EZTB

NASA's Jet Propulsion Laboratory, Pasadena, California

A software module that calculates magnetic properties of a semiconducting material has been written for incorporation into, and execution within, the Easy (Modular) Tight-Binding (EZTB) software infrastructure. [EZTB is designed to model the electronic structures of semiconductor devices ranging from bulk semiconductors, to quantum wells, quantum wires, and quantum dots. EZTB implements an empirical tight-binding mathematical model of the underlying physics.]

This module can model the effect of a magnetic field applied along any direction and does not require any adjustment of model parameters. The module has thus far been applied to study the performances of silicon-based quantum computers in the presence of magnetic fields and of miscut angles in quantum wells. The module is expected to assist experimentalists in fabricating a spin qubit in a Si/SiGe quantum dot. This software can be executed in almost any Unix operating

system, utilizes parallel computing, can be run as a Web-portal application program. The module has been validated by comparison of its predictions with experimental data available in the literature.

This program was written by Seungwon Lee and Paul von Allmen of Caltech for NASA's Jet Propulsion Laboratory.

This software is available for commercial licensing. Please contact Karina Edmonds of the California Institute of Technology at (626) 395-2322. Refer to NPO-44782.

Deep Space Network Antenna Logic Controller

NASA's Jet Propulsion Laboratory, Pasadena, California

The Antenna Logic Controller (ALC) software controls and monitors the motion control equipment of the 4,000-metric-ton structure of the Deep Space Network 70-meter antenna. This program coordinates the control of 42 hydraulic pumps, while monitoring several interlocks for personnel and equipment safety. Remote operation of the ALC runs via the Antenna Monitor &

Control (AMC) computer, which orchestrates the tracking functions of the entire antenna.

This software provides a graphical user interface for local control, monitoring, and identification of faults as well as, at a high level, providing for the digital control of the axis brakes so that the servo of the AMC may control the motion of the antenna. Specific

functions of the ALC also include routines for startup in cold weather, controlled shutdown for both normal and fault situations, and pump switching on failure.

The increased monitoring, the ability to trend key performance characteristics, the improved fault detection and recovery, the centralization of all control at a single panel, and the simplifi-

cation of the user interface have all reduced the required workforce to run 70-meter antennas. The ALC also increases the antenna availability by reducing the time required to start up the antenna, to diagnose faults, and by providing additional insight into the performance of key parameters that aid in preventive maintenance to avoid key element failure.

The ALC User Display (AUD) is a graphical user interface with hierarchi-

cal display structure, which provides high-level status information to the operation of the ALC, as well as detailed information for virtually all aspects of the ALC via drill-down displays. The operational status of an item, be it a function or assembly, is shown in the higher-level display. By pressing the item on the display screen, a new screen opens to show more detail of the function/assembly. Navigation tools and the map button allow immediate access to all screens.

This program was written by Harlow Ahlstrom, Scott Morgan, Peter Hames, Martha Strain, Christopher Owen, and Kenneth Shimizu of Caltech; Karen Wilson, David Shaller, and Said Doktormontaz of Modern Technologies Corp.; and Patrick Leung of Northrop Grumman Corp. for NASA's Jet Propulsion Laboratory.

This software is available for commercial licensing. Please contact Karina Edmonds of the California Institute of Technology at (626) 395-2322. Refer to NPO-44341.

Modeling Carbon and Hydrocarbon Molecular Structures in EZTB

NASA's Jet Propulsion Laboratory, Pasadena, California

A software module that models the electronic and mechanical aspects of hydrocarbon molecules and carbon molecular structures on the basis of first principles has been written for incorporation into, and execution within, the Easy (Modular) Tight-Binding (EZTB) software infrastructure, which is summarized briefly in the immediately preceding article. Of particular interest, this module can model carbon crystals and nanotubes characterized by

various coordinates and containing defects, without need to adjust parameters of the physical model.

The module has been used to study the changes in electronic properties of carbon nanotubes, caused by bending of the nanotubes, for potential utility as the basis of a nonvolatile, electric-charge-free memory devices. For example, in one application of the module, it was found that an initially 50-nm-long carbon, (10,10)-chirality nan-

otube, which is a metallic conductor when straight, becomes a semiconductor with an energy gap of ≈ 3 meV when bent to a lateral displacement of 4 nm at the middle.

This program was written by Seungwon Lee and Paul von Allmen of Caltech for NASA's Jet Propulsion Laboratory.

This software is available for commercial licensing. Please contact Karina Edmonds of the California Institute of Technology at (626) 395-2322. Refer to NPO-44781.

BigView Image Viewing on Tiled Displays

Ames Research Center, Moffett Field, California

BigView allows for interactive panning and zooming of images of arbitrary size on desktop PCs running Linux. Additionally, it can work in a multi-screen environment where multiple PCs cooperate to view a single, large image. Using this software, one can explore — on relatively modest machines — images such as the Mars Orbiter Camera mosaic [92,160×33,280 pixels].

The images must be first converted into “paged” format, where the image is stored in 256×256 “pages” to allow rapid movement of pixels into texture memory. The format contains an “image pyramid”: a set of scaled versions of the original image. Each scaled image is 1/2 the size of the previous, starting with the original down

to the smallest, which fits into a single 256×256 page.

This program was written by Timothy Sandstrom of Advanced Management Technology for Ames Research Center. For further information, access <http://opensource.arc.nasa.gov/> or contact the Ames Technology Partnerships Division at (650) 604-2954. ARC-15277-1

Imaging Sensor Flight and Test Equipment Software

Marshall Space Flight Center, Alabama

The Lightning Imaging Sensor (LIS) is one of the components onboard the Tropical Rainfall Measuring Mission (TRMM) satellite, and was designed to detect and locate lightning over the tropics. The LIS flight code was devel-

oped to run on a single onboard digital signal processor, and has operated the LIS instrument since 1997 when the TRMM satellite was launched.

The software provides controller functions to the LIS Real-Time Event

Processor (RTEP) and onboard heaters, collects the lightning event data from the RTEP, compresses and formats the data for downlink to the satellite, collects housekeeping data and formats the data for downlink to

the satellite, provides command processing and interface to the spacecraft communications and data bus, and provides watchdog functions for error detection.

The Special Test Equipment (STE) software was designed to operate specific test equipment used to support the LIS hardware through development, calibration, qualification, and integration with the TRMM spacecraft. The STE software provides the capability to control instrument activation, commanding (including both data formatting and user interfacing), data collection, decompression,

and display and image simulation.

The LIS STE code was developed for the DOS operating system in the C programming language. Because of the many unique data formats implemented by the flight instrument, the STE software was required to comprehend the same formats, and translate them for the test operator. The hardware interfaces to the LIS instrument using both commercial and custom computer boards, requiring that the STE code integrate this variety into a working system. In addition, the requirement to provide RTEP test capa-

bility dictated the need to provide simulations of background image data with short-duration lightning transients superimposed. This led to the development of unique code used to control the location, intensity, and variation above background for simulated lightning strikes at user-selected locations.

This program was written by Kathleen Freestone, Louis Simeone, Bryan Robertson, Maytha Frankford, David Trice, Kevin Wallace, and DeLisa Wilkerson of Marshall Space Flight Center. Further information is contained in a TSP (see page 1). MFS-32339-1

Processing AIRS Scientific Data Through Level 2

NASA's Jet Propulsion Laboratory, Pasadena, California

The Atmospheric Infrared Spectrometer (AIRS) Science Processing System (SPS) is a collection of computer programs, denoted product generation executives (PGEs), for processing the readings of the AIRS suite of infrared and microwave instruments orbiting the Earth aboard NASA's Aqua spacecraft. AIRS SPS at an earlier stage of development was described in "Initial Processing of Infrared Spectral Data" (NPO-35243), *NASA Tech Briefs*, Vol. 28, No. 11 (November 2004), page 39. To recapitulate: Starting from level 0 (representing raw AIRS data), the PGEs and their data products are denoted by alphanumeric labels (1A, 1B, and 2) that signify the

successive stages of processing. The cited prior article described processing through level 1B (the level-2 PGEs were not yet operational).

The level-2 PGEs, which are now operational, receive packages of level-1B geolocated radiance data products and produce such geolocated geophysical atmospheric data products such as temperature and humidity profiles. The process of computing these geophysical data products is denoted "retrieval" and is quite complex. The main steps of the process are denoted microwave-only retrieval, cloud detection and cloud clearing, regression, full retrieval, and rapid transmittance algorithm.

This program was written by Robert Oliphant, Sung-Yung Lee, Moustafa Chahine of Caltech; Joel Susskind of Goddard Space Flight Center; Christopher Barnett, Larry McMillin, and Mitchell Goldberg of the National Oceanic and Atmospheric Administration; John Blaisdell of Science Applications International Corp; Philip Rosenkranz of Massachusetts Institute of Technology; and Larrabee Strow of the University of Maryland, Baltimore County, for NASA's Jet Propulsion Laboratory.

This software is available for commercial licensing. Please contact Karina Edmonds of the California Institute of Technology at (626) 395-2322. Refer to NPO-40459.

Triaxial Probe Magnetic Data Analysis

NASA's Jet Propulsion Laboratory, Pasadena, California

The Triaxial Magnetic Moment Analysis software uses measured magnetic field test data to compute dipole and quadrupole moment information from a hardware element. It is used to support JPL projects needing magnetic control and an understanding of the spacecraft-generated magnetic fields.

Evaluation of the magnetic moment of an object consists of three steps: acquisition, conditioning, and analysis. This version of existing software was extensively rewritten for easier data acquisition, data analysis, and report presentation, including immediate feedback to the test operator during data acquisi-

tion.

While prior JPL computer codes provided the same data content, this program has a better graphic display including original data overlaid with reconstructed results to show "goodness of fit" accuracy and better appearance of the report graphic page. Data are acquired using three magnetometers and two rotations of the device under test. A clean acquisition user interface presents required numeric data and graphic summaries, and the analysis module yields the best fit (least squares) for the magnetic dipole and/or quadrupole moment of a device.

The acquisition module allows the user

to record multiple data sets, selecting the best data to analyze, and is repeated three times for each of the z-axial and y-axial rotations. In this update, the y-axial rotation starting position has been changed to an option, allowing either the x- or z-axis to point towards the magnetometer. The code has been rewritten to use three simultaneous axes of magnetic data (three probes), now using two "rotations" of the device under test rather than the previous three rotations, thus reducing handling activities on the device under test. The present version of the software gathers data in one-degree increments, which permits much better accuracy of the fit-

ted data than the coarser data acquisition of the prior software.

The data-conditioning module provides a clean data set for the analysis module. For multiple measurements at a given degree, the first measurement is used. For omitted measurements, the missing field is estimated by linear interpolation between the two nearest measurements.

The analysis module was rewritten for the dual rotation, triaxial probe measurement process and now has better moment estimation accuracy, based on the finer one degree of data acquisition resolution. The magnetic moments thus computed are used as an input to summarize the total spacecraft field.

This program was written by Kimberly Shultz, Albert Whittlesey, and Pablo Narvaez of Caltech for NASA's Jet Propulsion Laboratory. Further information is contained in a TSP (see page 1).

This software is available for commercial licensing. Please contact Karina Edmonds of the California Institute of Technology at (626) 395-2322. Refer to NPO-44192.

Analyzing Responses of Chemical Sensor Arrays

NASA's Jet Propulsion Laboratory, Pasadena, California

NASA is developing a third-generation electronic nose (ENose) capable of continuous monitoring of the International Space Station's cabin atmosphere for specific, harmful airborne contaminants. Previous generations of the ENose have been described in prior *NASA Tech Briefs* issues.

Sensor selection is critical in both (pre-fabrication) sensor material selection and (post-fabrication) data analysis of the ENose, which detects several analytes that are difficult to detect, or that are at very low concentration ranges. Existing sensor selection approaches usually include limited statistical measures, where selectivity is more important but reliability and sen-

sitivity are not of concern. When reliability and sensitivity can be major limiting factors in detecting target compounds reliably, the existing approach is not able to provide meaningful selection that will actually improve data analysis results.

The approach and software reported here consider more statistical measures (factors) than existing approaches for a similar purpose. The result is a more balanced and robust sensor selection from a less than ideal sensor array. The software offers quick, flexible, optimal sensor selection and weighting for a variety of purposes without a time-consuming, iterative search by performing sensor calibrations to a known linear or nonlin-

ear model, evaluating the individual sensor's statistics, scoring the individual sensor's overall performance, finding the best sensor array size to maximize class separation, finding optimal weights for the remaining sensor array, estimating limits of detection for the target compounds, evaluating fingerprint distance between group pairs, and finding the best event-detecting sensors.

This program was written by Hanying Zhou of Caltech for NASA's Jet Propulsion Laboratory.

This software is available for commercial licensing. Please contact Karina Edmonds of the California Institute of Technology at (626) 395-2322. Refer to NPO-43988.

PREDICTS

NASA's Jet Propulsion Laboratory, Pasadena, California

PREDICTS is a computer program that predicts the frequencies, as functions of time, of signals to be received by a radio science receiver — in this case, a special-purpose digital receiver dedicated to analysis of signals received by an antenna in NASA's Deep Space Network (DSN). Unlike other software used in the DSN, PREDICTS does not use interpolation early in the calculations; as a consequence, PREDICTS is more precise and more stable. The precision afforded by

the other DSN software is sufficient for telemetry; the greater precision afforded by PREDICTS is needed for radio-science experiments. In addition to frequencies as a function of time, PREDICTS yields the rates of change and interpolation coefficients for the frequencies and the beginning and ending times of reception, transmission, and occultation.

PREDICTS is applicable to S-, X-, and Ka-band signals and can accommodate the following link configurations: (1)

one-way (spacecraft to ground), (2) two-way (from a ground station to a spacecraft to the same ground station), and (3) three-way (from a ground transmitting station to a spacecraft to a different ground receiving station).

This work was done by Nicole Rappaport of Caltech for NASA's Jet Propulsion Laboratory.

This software is available for commercial licensing. Please contact Karina Edmonds of the California Institute of Technology at (626) 395-2322. Refer to NPO-40987.

Software Compensates Electronic-Nose Readings for Humidity

NASA's Jet Propulsion Laboratory, Pasadena, California

A computer program corrects for the effects of humidity on the readouts of an array of chemical sensors (an "electronic nose"). To enable the use of this program, the array must incorporate an in-

dependent humidity sensor in addition to sensors designed to detect analytes other than water vapor. The basic principle of the program was described in "Compensating for Effects of Humidity

on Electronic Noses" (NPO-30615), *NASA Tech Briefs*, Vol. 28, No. 6 (June 2004), page 63. To recapitulate: The output of the humidity sensor is used to generate values that are subtracted from

the outputs of the other sensors to correct for contributions of humidity to those readings. Hence, in principle, what remains after corrections are the contributions of the analytes only.

The outputs of the non-humidity sensors are then deconvolved to obtain the concentrations of the analytes. In addition,

the humidity reading is retained as an analyte reading in its own right. This subtraction of the humidity background increases the ability of the software to identify such events as spills in which contaminants may be present in small concentrations and accompanied by large changes in humidity.

This program was written by Hanying Zhou of Caltech for NASA's Jet Propulsion Laboratory.

This software is available for commercial licensing. Please contact Karina Edmonds of the California Institute of Technology at (626) 395-2322. Refer to NPO-30859.

Space Propulsion Design and Analysis

Marshall Space Flight Center, Alabama

This software provides an improved methodology for predicting launcher base pressure and heat loads for RSRM (Reusable Solid Rocket Motor) launchers by accounting for complex anisotropic stress/strains and variable turbulent Prandtl and Schmidt numbers. A "building block" approach to turbulence model development, and validation has been applied for improved missile/launcher base region analysis.

Modifications to existing $k - \epsilon$ turbulence models and application of scalar

variance models are incorporated into a RANS-based method for aeropropulsive flow modeling, directly related to base flow methodology. (RANS stands for Reynolds-averaged Navier-Stokes.) The models are applied in a RANS solver framework and can improve analysis of other complex flow fields.

The enhanced models provide a more accurate predictive capability for improving the design and analysis of RSRM launcher configuration. The $k - \epsilon$ model enhancements have been

shown to improve the capability for predicting turbulence effects in base blow environments. The scalar variance models have been assessed over a wide range of flow configurations to improve prediction of turbulent scalar mixing.

This program was written by Neeraj Sinha, Kevin Brinckman, Haritha Ayyalasomayajula, and Sanford Dash of CRAFT Tech for Marshall Space Flight Center. Further information is contained in a TSP (see page 1). Refer to MFS-32442-1.

Parallelization of the Coupled Earthquake Model

NASA's Jet Propulsion Laboratory, Pasadena, California

This Web-based tsunami simulation system allows users to remotely run a model on JPL's supercomputers for a given undersea earthquake. At the time of this reporting, predicting tsunamis on the Internet has never happened before. This new code directly couples the earthquake model and the ocean model on parallel computers and improves simulation speed.

Seismometers can only detect information from earthquakes; they cannot

detect whether or not a tsunami may occur as a result of the earthquake. When earthquake-tsunami models are coupled with the improved computational speed of modern, high-performance computers and constrained by remotely sensed data, they are able to provide early warnings for those coastal regions at risk.

The software is capable of testing NASA's satellite observations of

tsunamis. It has been successfully tested for several historical tsunamis, has passed all alpha and beta testing, and is well documented for users.

This program was written by Gary Block, P. Peggy Li, and Yuhe T. Song of Caltech for NASA's Jet Propulsion Laboratory.

This software is available for commercial licensing. Please contact Karina Edmonds of the California Institute of Technology at (626) 395-2322. Refer to NPO-44443.



Automated Recognition of 3D Features in GPIR Images

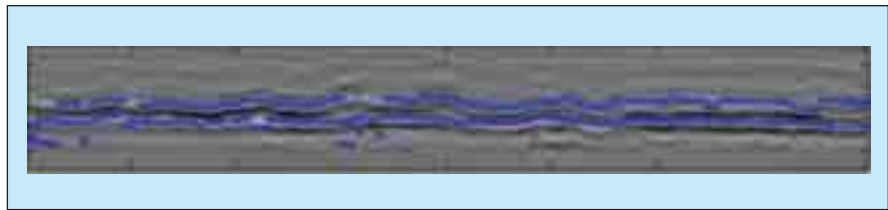
Enhanced images emphasizing features of interest are prepared for scrutiny by human analysts.

NASA's Jet Propulsion Laboratory, Pasadena, California

A method of automated recognition of three-dimensional (3D) features in images generated by ground-penetrating imaging radar (GPIR) is undergoing development. GPIR 3D images can be analyzed to detect and identify such subsurface features as pipes and other utility conduits. Until now, much of the analysis of GPIR images has been performed manually by expert operators who must visually identify and track each feature. The present method is intended to satisfy a need for more efficient and accurate analysis by means of algorithms that can automatically identify and track subsurface features, with minimal supervision by human operators.

In this method, data from multiple sources (for example, data on different features extracted by different algorithms) are fused together for identifying subsurface objects. The algorithms of this method can be classified in several different ways. In one classification, the algorithms fall into three classes: (1) image-processing algorithms, (2) feature-extraction algorithms, and (3) a multiaxis data-fusion/pattern-recognition algorithm that includes a combination of machine-learning, pattern-recognition, and object-linking algorithms.

The image-processing class includes preprocessing algorithms for reducing



Features Representing Two Pipes were generated by applying a feature-extraction algorithm to data from a GPIR scan of 110th Street in New York City. This synthetic image contains the detection marks overlaid on GPIR data from a mid-depth horizontal slice viewed from overhead. The gaps and undulations are minimized in subsequent processing by a multiaxis data-fusion/pattern-recognition algorithm.

noise and enhancing target features for pattern recognition. The feature-extraction algorithms operate on preprocessed data to extract such specific features in images as two-dimensional (2D) slices of a pipe. Then the multiaxis data-fusion/pattern-recognition algorithm identifies, classifies, and reconstructs 3D objects from the extracted features. In this process, multiple 2D features extracted by use of different algorithms and representing views along different directions are used to identify and reconstruct 3D objects. In object linking, which is an essential part of this process, features identified in successive 2D slices and located within a threshold radius of identical features in adjacent slices are linked in a directed-graph data structure. Relative to past approaches, this multiaxis approach offers the advantages of more re-

liable detections, better discrimination of objects, and provision of redundant information, which can be helpful in filling gaps in feature recognition by one of the component algorithms.

The image-processing class also includes postprocessing algorithms that enhance identified features to prepare them for further scrutiny by human analysts (see figure). Enhancement of images as a postprocessing step is a significant departure from traditional practice, in which enhancement of images is a preprocessing step.

This work was done by Han Park, Timothy Stough, and Amir Fijany of Caltech for NASA's Jet Propulsion Laboratory.

The software used in this innovation is available for commercial licensing. Please contact Karina Edmonds of the California Institute of Technology at (626) 395-2322. Refer to NPO-40698.

Algorithm Plans Collision-Free Path for Robotic Manipulator

This algorithm is designed to make minimal demands upon computational resources.

NASA's Jet Propulsion Laboratory, Pasadena, California

An algorithm has been developed to enable a computer aboard a robot to autonomously plan the path of the manipulator arm of the robot to avoid collisions between the arm and any obstacle, which could be another part of the robot or an external object in the vicinity of the robot. In simplified terms, the algorithm generates trial path segments and tests each segment for potential collisions in an iterative process that ends when a se-

quence of collision-free segments reaches from the starting point to the destination. The main advantage of this algorithm, relative to prior such algorithms, is computational efficiency: the algorithm is designed to make minimal demands upon the limited computational resources available aboard a robot.

This path-planning algorithm utilizes a modified version of the collision-detection method described in "Improved

Collision-Detection Method for Robotic Manipulator" (NPO-30356), *NASA Tech Briefs*, Vol. 27, No. 3 (June 2003), page 72. The method involves utilization of mathematical models of the robot constructed prior to operation and similar models of external objects constructed automatically from sensory data acquired during operation. This method incorporates a previously developed method, known in the art as the method of ori-

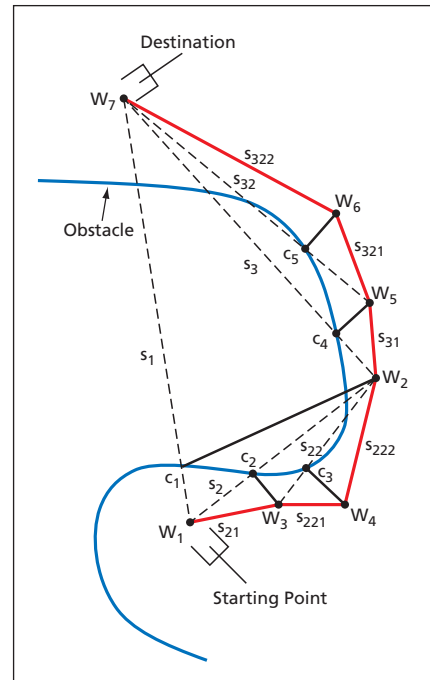
ented bounding boxes (OBBs), in which an object is represented approximately, for computational purposes, by a box that encloses its outer boundary. Because many parts of a robotic manipulator are cylindrical, the OBB method has been extended in this method to enable the approximate representation of cylindrical parts by use of octagonal or other multiple-OBB assemblies denoted oriented bounding prisms (OBPs).

A multiresolution OBB/OBP representation of the robot and its manipulator arm and a multiresolution OBB representation of external objects (including terrain) are constructed and used in a process in which collisions at successively finer resolutions are detected through computational detection of overlaps between the corresponding OBB and OBP models. For computational efficiency, the process is started at the coarsest resolution and stopped as soon as possible, preferably before reaching the finest resolution. At the coarsest resolution, there is a single OBB enclosing all relevant external objects and a single OBB enclosing the entire robot. At the next finer level of resolution, the coarsest-resolution OBB is divided into two OBBs, and so forth. If no collision is detected at the coarsest resolution, then there is no need for further computation to detect collisions. If a collision is detected at the coarsest resolution, then tests for collisions are performed at the next finer level of resolution. This process is continued to successively finer resolutions until either no more collisions are detected or the

finest resolution is reached.

The path-planning algorithm operates on a representation of the robot arm and obstacles in a Cartesian coordinate system. The figure schematically depicts a simplified example of the geometric effects of the algorithm. In this example, the robot arm has been commanded to move from a starting point to a destination. The problem to be solved by the algorithm is to choose waypoints (W_1, W_2, \dots) and straight-line path segments connecting the waypoints (including the starting point and destination as waypoints) so that there is no collision along any segment. The algorithm can be summarized as follows:

1. Generate a straight-line path (s_1) from the starting point (W_1) to the destination.
2. Using the collision-detection method described above, test for collisions along this path.
3. If there is a collision (denoted by collision point c_1), then by use of a geometry-based subalgorithm too complex to be described within the space available for this article, generate two new sub-paths (s_2 and s_3) that connect a new waypoint (W_2) with the ends of s_1 .
4. Test each new sub-path for collisions.
5. If a collision is detected on either sub-path (e.g., at collision point c_2 on s_2), then in the manner of step 3, generate new sub-sub paths (s_{21} and s_{22}) that connect new way point W_3 with W_1 and W_2 .
6. Test for collisions and generate new path segments in the manner described above until the starting and



A Multi-Segment Path is generated in an iterative process of generating candidate segments and testing them for collisions.

destination points are connected by collision-free path segments. In this example, the result is a total of seven waypoints connected by six path segments.

This work was done by Paul Backes and Antonio Diaz-Calderon of Caltech for NASA's Jet Propulsion Laboratory.

The software used in this innovation is available for commercial licensing. Please contact Karina Edmonds of the California Institute of Technology at (626) 395-2322. Refer to NPO-41697

Σ Hybrid Automated Diagnosis of Discrete/Continuous Systems

Integration of complementary tools offers new approach to hybrid diagnosis.

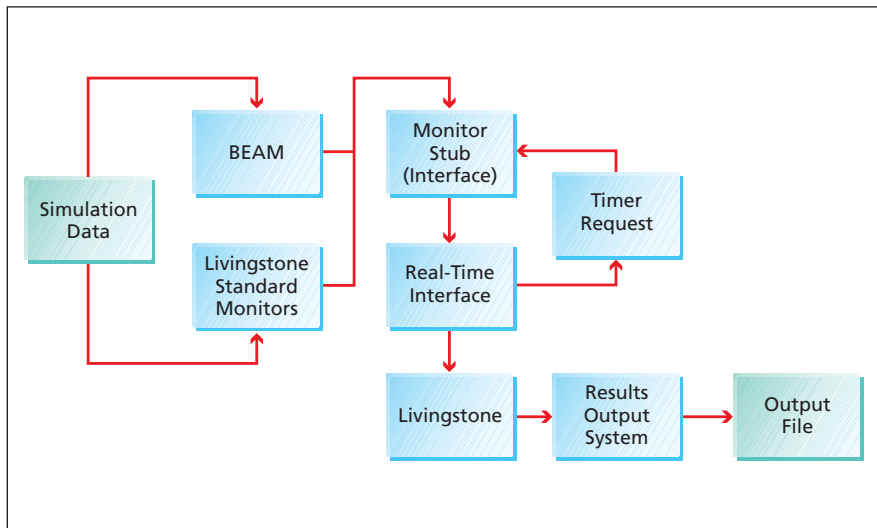
NASA's Jet Propulsion Laboratory, Pasadena, California

A recently conceived method of automated diagnosis of a complex electromechanical system affords a complete set of capabilities for hybrid diagnosis in the case in which the state of the electromechanical system is characterized by both continuous and discrete values (as represented by analog and digital signals, respectively). The method is an integration of two complementary diagnostic systems: (1) beacon-based exception analysis for multimissions (BEAM), which is primarily useful in the continuous domain and easily performs diagnoses in the presence of transients;

and (2) Livingstone, which is primarily useful in the discrete domain and is typically restricted to quasi-steady conditions. BEAM has been described in several prior *NASA Tech Briefs* articles: "Software for Autonomous Diagnosis of Complex Systems" (NPO-20803), Vol. 26, No. 3 (March 2002), page 33; "Beacon-Based Exception Analysis for Multimissions" (NPO-20827), Vol. 26, No. 9 (September 2002), page 32; "Wavelet-Based Real-Time Diagnosis of Complex Systems" (NPO-20830), Vol. 27, No. 1 (January 2003), page 67; and "Integrated Formulation of Beacon-Based Ex-

ception Analysis for Multimissions" (NPO-21126), Vol. 27, No. 3 (March 2003), page 74.

Briefly, BEAM is a complete data-analysis method, implemented in software, for real-time or off-line detection and characterization of faults. The basic premise of BEAM is to characterize a system from all available observations and train the characterization with respect to normal phases of operation. The observations are primarily continuous in nature. BEAM isolates anomalies by analyzing the deviations from nominal for each phase of operation. Livingstone is a



This Data-Flow Diagram illustrates the role of BEAM as a “smart” monitor for Livingstone.

model-based reasoner that uses a model of a system, controller commands, and sensor observations to track the system’s state, and detect and diagnose faults. Livingstone models a system within the discrete domain. Therefore, continuous sensor readings, as well as time, must be discretized. To reason about continuous systems, Livingstone uses “monitors”

that discretize the sensor readings using trending and thresholding techniques.

In development of the a hybrid method, BEAM results were sent to Livingstone to serve as an independent source of evidence that is in addition to the evidence gathered by Livingstone standard monitors. The figure depicts the flow of data in an early version of a

hybrid system dedicated to diagnosing a simulated electromechanical system. In effect, BEAM served as a “smart” monitor for Livingstone. BEAM read the simulation data, processed the data to form observations, and stored the observations in a file. A monitor stub synchronized the events recorded by BEAM with the output of the Livingstone standard monitors according to time tags. This information was fed to a real-time interface, which buffered and fed the information to Livingstone, and requested diagnoses at the appropriate times. In a test, the hybrid system was found to correctly identify a failed component in an electromechanical system for which neither BEAM nor Livingstone alone yielded the correct diagnosis.

This work was done by Han Park, Mark James, Ryan Mackey of Caltech; Howard Cannon and Anapa Bajwa of NASA’s Ames Research Center; and William Maul of NASA’s Glenn Research Center for NASA’s Jet Propulsion Laboratory.

The software used in this innovation is available for commercial licensing. Please contact Karina Edmonds of the California Institute of Technology at (626) 395-2322. Refer to NPO-40910.

State-Estimation Algorithm Based on Computer Vision

Available data are utilized optimally without incurring an excessive computational burden.

NASA’s Jet Propulsion Laboratory, Pasadena, California

An algorithm and software to implement the algorithm are being developed as means to estimate the state (that is, the position and velocity) of an autonomous vehicle, relative to a visible nearby target object, to provide guidance for maneuvering the vehicle. In the original intended application, the autonomous vehicle would be a spacecraft and the nearby object would be a small astronomical body (typically, a comet or asteroid) to be explored by the spacecraft. The algorithm could also be used on Earth in analogous applications — for example, for guiding underwater robots near such objects of interest as sunken ships, mineral deposits, or submerged mines.

For the purpose of the algorithm, it is assumed that the robot would be equipped with a vision system that would include one or more electronic cameras, image-digitizing circuitry, and an image-data-processing computer that would generate feature-recognition data products. Such products customarily include

bearing angles of lines of sight from the camera(s) [and, hence, from the vehicle] to recognized features. The data products that are processed by the present algorithm are of the following types:

- The Cartesian vector from the camera to a reference point on or in the target body;
- Bearing angles from the camera to the reference point;
- A landmark table (LMT);
- A paired-feature table (PFT); and
- A range point table (RPT).

The incorporation of the LMT and PFT is particularly important. LMT and PFT data are generated by typical computer-vision systems that could be used in the contemplated applications. In an LMT, a vision system recognizes landmarks from an onboard catalog and reports their bearing angles and associated known locations on the target body. In a PFT, a vision system reports bearing angles to features recognized as being common to two images taken at different times. Relative to the LMT, the PFT can

be generated with less computation because it is necessary only to track features frame-to-frame; it is not necessary to associate the features with landmarks. However, it is more challenging to incorporate the PFT in a state-estimation algorithm for reasons discussed below. The LMT and PFT are complementary in the sense that the LMT provides position-type information while the PFT provides velocity-type information. However, the velocity-type information from the PFT is incomplete because it includes an unknown scale factor. A state-estimation algorithm must fuse the aforementioned data types to make an optimal estimate.

The following three main challenges arise as parts of this data-fusion problem:

- The first challenge is posed by the large number of features (typically ≥ 50) that a typical computerized vision system can recognize during any given frame period. The large number of features imposes a heavy burden for real-time computation.

- The second challenge is associated with the lack of range information when camera measurements are the only measurements available. Camera's measurements consist only of bearings to specific feature points in images. The PFT data type is especially challenging inasmuch as recognized features do not necessarily represent known objects and do not contain location information.
- The third challenge is posed by the fact that computer vision information often relates to images taken in the past. For example, the PFT data type reports features that were recognized as being common to two images taken at earlier times. The need to update the current state estimate by use of information from the past presents a

challenge because prior recursive state-estimating algorithms typically only propagate the current state.

The present algorithm addresses these challenges by incorporating the following innovations:

The first innovation is a preprocessing step, based on QR factorization (a particular matrix factorization, a description of which would exceed the scope of this article), that provides for optimal compression of LMT, PFT, and RPT updates that involve large numbers of recognized features. This compression eliminates the need for a considerable amount of real-time computation.

The second innovation is a mathematical annihilation method for forming a linear measurement equation from the PFT data. The annihilation method is

equivalent to a mathematical projection that eliminates the dependence on the unknown scale factor.

The third innovation is a state-augmentation method for handling PFT and other data types that relate states from two or more past instants of time. The state-augmentation method stands in contrast to a prior stochastic cloning method. State augmentation provides an optimal solution to the state-estimation problem, while stochastic cloning can be shown to be suboptimal.

This work was done by David Bayard and Paul Brugarolas of Caltech for NASA's Jet Propulsion Laboratory.

The software used in this innovation is available for commercial licensing. Please contact Karina Edmonds of the California Institute of Technology at (626) 395-2322. Refer to NPO-41321

Σ Representing Functions in n Dimensions to Arbitrary Accuracy

Computation can be simplified in cases in which data are noiseless.

Langley Research Center, Hampton, Virginia

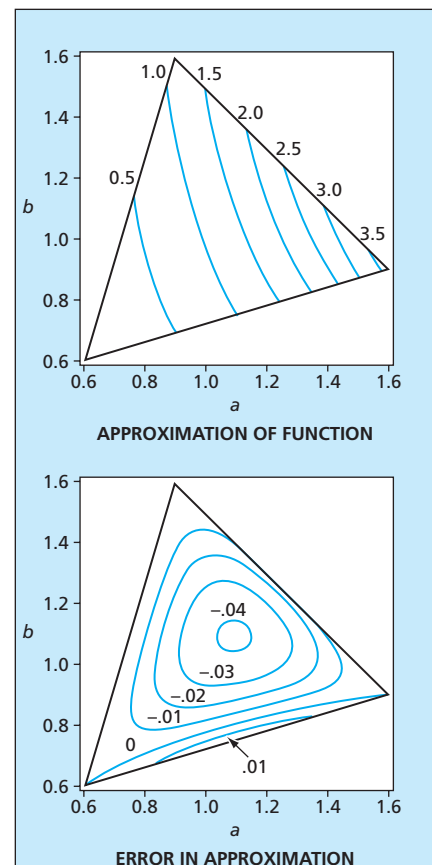
A method of approximating a scalar function of n independent variables (where n is a positive integer) to arbitrary accuracy has been developed. This method is expected to be attractive for use in engineering computations in which it is necessary to link global models with local ones or in which it is necessary to interpolate noiseless tabular data that have been computed from analytic functions or numerical models in n -dimensional spaces of design parameters.

This method is related to prior statistically based methods of fitting low-order approximate functional representations (response surfaces) to noisy experimental data. The prior methods are advantageous in situations in which large amounts of noisy data are available, but in situations in which the data and the functions that they represent are noiseless, it is computationally inefficient to generate the large quantities of data needed for fitting. Moreover, in the prior statistically based methods, the low-order functional representation cannot be defined to a specified degree of accuracy. The latter shortcoming limits the usefulness of response surfaces in design-optimization computations because (1) optimization calculations involve gradients of functions, which are approximated to orders lower than those of the functions themselves and, hence, can be so inaccurate

as to yield poor results; and (2) the accuracy of a response surface can vary widely over its domain. The present method overcomes these shortcomings of the prior methods.

Increasingly, modern computational-simulation programs generate values of gradients of functions in addition to values of the functions themselves, in order to satisfy the need for accurate gradient as well as function values for optimizations. Taking advantage of this trend, the present method relies on the availability of both gradient and function data. In this method, the space of n independent variables is subdivided into an n -dimensional mesh of simplex elements (simplices) that amount to n -dimensional generalizations of modeling techniques used in the finite-element method. The exact values of the scalar function and its gradient, as generated by the applicable computational model, are specified at the simplex nodes, which are intersections of coordinate axes of the n -dimensional mesh. Within each simplex, the function and its gradient are interpolated approximately by a set of basis functions of the n coordinates.

In order to minimize the computational burden, one tries to use basis functions of order no higher than that needed to limit the error in the approximation to an acceptably low value. It would be preferable if, in a given case,



In a **Simple Example**, the function ba^2 is approximated by a third-order (complete to second order) polynomial on a triangular simplex. The error is zero at the nodes of the simplex and greatest near the middle.

one could obtain acceptable accuracy from polynomial functions of order no higher than third, complete to second order (see figure). The advantage of using such low-order polynomials is that the interpolation could be performed

without need for matrix operations (which would, if needed, add to the computational burden). Approximate-error-indicator quantities, defined on the edges of the simplices, have been derived as guides to whether there is a

need to refine the simplices to reduce the errors.

This work was done by Stephen J. Scotti of Langley Research Center. Further information is contained in a TSP (see page 1). LAR-16297-1

Accumulate-Repeat-Accumulate-Accumulate Codes

Fast, high-performance coders and decoders could be designed.

NASA's Jet Propulsion Laboratory, Pasadena, California

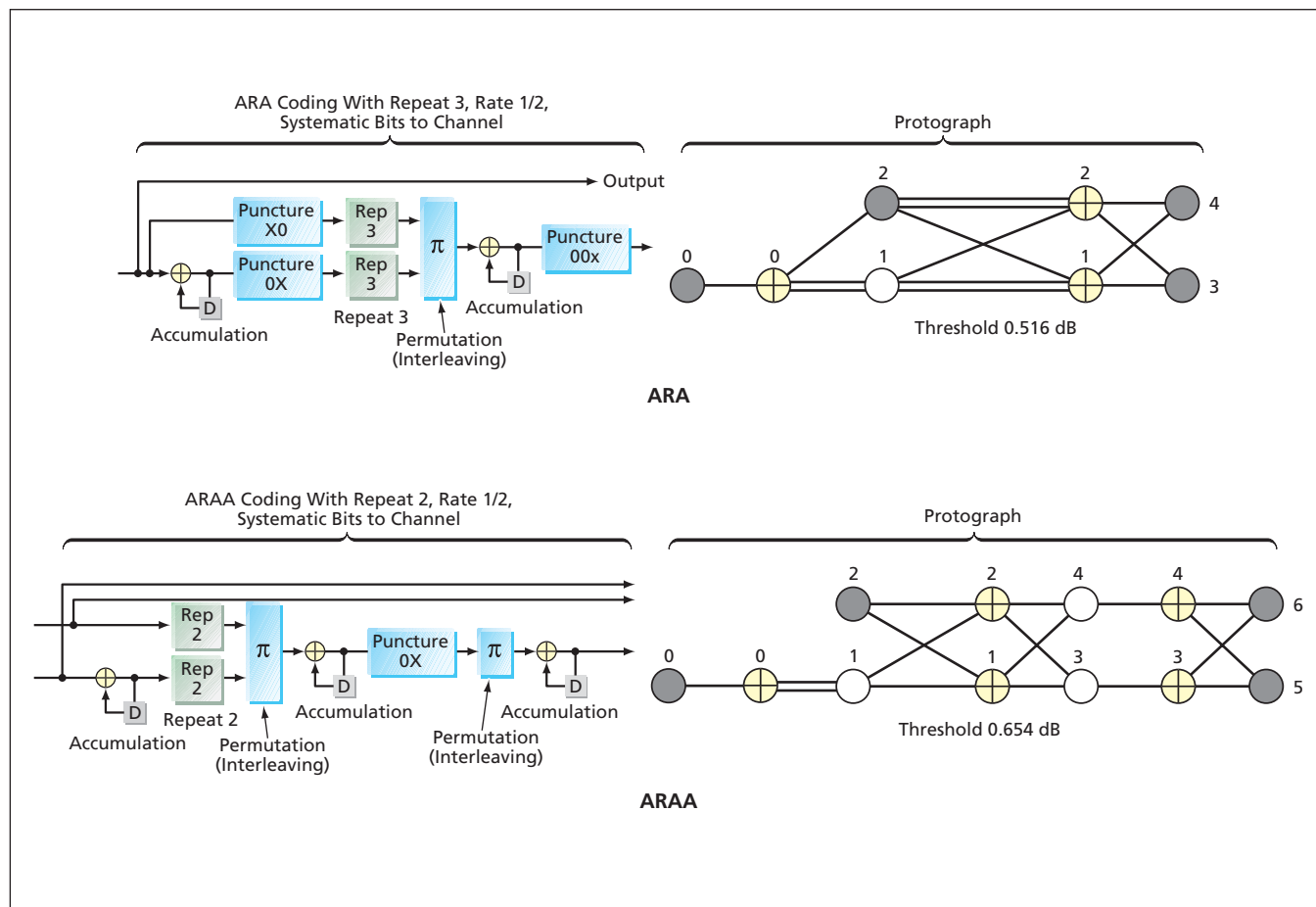
Accumulate-repeat-accumulate-accumulate (ARAA) codes have been proposed, inspired by the recently proposed accumulate-repeat-accumulate (ARA) codes. These are error-correcting codes suitable for use in a variety of wireless data-communication systems that include noisy channels. ARAA codes can be regarded as serial turbo-like codes or as a subclass of low-density parity-check (LDPC) codes, and, like ARA codes they have projected graph or protograph representations; these characteristics make it possible to design high-speed iterative decoders that

utilize belief-propagation algorithms. The objective in proposing ARAA codes as a subclass of ARA codes was to enhance the error-floor performance of ARA codes while maintaining simple encoding structures and low maximum variable node degree.

A rate-1/2 classical repeat-and-accumulate (RA) code has a high threshold (3.01 dB). An ARAA code can be viewed as a preceded RA code with puncturing in concatenation with another accumulation; these characteristics make it possible to design very fast

encoders. The top part of the figure illustrates the simplest example of the encoding process for a rate-1/2 ARA code, its protograph (filled nodes correspond to transmitted code symbols), and the corresponding decoding threshold of 0.516 dB. Other rate-1/2 ARA examples with maximum variable node degree 5 have thresholds as low as 0.26 dB, which can be compared to the Shannon capacity limit of 0.19 dB.

The bottom part of the figure illustrates a simple example of the encoding process for a rate-1/2 ARAA code, its protograph, and the corresponding



These Block Diagrams and Protographs illustrate the similarities and differences between a simple rate-1/2 ARA code and a simple rate-1/2 ARAA code.

threshold of 0.654 dB. The protograph of this code is similar to the ARA-code protograph shown in the top part of the figure, except for the additional accumulator stage and fewer parallel edges. The maximum variable node degree (4) of this ARAA protograph is less than that of the ARA protograph, but the total number of nodes is greater than in the ARA protograph.

Other rate-1/2 ARAA examples with maximum variable node degree 4 (but with larger protographs) can reduce the threshold further. ARAA codes with higher code rates can be obtained by puncturing the output of the middle accumulator: For example, one can obtain thresholds of 1.46 dB and 2.00 dB for rates 2/3 and 3/4, respectively, for punctured versions of the ARAA code represented in the bottom part of the figure. A single fast decoder using a belief-propagation algo-

rithm with depuncturing can be implemented to handle different code rates.

By use of density evolution (a computational-simulation technique for analyzing performances of LDPC codes) on protographs of ARAA codes of maximum variable node degree 4, it has been found that a minimum bit signal-to-noise ratio as low as 0.21 dB above the channel capacity limit can be achieved as the block size goes to infinity. Such a low threshold cannot be achieved by RA, irregular RA (IRA), or unstructured irregular LDPC codes with the same constraint on the maximum variable node degree. Furthermore, by puncturing the accumulators, one can construct families of higher rate ARAA codes with thresholds that stay close to their respective channel capacity thresholds. Results of simulations of iterative decoding have shown that ARAA codes would perform comparably to the

best previously known LDPC codes but with very low error floors, even at moderate block sizes.

This work was done by Dariush Divsalar, Samuel Dolinar, and Jeremy Thorpe of Caltech for NASA's Jet Propulsion Laboratory. Further information is contained in a TSP (see page 1).

In accordance with Public Law 96-517, the contractor has elected to retain title to this invention. Inquiries concerning rights for its commercial use should be addressed to:

*Innovative Technology Assets Management
JPL*

Mail Stop 202-233

4800 Oak Grove Drive

Pasadena, CA 91109-8099

(818) 354-2240

E-mail: iaoffice@jpl.nasa.gov

Refer to NPO-41305, volume and number of this NASA Tech Briefs issue, and the page number.

Interface for Physics Simulation Engines

Ames Research Center, Moffett Field, California

DSS-Prototyper is an open-source, real-time 3D virtual environment software that supports design simulation for the new Vision for Space Exploration (VSE). This is a simulation of NASA's proposed Robotic Lunar Exploration Program, second mission (RLEP2). It simulates the Lunar Surface Access Module (LSAM), which is designed to carry up to four astronauts to the lunar surface for durations of a week or longer. This simulation (see figure) shows the virtual vehicle making approaches and landings on a variety of lunar terrains. The physics of the descent engine thrust vector, production of dust,

and the dynamics of the suspension are all modeled in this set of simulations.

The RLEP2 simulations are drivable (by keyboard or joystick) virtual rovers with controls for speed and motor torque, and can be articulated into higher or lower centers of gravity (depending on driving hazards) to enable drill placement. Gravity also can be set to lunar, terrestrial, or zero-g.

This software has been used to support NASA's Marshall Space Flight Center in simulations of proposed vehicles for robotically exploring the lunar surface for water ice, and could be used to

model all other aspects of the VSE from the Ares launch vehicles and Crew Exploration Vehicle (CEV) to the International Space Station (ISS). This simulator may be installed and operated on any Windows PC with an installed 3D graphics card.

This program was written by Bruce Damer of DigitalSpace Corporation for Ames Research Center. For further information, visit <http://www.digitalspace.com/projects/showcase.html>.

Inquiries concerning rights for the commercial use of this invention should be addressed to DigitalSpace Corporation at (831) 338-9400. Refer to ARC-15593-1.



RLEP2 lunar rover simulation and LSAM human lunar lander simulation using DigitalSpace software.

ISPATOM: A Generic Real-Time Data Processing Tool Without Programming

Lyndon B. Johnson Space Center, Houston, Texas

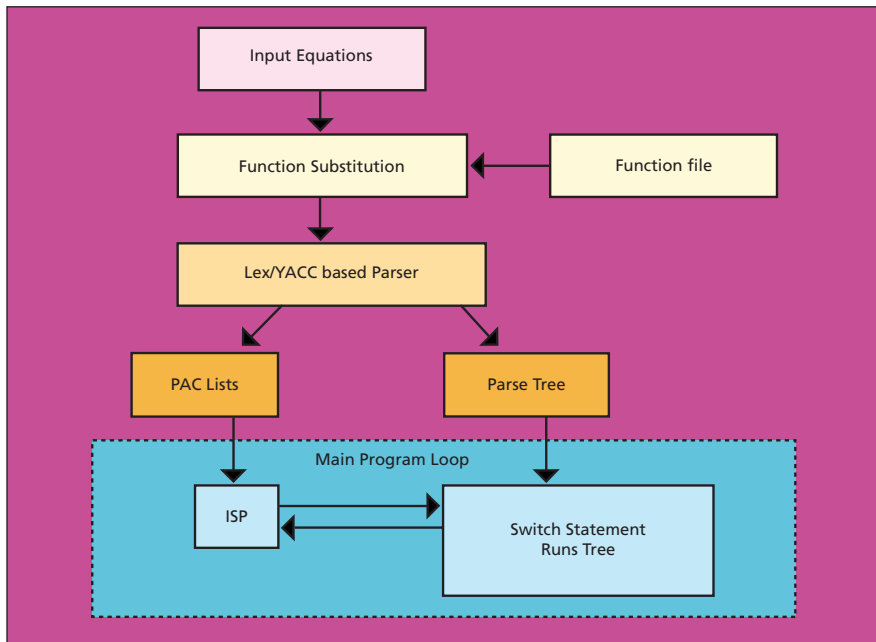
Information Sharing Protocol Advanced Tool of Math (ISPATOM) is an application program allowing for the streamlined generation of “comps,”

which subscribe to streams of incoming telemetry data, perform any necessary computations on the data, then send the data to other programs for display

and/or further processing in NASA mission control centers (see figure). Heretofore, the development of comps was difficult, expensive, and time-consuming: Each comp was custom written manually, in a low-level computing language, by a programmer attempting to follow requirements of flight controllers.

ISPATOM enables a flight controller who is not a programmer to write a comp by simply typing in one or more equation(s) at a command line or retrieving the equation(s) from a text file. ISPATOM then subscribes to the necessary input data, performs all of necessary computations, and sends out the results. It sends out new results whenever the input data change. The use of equations in ISPATOM is no more difficult than is entering equations in a spreadsheet. The time involved in developing a comp is thus limited to the time taken to decide on the necessary equations. Thus, ISPATOM is a real-time dynamic calculator.

This work was done by Adam Dershowitz of United Space Alliance for Johnson Space Center. Further information is contained in a TSP (see page 1).MSC-23799



Overview of ISPATOM application flow structure.

Automated Diagnosis and Control of Complex Systems

Ames Research Center, Moffett Field, California

Livingstone2 is a reusable, artificial intelligence (AI) software system designed to assist spacecraft, life support systems, chemical plants, or other com-

plex systems by operating with minimal human supervision, even in the face of hardware failures or unexpected events. The software diagnoses the current state of the spacecraft or other system, and recommends commands or repair actions that will allow the system to continue operation. Livingstone2 is an enhancement of the Livingstone diagnosis system that was flight-tested onboard the Deep Space One spacecraft in 1999 (see figure). This version tracks multiple diagnostic hypotheses, rather than just a single hypothesis as in the previous version. It is also able to revise diagnostic decisions made in the past when additional observations become available. In such cases, Livingstone might arrive at an incorrect hypothesis.

Re-architecting and re-implementing the system in C++ has increased performance. Usability has been improved by creating a set of development tools

that is closely integrated with the Livingstone2 engine. In addition to the core diagnosis engine, Livingstone2 includes a compiler that translates diagnostic models written in a Java-like language into Livingstone2's language, and a broad set of graphical tools for model development.

This program was written by James Kurien, Christian Plaunt, Howard Cannon, Mark Shirley, and Will Taylor of Ames Research Center; P. Nayak of USRA-RACS; Benoit Hudson, Andrew Bachmann, Lee Brownston, Sandra Hayden, and Steve Wragg of QSS Group, Inc.; William Millar and Shirley Pepke of Caelum Research Corp.; Scott Christa of Aerospace Computing, Inc.; and Ray Garcia of Foothill-DeAnza Community College. For further information, access <http://opensource.arc.nasa.gov/> or contact the Ames Technology Partnerships Division at (650) 604-2954. ARC-14725-1



Artist's conception of the New Millennium Deep Space One Probe.

Σ Program Management Tool

Ames Research Center, Moffett Field, California

The Program Management Tool (PMT) is a comprehensive, Web-enabled business intelligence software tool for assisting program and project managers within NASA enterprises in gathering, comprehending, and disseminating information on the progress of their programs and projects. The PMT provides planning and management support for implementing NASA programmatic and project management processes and requirements. It provides an online environment for program and line management to develop, communicate, and manage their programs, projects, and tasks in a comprehensive tool suite. The information managed by use of the PMT can include monthly reports as well as data on goals, deliverables, milestones, business processes, personnel, task plans, monthly reports, and budgetary allocations.

The PMT provides an intuitive and enhanced Web interface to automate the

tedious process of gathering and sharing monthly progress reports, task plans, financial data, and other information on project resources based on technical, schedule, budget, and management criteria and merits. The PMT is consistent with the latest Web standards and software practices, including the use of Extensible Markup Language (XML) for exchanging data and the WebDAV (Web Distributed Authoring and Versioning) protocol for collaborative management of documents. The PMT provides graphical displays of resource allocations in the form of bar and pie charts using Microsoft Excel Visual Basic for Application (VBA) libraries.

The PMT has an extensible architecture that enables integration of PMT with other strategic-information software systems, including, for example, the Erasmus reporting system, now part of the NASA Integrated Enterprise Man-

agement Program (IEMP) tool suite, at NASA Marshall Space Flight Center (MSFC). The PMT data architecture provides automated and extensive software interfaces and reports to various strategic information systems to eliminate duplicative human entries and minimize data integrity issues among various NASA systems that impact schedules and planning.

This work was done by Yuri Gawdiak and Alan Wong of Ames Research Center; David Maluf, David Bell, and Mohana Gurram of Universities Space Research Association/RIACS; Khai Peter Tran, Jennifer Hsu, and Kenji Yagi of QSS Group, Inc.; and Hemil Patel of SAIC.

This invention is owned by NASA and a patent application has been filed. Inquiries concerning rights for the commercial use of this invention should be addressed to the Ames Technology Partnerships Division at (650) 604-2954. Refer to ARC-14950-1.

Σ Flyby Geometry Optimization Tool

Langley Research Center, Hampton, Virginia

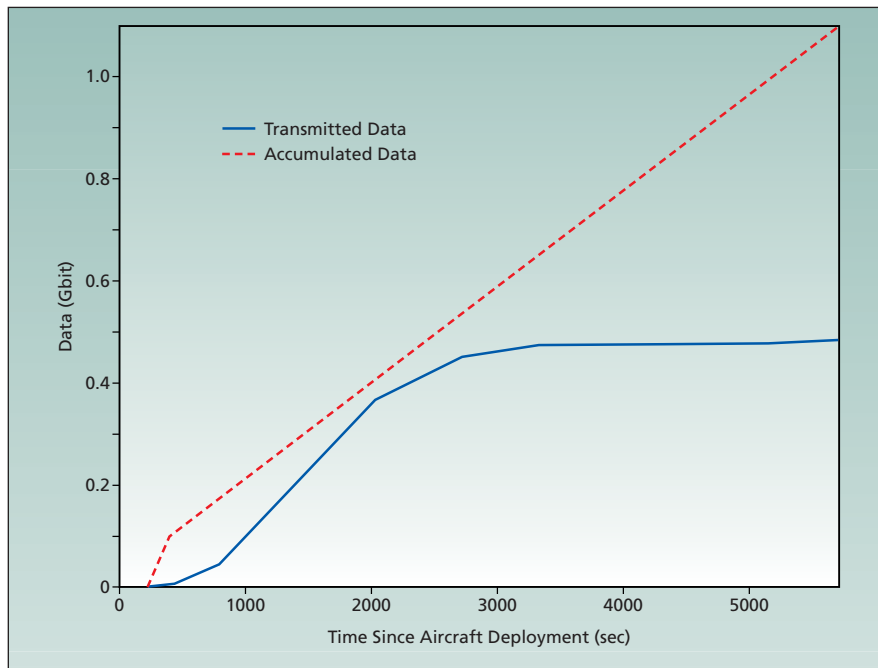
The Flyby Geometry Optimization Tool is a computer program for computing trajectories and trajectory-altering impulsive maneuvers for spacecraft used

in radio relay of scientific data to Earth from an exploratory airplane flying in the atmosphere of Mars. This program implements a genetic algorithm (GA) to

choose trajectories to maximize the volume of data relayed via at least one of three spacecraft: a main spacecraft in a hyperbolic orbit and two alternate spacecraft in elliptical orbits about Mars. [The GA approach is ideal for this type of optimization problem, wherein discrete data-transmission rates lead to discontinuities in data-collection volumes that one seeks to maximize. Such discontinuities are typically problematic for other optimization methods — especially, gradient search methods.]

The GA code is used to calculate a maneuver made by the main spacecraft prior to its periapse passage, to set up a favorable orbital geometry for communication with the airplane. The maneuver is chosen to maximize the total volume of data (see figure) transmitted from the airplane to the spacecraft. Then the program causes the data to be transmitted from the airplane to whichever spacecraft offers the highest data rate.

This program was written by Christopher D. Karlgaard of Analytical Mechanics Associates, Inc. for Langley Research Center. Further information is contained in a TSP (see page 1). LAR-16884-1



Accumulated and Transmitted Data are shown as a function of time.

Σ Displaying Properties of PDFs

Ames Research Center, Moffett Field, California

PDFVis is a computer program that assists in visualization of uncertainty as represented by a probability density function (PDF) located at each grid cell in a spatial domain. PDFVis performs the following functions:

- Creates maps of first-, second-, and third-order statistics of the PDFs, displaying the maps simultaneously in one image;
- Provides an interactive probe that displays various forms of density estimates (e.g., histogram or kernel density estimator) of the PDF at a grid cell or

larger region selected by the user;

- For grid cells in a row or column selected by the user, it displays surfaces of the PDFs as shaded walls and as color-mapped wall according to a scalar variable selectable by the user;
- Displays the modality (basically, the number of peaks) and the locality of the peaks of the PDF in each grid cell;
- Provides a capability for querying the modalities of the PDFs on the basis of ranges and other criteria specified by the user; and

- Facilitates interactivity by providing simple user command keys.

This program was written by David Kao and Jennifer Dungan of Ames Research Center and David Kao of The Regents of the University of California Santa Cruz. Further information is contained in a TSP (see page 1).

Inquiries concerning rights for the commercial use of this invention should be addressed to the Ames Technology Partnerships Division at (650) 604-2954. Refer to ARC-15039-1

Σ Modular Filter and Source-Management Upgrade of RADAC

Goddard Space Flight Center, Greenbelt, Maryland

In an upgrade of the Range Data Acquisition Computer (RADAC) software, a modular software object library was developed to implement required functionality for filtering of flight-vehicle-tracking data and management of tracking-data sources. (The RADAC software is used to process flight-vehicle metric data for real-time display in the Wallops Flight Facility Range Control Center and Mobile Control Center. This software is part of the Range Control/Range Safety System used to contain impacts of debris from

flight-vehicle operations.) The library includes implementations of tracking-data-editing and -filtering techniques that can be readily found in the literature and was constructed to facilitate future incorporation of implementations of other, more-exotic filtering techniques. A pragmatic technique is used to maintain statistics on differences between measurements and estimates of positions in order to compute a figure of merit for each radar, Global-Positioning-System, or inertial-navigation-system source of tracking data.

An automatic source-qualification technique is implemented to enable optional replacement of a pre-existing manual data-qualification function. The library was written in the C++ language and was designed to be hosted within an application program running on virtually any computing platform.

This program was written by R. James Lanzi and Donna C. Smith of Goddard Space Flight Center. Further information is contained in a TSP (see page 1).
GSC-14974-1

Σ Automatic Command Sequence Generation

NASA's Jet Propulsion Laboratory, Pasadena, California

Automatic Sequence Generator (Autogen) Version 3.0 software automatically generates command sequences for the Mars Reconnaissance Orbiter (MRO) and several other JPL spacecraft operated by the multi-mission support team. Autogen uses standard JPL sequencing tools like APGEN, ASP, SEQGEN, and the DOM database to automate the generation of uplink command products, Spacecraft Command Message Format (SCMF) files, and the corresponding ground command products, DSN Keywords Files (DKF). Autogen supports all the major multi-mission mission phases including the cruise, aerobraking, mapping/science, and relay mission phases.

Autogen is a Perl script, which functions within the 'mission operations'

UNIX environment. It consists of two parts: a set of model files and the autogen Perl script. Autogen encodes the behaviors of the system into a model and encodes algorithms for context-sensitive customizations of the modeled behaviors. The model includes knowledge of different mission phases and how the resultant command products must differ for these phases. The executable software portion of Autogen, automates the setup and use of APGEN for constructing a spacecraft activity sequence file (SASF). The setup includes file retrieval through the DOM (Distributed Object Manager), an object database used to store project files. This step retrieves all the needed input files for generating the command products.

Depending on the mission phase, Autogen also uses the ASP (Automated Sequence Processor) and SEQGEN to generate the command product sent to the spacecraft. Autogen also provides the means for customizing sequences through the use of configuration files. By automating the majority of the sequencing generation process, Autogen eliminates many sequence generation errors commonly introduced by manually constructing spacecraft command sequences. Through the layering of commands into the sequence by a series of scheduling algorithms, users are able to rapidly and reliably construct the desired uplink command products.

With the aid of Autogen, sequences may be produced in a matter of hours instead of weeks, with a significant reduc-

tion in the number of people on the sequence team. As a result, the uplink product generation process is significantly streamlined and mission risk is significantly reduced. Autogen is used for operations of MRO, Mars Global Surveyor (MGS), Mars Exploration Rover

(MER), Mars Odyssey, and will be used for operations of Phoenix. Autogen Version 3.0 is the operational version of Autogen including the MRO adaptation for the cruise mission phase, and was also used for development of the aerobraking and mapping mission phases for MRO.

This program was written by Forest Fisher, Roy Gladded, and Teerapat Khanampompan for NASA's Jet Propulsion Laboratory.

This software is available for commercial licensing. Please contact Karina Edmonds of the California Institute of Technology at (626) 395-2322. Refer to NPO-43638.

Σ Generating Scenarios When Data Are Missing

NASA's Jet Propulsion Laboratory, Pasadena, California

A computer program implements the algorithm described in "Hypothetical Scenario Generator for Fault-Tolerant Diagnosis" (NPO-42516), *NASA Tech Briefs*,

Vol. 31, No. 6 (June 2007), page 71. To recapitulate: the Hypothetical Scenario Generator (HSG) is being developed in conjunction with other components of

artificial-intelligence systems for automated diagnosis and prognosis of faults in spacecraft, aircraft, and other complex engineering systems. The HSG accepts, as input, possibly incomplete data on the current state of a system (see figure).

The HSG models a potential fault scenario as an ordered disjunctive tree of conjunctive consequences, wherein the ordering is based upon the likelihood that a particular conjunctive path will be taken for the given set of inputs. The computation of likelihood is based partly on a numerical ranking of the degree of completeness of data with respect to satisfaction of the antecedent conditions of prognostic rules. The results from the HSG are then used by a model-based artificial-intelligence subsystem to predict realistic scenarios and states.

This program was written by Mark James and Ryan Mackey of Caltech for NASA's Jet Propulsion Laboratory. Further information is contained in a TSP (see page 1).

This software is available for commercial licensing. Please contact Karina Edmonds of the California Institute of Technology at (626) 395-2322. Refer to NPO-43097.



End-to-End Prognostic Architecture uses existing diagnostic models to generate predictions.

Σ CASPER Version 2.0

NASA's Jet Propulsion Laboratory, Pasadena, California

The Continuous Activity Scheduling Planning Execution and Replanning (CASPER) computer program has been updated to version 2.0. A prototype version was reported in "Software for Continuous Replanning During Execution" (NPO-20972), *NASA Tech Briefs*, Vol. 26, No. 7 (April 2002), page 67. To recapitulate: CASPER is designed to perform automated planning of interdependent activities within a system subject to requirements, constraints, and limitations on resources.

In contradistinction to the traditional concept of batch planning followed by

execution, CASPER implements a concept of continuous planning and replanning in response to unanticipated changes (including failures), integrated with execution. Improvements over other, similar software that have been incorporated into CASPER version 2.0 include an enhanced executable interface to facilitate integration with a wide range of execution software systems and supporting software libraries; features to support execution while reasoning about urgency, importance, and impending deadlines; features that enable accommodation to a wide range of com-

puting environments that include various central processing units and random-access-memory capacities; and improved generic time-server and time-control features.

This program was written by Steve Chien, Gregg Rabideau, Daniel Tran, Russell Knight, Caroline Chouinard, Tara Estlin, Daniel Gaines, Bradley Clement, and Anthony Barrett of Caltech for NASA's Jet Propulsion Laboratory.

This software is available for commercial licensing. Please contact Karina Edmonds of the California Institute of Technology at (626) 395-2322. Refer to NPO-41987.

Σ Mission Simulation Toolkit

Ames Research Center, Moffett Field, California

The Mission Simulation Toolkit (MST) is a flexible software system for autonomy research. It was developed as part of the Mission Simulation Facility (MSF) project that was started in 2001 to facilitate the development of autonomous planetary robotic missions. Autonomy is a key enabling factor for robotic exploration. There has been a large gap between autonomy software (at the research level), and software that is ready for insertion into near-term space missions. The MST bridges this gap by providing a simulation framework and a suite of tools for supporting research and maturation of autonomy.

MST uses a distributed framework based on the High Level Architecture (HLA) standard. A key feature of the MST framework is the ability to plug in new models to replace existing ones with the same services. This enables significant simulation flexibility, particularly the mixing and control of fidelity level. In addition, the MST provides automatic code generation from robot interfaces defined with the Unified Modeling Language (UML), methods for maintaining synchronization across distributed simulation systems, XML-based robot description, and an environment server. Finally, the MSF supports a number of third-party

products including dynamic models and terrain databases. Although the communication objects and some of the simulation components that are provided with this toolkit are specifically designed for terrestrial surface rovers, the MST can be applied to any other domain, such as aerial, aquatic, or space.

This project was developed by Gregory Pisanich, Lorenzo Flueckiger, Christian Neukom, Mike Wagner, Eric Buchanan, and Laura Plice of QSS Group, Inc. for Ames Research Center. For further information, access <http://opensource.arc.nasa.gov/> or contact the Ames Technology Partnerships Division at (650) 604-2954. ARC-14932-1.

Σ Solving Equations of Multibody Dynamics

NASA's Jet Propulsion Laboratory, Pasadena, California

Darts++ is a computer program for solving the equations of motion of a multibody system or of a multibody model of a dynamic system. It is intended especially for use in dynamical simulations performed in designing and analyzing, and developing software for the control of, complex mechanical systems. Darts++ is based on the Spatial-Operator-Algebra formulation for multibody dynamics. This software reads a description of a multibody system from a

model data file, then constructs and implements an efficient algorithm that solves the dynamical equations of the system. The efficiency and, hence, the computational speed is sufficient to make Darts++ suitable for use in real-time closed-loop simulations. Darts++ features an object-oriented software architecture that enables reconfiguration of system topology at run time; in contrast, in related prior software, system topology is fixed during initialization.

Darts++ provides an interface to scripting languages, including Tcl and Python, that enable the user to configure and interact with simulation objects at run time.

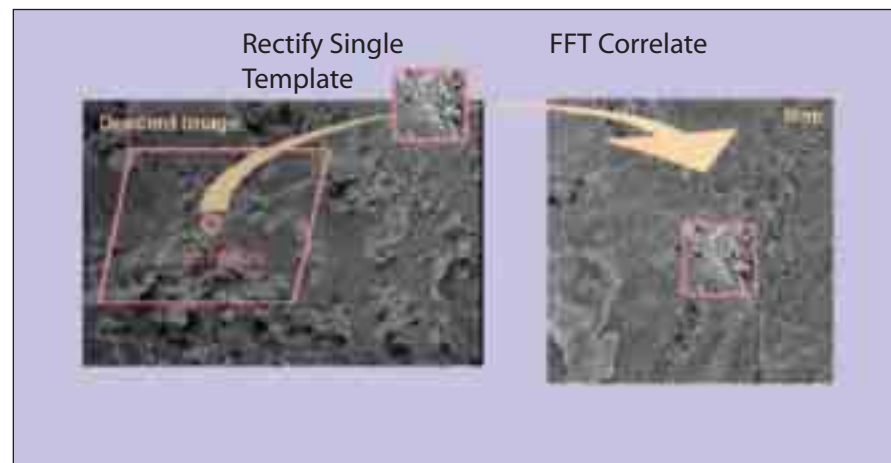
This program was written by Abhinandan Jain and Christopher Lim of Caltech for NASA's Jet Propulsion Laboratory.

This software is available for commercial licensing. Please contact Karina Edmonds of the California Institute of Technology at (626) 395-2322. Refer to NPO-42890.

Σ Mapped Landmark Algorithm for Precision Landing

NASA's Jet Propulsion Laboratory, Pasadena, California

A report discusses a computer vision algorithm for position estimation to enable precision landing during planetary descent. The Descent Image Motion Estimation System for the Mars Exploration Rovers has been used as a starting point for creating code for precision, terrain-relative navigation during planetary landing. The algorithm is designed to be general because it handles images taken at different scales and resolutions relative to the map, and can produce mapped landmark matches for any planetary terrain of sufficient texture. These matches provide a measurement of horizontal position relative to a known landing site specified on the surface map. Multiple



FFT Map-Matching Concept.

mapped landmarks generated per image allow for automatic detection and elimination of bad matches. Attitude and position can be generated from each image; this image-based attitude measurement can be used by the onboard navigation filter to improve the attitude estimate, which will improve the position estimates.

The algorithm uses normalized correlation of grayscale images, producing

precise, sub-pixel images. The algorithm has been broken into two sub-algorithms: (1) FFT Map Matching (see figure), which matches a single large template by correlation in the frequency domain, and (2) Mapped Landmark Refinement, which matches many small templates by correlation in the spatial domain. Each relies on feature selection, the homography transform, and 3D image correlation. The algorithm is implemented in C++ and is

rated at Technology Readiness Level (TRL) 4.

This work was done by Andrew Johnson, Adnan Ansar, and Larry Matthies of Caltech for NASA's Jet Propulsion Laboratory. Further information is contained in a TSP (see page 1).

The software used in this innovation is available for commercial licensing. Please contact Karina Edmonds of the California Institute of Technology at (626) 395-2322. Refer to NPO-44463.

Σ WMAP C&DH Software

Goddard Space Flight Center, Greenbelt, Maryland

The command-and-data-handling (C&DH) software of the Wilkinson Microwave Anisotropy Probe (WMAP) spacecraft functions as the sole interface between (1) the spacecraft and its instrument subsystem and (2) ground operations equipment. This software includes a command-decoding and -distribution system, a telemetry/data-handling system, and a data-storage-and-playback system. This software performs onboard processing of attitude sensor data and generates

commands for attitude-control actuators in a closed-loop fashion. It also processes stored commands and monitors health and safety functions for the spacecraft and its instrument subsystems. The basic functionality of this software is the same of that of the older C&DH software of the Rossi X-Ray Timing Explorer (RXTE) spacecraft, the main difference being the addition of the attitude-control functionality. Previously, the C&DH and attitude-control computations were performed by differ-

ent processors because a single RXTE processor did not have enough processing power. The WMAP spacecraft includes a more-powerful processor capable of performing both computations.

This program was written by Alan Cudmore, Tim Leath, Art Ferrer, Todd Miller, Mark Walters, Bruce Savadkin, and Ji-Wei Wu of Goddard Space Flight Center; Steve Slegel of Daedalian Systems Corp.; and Emory Stagmer of Litton/PRC. Further information is contained in a TSP (see page 1). GSC-14964-1

Σ Web-Based Environment for Maintaining Legacy Software

Lyndon B. Johnson Space Center, Houston, Texas

"Advanced Tool Integration Environment" ("ATIE") is the name of both a software system and a Web-based environment created by the system for maintaining an archive of legacy software and expertise involved in developing the legacy software. ATIE can also be used in modifying legacy software and developing new software. The information that can be encapsulated in ATIE includes experts' documentation, input and output data of tests cases, source code, and compilation scripts. All of this informa-

tion is available within a common environment and retained in a database for ease of access and recovery by use of powerful search engines. ATIE also accommodates the embedment of supporting software that users require for their work, and even enables access to supporting commercial-off-the-shelf (COTS) software within the flow of the experts' work.

The flow of work can be captured by saving the sequence of computer programs that the expert uses. A user gains

access to ATIE via a Web browser. A modern Web-based graphical user interface promotes efficiency in the retrieval, execution, and modification of legacy code. Thus, ATIE saves time and money in the support of new and pre-existing programs.

This program was written by Michael Tigges of Johnson Space Center; Nelson Thompson, Mark Orr, and Richard Fox of Dynacs, Inc.; and Rick Rohan of Lockheed Martin Corp. Further information is contained in a TSP (see page 1). MSC-23810-1

Σ Information Metacatalog for a Grid

Ames Research Center, Moffett Field, California

SWIM is a Software Information Metacatalog that gathers detailed information about the software components and packages installed on a grid resource. Information is currently gathered for Executable and Linking

Format (ELF) executables and shared libraries, Java classes, shell scripts, and Perl and Python modules. SWIM is built on top of the POUR framework, which is described in the preceding article. SWIM consists of a set of Perl

modules for extracting software information from a system, an XML schema defining the format of data that can be added by users, and a POUR XML configuration file that describes how these elements are used to generate pe-

riodic, on-demand, and user-specified information.

Periodic software information is derived mainly from the package managers used on each system. SWIM collects information from native package managers in FreeBSD, Solaris, and IRIX as well as the RPM, Perl, and Python package managers on multiple platforms. Because not all software is avail-

able, or installed in package form, SWIM also crawls the set of relevant paths from the File System Hierarchy Standard that defines the standard file system structure used by all major UNIX distributions. Using these two techniques, the vast majority of software installed on a system can be located. SWIM computes the same information gathered by the periodic

routines for specific files on specific hosts, and locates software on a system given only its name and type.

This program was written by Paul Kolano of Advanced Management Technology for Ames Research Center. For further information, access <http://opensource.arc.nasa.gov/> or contact the Ames Technology Partnerships Division at (650) 604-2954. ARC-15469-1

Σ Grid Task Execution

Ames Research Center, Moffett Field, California

IPG Execution Service is a framework that reliably executes complex jobs on a computational grid, and is part of the IPG service architecture designed to support location-independent computing. The new grid service enables users to describe the platform on which they need a job to run, which allows the service to locate the desired platform, configure it for the required application, and execute the job. After a job is submitted, users can monitor it through periodic notifications, or through queries.

Each job consists of a set of tasks that performs actions such as executing applications and managing data. Each task is executed based on a starting condition that is an expression of the states of other tasks. This formulation allows tasks to be executed in parallel, and also allows a user to specify tasks to execute when other tasks succeed, fail, or are canceled.

The two core components of the Execution Service are the Task Database, which stores tasks that have been submit-

ted for execution, and the Task Manager, which executes tasks in the proper order, based on the user-specified starting conditions, and avoids overloading local and remote resources while executing tasks.

This program was written by Chaumin Hu of Advanced Management Technology for Ames Research Center. For further information, access <http://opensource.arc.nasa.gov/> or contact the Ames Technology Partnerships Division at (650) 604-2954. ARC-15529-1

Σ Parallel-Processing Software for Correlating Stereo Images

NASA's Jet Propulsion Laboratory, Pasadena, California

A computer program implements parallel-processing algorithms for correlating images of terrain acquired by stereoscopic pairs of digital stereo cameras on an exploratory robotic vehicle (e.g., a Mars rover). Such correlations are used to create three-dimensional computational models of the terrain for navigation. In this program, the scene viewed by the cameras is segmented into subimages. Each subimage is assigned to one of a number of central processing units (CPUs) operating simultaneously. Be-

cause each subimage is smaller than a full image, the correlation process takes less time than it would if full images were processed on one CPU. Segmentation and parallelization also make the process more robust in that the smaller subimages present fewer opportunities for a correlation algorithm to "get lost" and thereby fail to converge on a solution. The effectiveness of this program has been demonstrated on several parallel-processing computer systems. Whereas correlation processing of a typ-

ical stereoscopic pair of test images on a single CPU was found to take on the order of one hour, parallel processing of the same images on a 16-CPU cluster was found to take about 3 minutes.

This program was written by Gerhard Klimeck, Robert Deen, Michael McAuley, and Eric De Jong of Caltech for NASA's Jet Propulsion Laboratory.

This software is available for commercial licensing. Please contact Karina Edmonds of the California Institute of Technology at (626) 395-2322. Refer to NPO-30631.

Σ Knowledge Base Editor (SharpKBE)

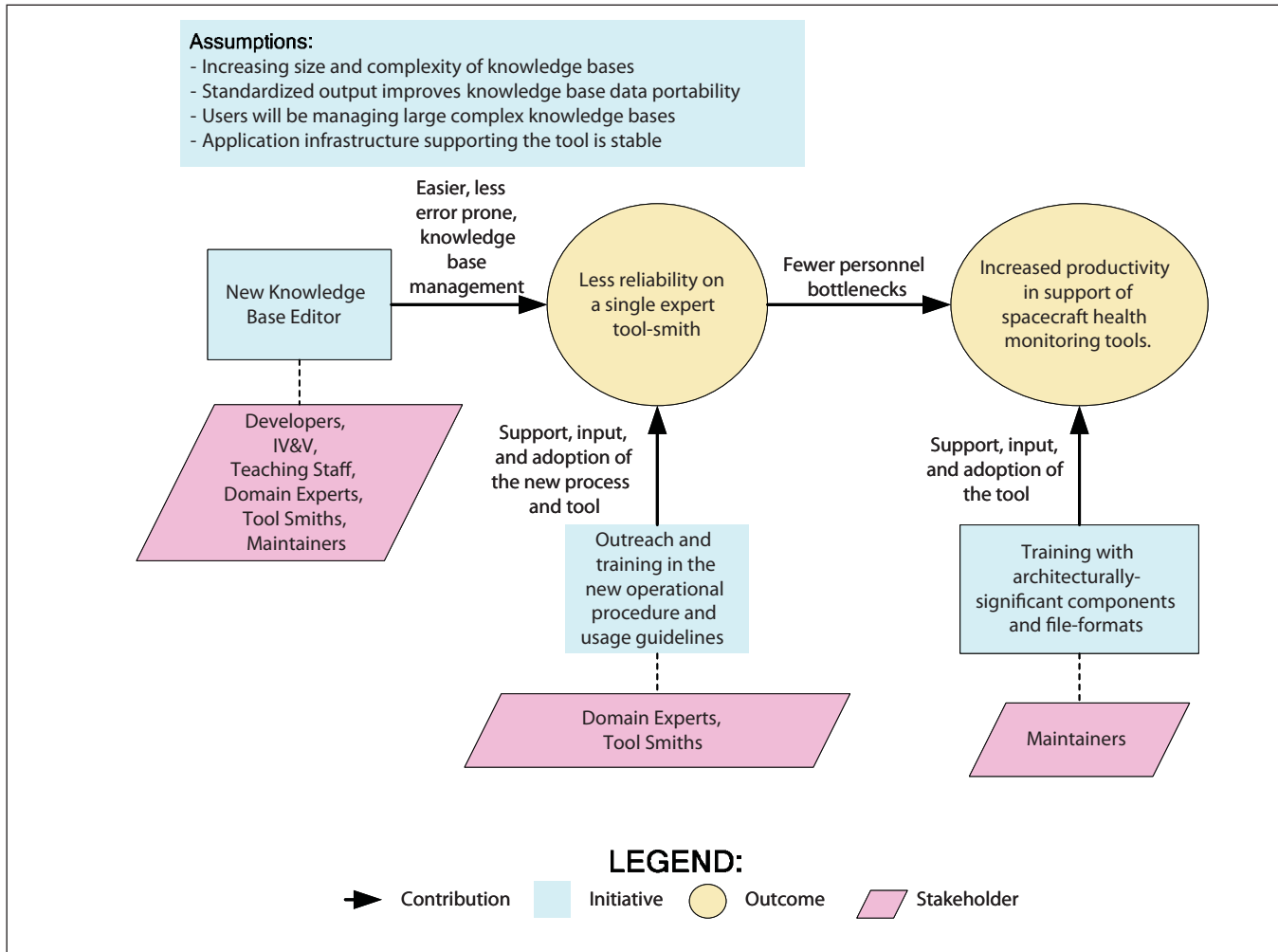
NASA's Jet Propulsion Laboratory, Pasadena, California

The SharpKBE software provides a graphical user interface environment for domain experts to build and manage knowledge base systems. Knowledge bases can be exported/translated to various target languages automatically, including customizable target languages.

The tool enhances current practices by minimizing reliance on toolsmiths for system workflow management, and also improves the quality and maintenance of those systems by reducing the number of errors within the knowledge bases. This tool's primary capability is in the

area of expert systems modeling, specifically where there is a need to capture and efficiently manage large quantities of domain information (see figure).

The SharpKBE supports C# and SHINE targets, and in concert with SHINE additionally produces C and



Benefits Chain Diagram

C++ targets. The knowledge base, which is created via graphical expression editors, is saved to a standardized XML document structure that is more flexible than previously existing formats, which were written in LISP-style syntax. This provides the user with intuitive mechanisms for viewing and modifying

knowledge bases (see example) as well as the ability to produce customized style sheets. The editor can support the auto-coding paradigm for fault detection systems in flight software applications with reduced cost.

This program was written by Raffi Tikidjian, Mark James, and Ryan Mackey of Cal-

tech for NASA's Jet Propulsion Laboratory. Further information is contained in a TSP (see page 1).

This software is available for commercial licensing. Please contact Karina Edmonds of the California Institute of Technology at (626) 395-2322. Refer to NPO-44476.

Parallel Computing With Satellite Orbit Analysis Program

NASA's Jet Propulsion Laboratory, Pasadena, California

This software innovation speeds up the computation time of the Satellite Orbit Analysis Program (SOAP) tool by parallelizing the code using the message-passing interface (MPI) library. The speed increases almost linearly with the number of processors, allowing the per-study duration of the visualization and analysis of space missions to take place in hours, rather than overnight. The software can conduct a parametric study involving millions of design vec-

tors in a few hours of computational time by distributing the design scenarios among multiple processors. This allows SOAP to run in a parallel mode on JPL's new, high-performance computer cluster, which has 1024 Intel Xeon processors.

Parametric Study and Contours in SOAP were the first targets of parallelization. The two functions compute one or more variables over a given time period and become quickly com-

putationally intensive as report duration, time resolution, and variable complexity increase. The spatial and variable domains are sliced and distributed to each processor proportionally to its processing power. The result of the computation over the slice is collected at the end of the computation, and a single processor handles the file-writing task. Each space and variable domain contribution is completely independent so that message

passing is needed only at the beginning and end of the computation. The minimal message passing ensures the high speed of the proposed parallel implementation.

Trade analyses can be performed and optimization problems can be solved for space mission design with respect to rel-

evant figures of merit. The mission merits/objectives/requirements are calculated with the set of design variables. The tradeoff space given by the design problem is visualized. SOAP is used for DAWN mission design, Cassini mission analyses, Team X mission concept studies, and DOD and Air Force projects.

This program was written by John M. Coggi and David Y. Stodden of Aerospace Corporation and Seungwon Lee and Robert C. Carrwright of Caltech for NASA's Jet Propulsion Laboratory.

This software is available for commercial licensing. Please contact Karina Edmonds of the California Institute of Technology at (626) 395-2322. Refer to NPO-44486.

Σ Automated Sequence Generation Process and Software

NASA's Jet Propulsion Laboratory, Pasadena, California

"Automated sequence generation" (autogen) signifies both a process and software used to automatically generate sequences of commands to operate various spacecraft. Autogen requires fewer workers than are needed for older manual sequence-generation processes and reduces sequence-generation times from weeks to minutes. The autogen software comprises the autogen script plus the Activity Plan Generator (APGEN) program. APGEN can be used for planning missions and command sequences. APGEN includes a graphical user interface that facilitates scheduling

of activities on a time line and affords a capability to automatically expand, decompose, and schedule activities. The autogen script performs the following tasks:

- Gathers needed data files from data repositories on the mission operations network.
- Builds other data files needed for the APGEN scheduling algorithms, based on inputs specified by the user.
- Sets up the environment to run APGEN, including scheduling instructions.
- Runs APGEN, which schedules activi-

ties and writes the corresponding sequences of commands to files.

- Manipulates the resultant sequence and other files, if needed.
- Initiates any automated sequence processors to prepare the sequence for uplink, if appropriate.

This work was done by Roy Gladden of Caltech for NASA's Jet Propulsion Laboratory. Further information is contained in a TSP (see page 1).

This software is available for commercial licensing. Please contact Karina Edmonds of the California Institute of Technology at (626) 395-2322. Refer to NPO-30746.

Σ Periodic, On-Demand, and User-Specified Information Reconciliation

Ames Research Center, Moffett Field, California

POUR is a framework that accepts periodic information updates, collects information on demand, and accepts user-specified information while presenting a single unified view to the user. The primary functionality of POUR is through its query interface. A query consists of any number of XPath's, where each XPath returns a list of XML strings that satisfies the query. Depending on the XPath's specified and the contents of the POUR database, query processing may be as simple as a database lookup, or as complex as a series of

queries down a POUR hierarchy to a set of POUR repositories that compute the requested information on the fly before the appropriate results are returned.

Users may use any valid XPath to retrieve results integrated from across the relevant periodic, on-demand, and user-specified sources. Periodic information comes from trusted sources at an unknown frequency such that any previous information from the same source can be completely overwritten. On-demand information is computed when needed

using queries to other POUR instances or using scripts dynamically executed by the Globus GRAM service. Finally, users may add their own information into a POUR repository if it conforms to a site-defined XML schema.

This program was written by Paul Kolano of Advanced Management Technology for Ames Research Center. For further information, access <http://opensource.arc.nasa.gov/> or contact the Ames Technology Partnerships Division at (650) 604-2954. ARC-15468-1

Σ Simulating Operations at a Spaceport

John F. Kennedy Space Center, Florida

SPACESIM is a computer program for detailed simulation of operations at a spaceport. SPACESIM is being developed to greatly improve existing spaceports and to aid in designing, building,

and operating future spaceports, given that there is a worldwide trend in spaceport operations from very expensive, research-oriented launches to more frequent commercial launches. From an

operational perspective, future spaceports are expected to resemble current airports and seaports, for which it is necessary to resolve issues of safety, security, efficient movement of machinery and

people, cost effectiveness, timeliness, and maximizing effectiveness in utilization of resources.

Simulations can be performed, for example, to (1) simultaneously analyze launches of reusable and expendable rockets and identify bottlenecks arising from competition for limited resources or (2) perform "what-if" scenario analyses to identify optimal scenarios prior to making large capital investments. SPACESIM includes an object-oriented discrete-event-simulation engine. (Dis-

crete-event simulation has been used to assess processes at modern seaports.) The simulation engine is built upon the Java programming language for maximum portability. Extensible Markup Language (XML) is used for storage of data to enable industry-standard interchange of data with other software. A graphical user interface facilitates creation of scenarios and analysis of data.

This program was written by Michael R. Nevins of Nevins Software, Inc. for Kennedy Space Center.

In accordance with Public Law 96-517, the contractor has elected to retain title to this invention. Inquiries concerning rights for its commercial use should be addressed to:

*Mr. Mike Nevins
Nevins Software, Inc.
P.O. Box 308
Morris, IL 60450
Phone No.: (815) 941-2406*

*E-mail: mnevins@nevinssoftware.com
Refer to KSC-12943, volume and number of this NASA Tech Briefs issue, and the page number.*

Web-Based Real-Time Emergency Monitoring

Stennis Space Center, Mississippi

The Web-based Real-Time Asset Monitoring (RAM) module for emergency operations and facility management enables emergency personnel in federal agencies and local and state governments to monitor and analyze data in the event of a natural disaster or other crisis that threatens a large number of people and property. The software can manage many disparate sources of data within a facility, city, or county. It was developed on industry-standard Geo-Spatial software and is compliant with open GIS standards.

RAM View can function as a stand-alone system, or as an integrated plug-in module to Emergency Operations Center (EOC) software suites such as REACT (Real-time Emergency Action

Coordination Tool), thus ensuring the widest possible distribution among potential users. RAM has the ability to monitor various data sources, including streaming data. Many disparate systems are included in the initial suite of supported hardware systems, such as mobile GPS units, ambient measurements of temperature, moisture and chemical agents, flow meters, air quality, asset location, and meteorological conditions.

RAM View displays real-time data streams such as gauge heights from the U.S. Geological Survey gauging stations, flood crests from the National Weather Service, and meteorological data from numerous sources. Data points are clearly visible on the map in-

terface, and attributes as specified in the user requirements can be viewed and queried.

This program was written by Craig A. Harvey and Joel Lawhead of NVision Solutions, Inc. for Stennis Space Center.

In accordance with Public Law 96-517, the contractor has elected to retain title to this invention. Inquiries concerning rights for its commercial use should be addressed to:

*NVision Solutions, Inc.
NASA Stennis Space Center
Building 1103, Suite 147C
Stennis Space Center, MS 39529
Phone No.: (228) 688-2205*

*E-mail: Charvey@nvs-inc.com
Refer to SSC-00244, volume and number of this NASA Tech Briefs issue, and the page number.*

Real-Time Data Display

Marshall Space Flight Center, Alabama

RT-Display is a MATLAB-based data acquisition environment designed to use a variety of commercial off-the-shelf (COTS) hardware to digitize analog signals to a standard data format usable by other post-acquisition data analysis tools. This software presents the acquired data in real time using a variety of signal-processing algorithms. The acquired data is stored in a standard Operator Interactive Signal Processing Software (OISPS) data-formatted file.

RT-Display is primarily configured to use the Agilent VXI (or equivalent) data acquisition boards used in such systems as MIDDAS (Multi-channel Integrated Dynamic Data Acquisition Sys-

tem). The software is generalized and deployable in almost any testing environment, without limitations or proprietary configuration for a specific test program or project. With the Agilent hardware configured and in place, users can start the program and, in one step, immediately begin digitizing multiple channels of data. Once the acquisition is completed, data is converted into a common binary format that also can be translated to specific formats used by external analysis software, such as OISPS and PC-Signal (product of AI Signal Research Inc.).

RT-Display at the time of this reporting was certified on Agilent hardware capa-

ble of acquisition up to 196,608 samples per second. Data signals are presented to the user on-screen simultaneously for 16 channels. Each channel can be viewed individually, with a maximum capability of 160 signal channels (depending on hardware configuration). Current signal presentations include: time data, fast Fourier transforms (FFT), and power spectral density plots (PSD). Additional processing algorithms can be easily incorporated into this environment.

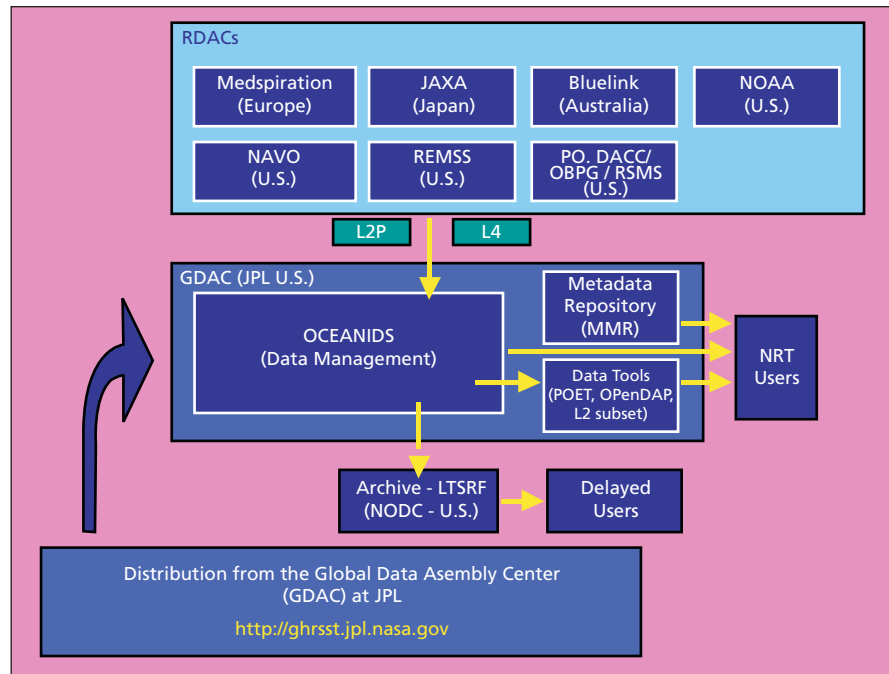
This program was written by Marc Pedings of Optical Sciences Corporation for Marshall Space Flight Center. Further information is contained in a TSP (see page 1). MFS-32325-1

Master Metadata Repository and Metadata-Management System

NASA's Jet Propulsion Laboratory, Pasadena, California

A master metadata repository (MMR) software system manages the storage and searching of metadata pertaining to data from national and international satellite sources of the Global Ocean Data Assimilation Experiment (GODAE) High Resolution Sea Surface Temperature Pilot Project [GHRSS-PP]. These sources (see figure) produce a total of hundreds of data files daily, each file classified as one of more than ten data products representing global sea-surface temperatures. The MMR is a relational database wherein the metadata are divided into granule-level records [denoted file records (FRs)] for individual satellite files and collection-level records [denoted data set descriptions (DSDs)] that describe metadata common to all the files from a specific data product. FRs and DSDs adhere to the NASA Directory Interchange Format (DIF). The FRs and DSDs are contained in separate sub-databases linked by a common field.

The MMR is configured in MySQL database software with custom Practical Extraction and Reporting Language (PERL) programs to validate and ingest the metadata records. The database contents are converted into the Federal Geographic Data Committee (FGDC) standard format by use of the Extensible



An Overview of the GHRSS-PP is shown and the JPL Global Data Assembly Center (GDAC). Note NRT is near real time.

Markup Language (XML). A Web interface enables users to search for availability of data from all sources.

This software was written by Edward Armstrong of Caltech and Nate Reed and Wen Zhang of Raytheon ITSS for NASA's Jet

Propulsion Laboratory. Further information is contained in a TSP (see page 1).

This software is available for commercial licensing. Please contact Karina Edmonds of the California Institute of Technology at (626) 395-2322. Refer to NPO-44552.

Collaborative Resource Allocation

NASA's Jet Propulsion Laboratory, Pasadena, California

Collaborative Resource Allocation Networking Environment (CRANE) Version 0.5 is a prototype created to prove the newest concept of using a distributed environment to schedule Deep Space Network (DSN) antenna times in a collaborative fashion. This program is for all space-flight and terrestrial science project users and DSN schedulers to perform scheduling activities and conflict resolution, both synchronously and asynchronously. Project schedulers can, for the first time, participate directly in scheduling their tracking times into the official DSN schedule, and negotiate directly with other projects in an integrated scheduling system.

A master schedule covers long-range,

mid-range, near-real-time, and real-time scheduling time frames all in one, rather than the current method of separate functions that are supported by different processes and tools. CRANE also provides private workspaces (both dynamic and static), data sharing, scenario management, user control, rapid messaging (based on Java Message Service), data/time synchronization, workflow management, notification (including e-mails), conflict checking, and a linkage to a schedule generation engine.

The data structure with corresponding database design combines object trees with multiple associated mortal instances and relational database to provide unprecedented traceability and simplify the existing DSN XML schedule

representation. These technologies are used to provide traceability, schedule negotiation, conflict resolution, and load forecasting from real-time operations to long-range loading analysis up to 20 years in the future. CRANE includes a database, a stored procedure layer, an agent-based middle tier, a Web service wrapper, a Windows Integrated Analysis Environment (IAE), a Java application, and a Web page interface.

This program was written by Yeou-Fang Wang, Allan Wax, Raymond Lam, John Baldwin, and Chester Borden of Caltech for NASA's Jet Propulsion Laboratory.

This software is available for commercial licensing. Please contact Karina Edmonds of the California Institute of Technology at (626) 395-2322. Refer to NPO-44053.

Model Checker for Java Programs

Ames Research Center, Moffett Field, California

Java Pathfinder (JPF) is a verification and testing environment for Java that integrates model checking, program analysis, and testing. JPF consists of a custom-made Java Virtual Machine (JVM) that interprets bytecode, combined with a search interface to allow the complete behavior of a Java program to be analyzed, including interleavings of concurrent programs. JPF is implemented in Java, and its architecture is highly modular to support rapid prototyping of new features.

JPF is an explicit-state model checker, because it enumerates all visited states and, therefore, suffers from the state-explosion problem inherent in analyzing large programs. It is suited to analyzing

programs less than 10kLOC, but has been successfully applied to finding errors in concurrent programs up to 100kLOC. When an error is found, a trace from the initial state to the error is produced to guide the debugging.

JPF works at the bytecode level, meaning that all of Java can be model-checked. By default, the software checks for all runtime errors (uncaught exceptions), assertions violations (supports Java's assert), and deadlocks. JPF uses garbage collection and symmetry reductions of the heap during model checking to reduce state-explosion, as well as dynamic partial-order reductions to lower the number of interleavings analyzed.

JPF is capable of symbolic execution of Java programs, including symbolic execution of complex data such as linked lists and trees. JPF is extensible as it allows for the creation of listeners that can subscribe to events during searches. The creation of dedicated code to be executed in place of regular classes is supported and allows users to easily handle native calls and to improve the efficiency of the analysis.

This work was done by Willem Visser of Research Institute for Advanced Computer Science for Ames Research Center. For further information, access <http://ti.arc.nasa.gov/ase/jpf/index.html> or contact the Ames Technology Partnerships Division at (650) 604-2954. Refer to ARC-15388-1.



Books & Reports

Telescope Formation at L2 for Observing Earth's Atmosphere

Two documents describe a proposed Earth-atmosphere observatory to orbit the Sun at the Sun-Earth L2 Lagrange point — a point of unstable equilibrium in the shadow of the Earth, about 1.5 million km from the Earth along an outward projection of the Earth-Sun axis. The observatory would comprise two spacecraft flying in precision formation: (1) a primary-aperture spacecraft, from which would be deployed a 25-m diameter membrane primary mirror aimed at the Earth, and (2) a secondary-telescope spacecraft at the focal plane of the primary mirror, 125-m distant along the axis towards the Earth. The secondary telescope would be aimed at the primary mirror and slowly rotated to scan the focused annular image of the visible illuminated portion of the Earth's atmosphere during continuous occultation of the Sun.

The purpose of the observations is to gather spectroscopic data of chemical signatures from ultraviolet to near-infrared that could contribute to major advances in understanding atmospheric dynamics and development of models for prediction of climate change. The documents present an overview of the scientific mission, the rationale for the choice of L2, and numerous engineering issues, including the overall architecture of the telescope formation, delivery to L2, design of the telescope and associated metrology instrumentation, formation maneuvering to follow a unique powered solar occultation orbit in the vicinity of L2, and strategies for observatory initialization and mission operations.

*This work was done by Edward Mettler, Beçet Açıkmeşe, William Breckenridge, Steven Macenka, Randall Hein, and Eldred Tubbs of Caltech for NASA's Jet Propulsion Laboratory. Further information is contained in a TSP (see page 1).
NPO-40973*

Ultraviolet-Resistant Bacterial Spores

A document summarizes a study in which it was found that spores of the SAFR-032 strain of *Bacillus pumilus* can survive doses of ultraviolet (UV) radiation, γ radiation, and hydrogen perox-

ide in proportions much greater than those of other bacteria. The study was part of a continuing effort to understand the survivability of bacteria under harsh conditions and develop means of sterilizing spacecraft to prevent biocontamination of Mars that could interfere with the search for life there.

A major conclusion stated in the document is that standard UV treatments that are effective against spores of other bacteria may not be sufficient to inactivate spores of SAFR-032 and, hence, may not be sufficient to inactivate all bacterial spores. Noting that heretofore, spores of *B. subtilis* have been used as a biodosimetry model for the UV inactivation of spores, the document presents the further conclusion that *B. subtilis* should now be considered unreliable as such a model. It is further suggested that because of its greater resistance to sterilization processes, SAFR-032 should be substituted for other biological indicators that have been used in hospitals and government facilities as indicators for quality control of sterilization.

This work was done by Kasthuri Venkateswaran, David Neucombe, Myron T. La Duc, and Shariff R. Osman of Caltech for NASA's Jet Propulsion Laboratory.

In accordance with Public Law 96-517, the contractor has elected to retain title to this invention. Inquiries concerning rights for its commercial use should be addressed to:

*Innovative Technology Assets Management
JPL*

*Mail Stop 202-233
4800 Oak Grove Drive
Pasadena, CA 91109-8099
(818) 354-2240*

E-mail: iaoffice@jpl.nasa.gov

Refer to NPO-40953, volume and number of this NASA Tech Briefs issue, and the page number.

Launching Payloads Into Orbit at Relatively Low Cost

A report proposes the development of a system for launching payloads into orbit at about one-fifth the cost per unit payload weight of current systems. The system would be based on the formerly secret PILOT microsatellite-launching system developed in response to the Soviet launch of Sputnik-1. The PILOT sys-

tem was a solid-fuel, aerodynamically spun and spin-stabilized, five-stage rocket with onboard controls including little more than an optoelectronic horizon sensor and a timer for triggering the second and fifth stages, respectively. The proposal calls for four improvements over the PILOT system to enable control of orbital parameters:

- (1) the aerodynamic tipover of the rocket at the top of the atmosphere could be modeled as a nonuniform gyroscopic precession and could be controlled by selection of the initial rocket configuration and launch conditions;
- (2) the attitude of the rocket at the top of the first-stage trajectory could be measured by use of radar tracking or differential Global Positioning System receivers to determine when to trigger the second stage;
- (3) the final-stage engines could be configured around the payload to enhance spin stabilization during a half-orbit coast up to apoapsis where the final stage would be triggered; and
- (4) the final payload stage could be equipped with a "beltline" of small thrusters for correcting small errors in the trajectory as measured by an off-board tracking subsystem.

This work was done by Brian Wilcox of Caltech for NASA's Jet Propulsion Laboratory. Further information is contained in a TSP (see page 1).

In accordance with Public Law 96-517, the contractor has elected to retain title to this invention. Inquiries concerning rights for its commercial use should be addressed to:

*Innovative Technology Assets Management
JPL*

*Mail Stop 202-233
4800 Oak Grove Drive
Pasadena, CA 91109-8099
(818) 354-2240*

E-mail: iaoffice@jpl.nasa.gov

Refer to NPO-20908, volume and number of this NASA Tech Briefs issue, and the page number.

Effects of Bone Morphogenic Proteins on Engineered Cartilage

A report describes experiments on the effects of bone morphogenic proteins (BMPs) on engineered cartilage grown

in vitro. In the experiments, bovine calf articular chondrocytes were seeded onto biodegradable polyglycolic acid scaffolds and cultured in, variously, a control medium or a medium supplemented with BMP-2, BMP-12, or BMP-13 in various concentrations. Under all conditions investigated, cell-polymer constructs cultivated for 4 weeks macroscopically and histologically resembled native cartilage. At a concentration of 100 ng/mL, BMP-2, BMP-12, or BMP-13 caused (1) total masses of the constructs to exceed those of the controls by 121, 80, or 62 percent, respectively; (2) weight percentages of gly-

cosaminoglycans in the constructs to increase by 27, 18, or 15, respectively; and (3) total collagen contents of the constructs to decrease to 63, 89, or 83 percent of the control values, respectively. BMP-2, but not BMP-12 or BMP-13, promoted chondrocyte hypertrophy.

These observations were interpreted as suggesting that the three BMPs increase the growth rates and modulate the compositions of engineered cartilage. It was also concluded that *in vitro* engineered cartilage is a suitable system for studying effects of BMPs on chondrogenesis in a well-defined environment.

This work was done by Keith J. Gooch,

Torsten Blunk, Donald L. Courter, Alisha Sieminski, Gordana Vunjak-Novakovic, and Lisa E. Freed of Massachusetts Institute of Technology for Johnson Space Center.

In accordance with Public Law 96-517, the contractor has elected to retain title to this invention. Inquiries concerning rights for its commercial use should be addressed to:

L.E. Freed, M.D., Ph.D.

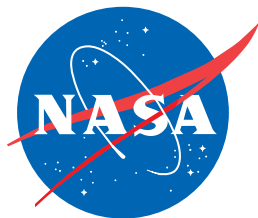
M.I.T. E25-330

45 Carleton St.

Cambridge, MA 02139

E-mail: Lfreed@mit.edu

Refer to MSC-23647, volume and number of this NASA Tech Briefs issue, and the page number.



National Aeronautics and
Space Administration